Student thesis series INES nr 408

Assessment of forcing mechanisms on net community production and dissolved inorganic carbon dynamics in the Southern Ocean using glider data

Julia Schütt

2017
Department of
Physical Geography and Ecosystem Science
Lund University
Sölvegatan 12
S-223 62 Lund
Sweden

Julia Schütt (2017).
Assessment of forcing mechanisms on net community production and dissolved inorganic carbon dynamics in the Southern Ocean using glider data
Master degree thesis, 30 credits in *Atmospheric Sciences and Biogeochemical Cycles*
Department of Physical Geography and Ecosystem Science, Lund University

Level: Master of Science (MSc)

Course duration: *January* 2016 until *January* 2017

Assessment of forcing mechanisms on net community production and dissolved inorganic carbon dynamics in the Southern Ocean using glider data

---

Julia Schütt

Master thesis, 30 credits, in *Atmospheric Sciences and Biogeochemical Cycles*

Martin Berggren
Department of Physical Geography and Ecosystem Science

Sandy Thomalla
CSIR/ SOCCO, South Africa

Exam committee:
Vaughan Phillips, Department of Physical Geography and Ecosystem Science
Ana Soares, Department of Physical Geography and Ecosystem Science

Abstract

In the Subantarctic Zone of the Southern Ocean, a combination of physical forcings, chemical solubility and biological fixation is controlling the carbon uptake and thus the role the Southern Ocean is playing in the remediation of global climate change. Therefore, it is necessary to understand the mechanisms controlling oceanic carbon budgets and to quantify biological uptake rates to make reliable future climate predictions. In this study, the data of two ocean gliders simultaneously sampling the ocean interior and the CO_2 exchange processes at the ocean surface were used to model the biological net community production (NCP) based on Chlorophyll *a*. A comparison was made to the seasonal development of surface water diurnal changes in dissolved inorganic carbon (DIC) concentration, as well as to the physical forcing mechanisms controlling both processes.
The cross-seasonal net community production was found to range between -90 and 242 mg m^{-2} d^{-1} with 118 mg m^{-2} d^{-1} on average and the seasonal average daily change in dissolved inorganic carbon concentration was -235 mg m^{-2} d^{-1}, leaving the two processes at overlapping and comparable ranges. It was shown that both time series were following similar seasonal trends of daily carbon drawdown and release when comparing the time series smoothed with a running mean filter, leading to the conclusion that the here modeled daily dissolved inorganic carbon fluxes are largely controlled by the biology. Although, the dissolved inorganic carbon data is fluctuating with a higher amplitude and holds higher daily variability. The net community production was largely controlled by the mixed layer depth and by light, the dissolved inorganic carbon flux did not show any correlation with any of the physical drivers.
It was reasoned that contrary to biological processes, the DIC dynamics are subject to chemical and thermodynamical forcings that are evident during short-lived events and might be most prominently occurring during spring. In the beginning of the productive season, variations in temperature and windstress could be held responsible in controlling an outgassing CO_2 flux which reduces the daily dissolved inorganic carbon rate. During the latter half of the season the days of where net community production and dissolved inorganic carbon had the same sign coincide with periods of mixed layer depth entrainment. The comparison of the seasonal development of net community production and daily dissolved inorganic carbon fluxes and their physical drivers shows the analogy of both time series during summer and thus the possibility of using dissolved inorganic carbon data in the here presented way for deriving information about biological community production and carbon uptake.

Contents

List of Figures

1 Introduction

The world's oceans represent a major carbon reservoir and the Southern Ocean is responsible for taking up 40-50% of the anthropogenically emitted CO_2 that is taken up by the oceans globally (Sallée et al., 2012; Landschützer et al., 2014), which underlines the importance of this part of the world's influence on the global climate. The part of the Southern Ocean (SO) between 30 and 50°S has been recognized as a major sink for atmospheric CO_2 (Takahashi et al., 2012). The uptake and release rate of inorganic carbon is driven by biotic as well as abiotic processes. Quantifying the impacts both of these components have on the air-sea CO_2 flux is crucial to correctly model and identify source and sink regions of CO_2 on the planet.

According to Takahashi et al. (1989) three processes govern the uptake of CO_2 by the ocean: Its chemical solubility, ocean circulations and biological uptake. Ocean circulations are distributing organic and inorganic carbon species around the globe and have the ability to either enhance exchange with the atmospheric reservoir, by providing the conditions necessary for either biological production or outgassing, or suppress the exchange with the atmosphere, by allowing the carbon species to get carried out, or isolating them, from the rest of the cycle for many years. Physical conditions within the water, like stratification, the depth of mixing, entertainment from deeper water layers, horizontal advection and eddies, are driving the seasonal cycle of inorganic carbon (Merlivat et al., 2014). However, factors outside the waterbody, like windstress and solar heat flux, simultaneously influence its physical processes (Chester, 2000).

The solubility pump is responsible for driving the transfer of CO_2 from the atmosphere to the ocean (Chester, 2000). The solubility of gases in seawater is generally a function of temperature, pressure and salinity, causing the oceanic uptake by solubility alone to be greatest when sea surface temperatures (SST) are low. Thermodynamically, the partitioning of CO_2 between atmosphere and ocean is determined by the difference in partial pressures (pCO_2) between sea and atmosphere, where a higher pCO_2 in the air will drive the flux into the water (Takahashi et al., 2009).

Phytoplanktonic primary production is the main driver of the biological pump, which is controlling the export of dissolved inorganic carbon species from the productive layer to the deep ocean and thus controlling atmospheric partial pressure of CO_2 (Volk and Hoffert, 1985) by reducing the amount of dissolved inorganic carbon (DIC) in the surface waters. The biological production is tightly coupled with remineralization and heterotrophic respiration. The difference of production and consumption in a marine community is described by the term net community production (NCP) and is restricted by irradiance and nutrient levels, which are, in turn, a function of ocean physics. Time- and depth-integrated NCP is a proxy used to estimate export production (Munro et al., 2015), i.e. the amount of organic matter produced in the ocean that is not recycled before it sinks into the deep ocean where it stays for more than thousand years. When favorable light and nutrient conditions promote the development of a phytoplankton bloom, large amounts of carbon are fixed in the surface waters (Takahashi et al., 2009). This process is an important feedback on the global climate (Raven and Falkowski, 1999), but simultaneously is the climate a driver for the phytoplankton bloom (Monteiro et al., 2011). The seasonality of physical forcings and resulting chemical as well as biological responses is complex in the SO (Takahashi et al., 2009) and up to date still bears large uncertainties in global climate models and atmosphere-water CO_2 flux estimates (Landschützer et al., 2014).

Recent studies (Resplandy et al., 2014) showed the importance of resolving the Southern Ocean at fine spacial scales to fully adhere for their share to the overall role in the global circulation and climate system. The contribution of not only seasonal but also intra-seasonal variability in productivity and thus CO_2 dynamics is an important factor when assessing future climate scenarios and the role the Southern Ocean has played in the past and will play in the future (Resplandy et al., 2014). Mesoscale (10-200km) and sub-mesoscale (<10km) variances in oceanographical phenomenons such as stratification, mixing, air-sea exchange rates driven by wind, waves and temperature, can result in biological patchiness (Mahadevan et al., 2012). Monteiro et al. (2015) showed that resolving CO_2 fluxes at very fine temporal scales is necessary to reduce the uncertainty in climate modeling to below 10%. Autonomous gliders are able to resolve and sample at these fine temporal and spacial scales and thus provide important information about processes that are not being captured by other modes of observations (Monteiro et al., 2015). This way, a variety of oceanographical and bio-optical properties of the ocean interior, as well as surface water measurements of partial pressure of CO_2 (pCO_2) in the water as well as in the overlaying atmosphere, can be obtained.

Although model results point out the importance of the Southern Ocean's role in the uptake of anthropogenic CO_2 (Landschützer et al., 2014), it is the area where the uncertainties of air-sea CO_2 fluxes and thus the carbon storage capacity are highest (Gruber et al., 2009). Model results vary between 0.15 and 0.72 Pg C yr^{-1} in Gruber et al. (2009) (the SO as carbon sink) and between -0.3 (SO as carbon source) and 0.3 Pg C yr^{-1} in Lenton et al. (2013). These uncertainties are partly due to unresolved spatiotemporal variability (Resplandy et al, 2014). Concerning the physical drivers of carbon fluxes, model results suggest warming, increased stratification and altered mixed layer depths (Boyd, 2002; Lovenduski and Ito, 2009; Moore et al., 2013 and references therein) that might decrease the uptake capacity of the Southern Ocean (Lovenduski and Ito, 2009), whereas others estimate that the HNLC regions (high nutrient low chlorophyll) will increase their productivity by lateral input of iron (Moore et al., 2013). How the biology in the ocean will react to future changes in the physical conditions is harder to estimate (Moore et al., 2013) and currently models have difficulties in giving estimations without large uncertainties (Munro et al., 2015).

While a variety of approaches based on atmospheric and ocean physics, biogeochemistry and ecosystem science are necessary to link interactions regulating CO_2 partitioning, this study will focus on the role of biological production as a driver for carbon dynamics. With altering climatic conditions, it is unknown how and to what extent ocean physics, chemistry and biology will behave and additionally, how they will influence each other. It is thus necessary to quantify the impact of each process on the carbon cycle for being able to evaluate the Southern Ocean's function as a source or sink of CO_2 under future climate warming. The role of small scale structures in the biology on the carbon budget remains one of the greatest challenges (Resplandy et al., 2014) where some studies suggest a reduction in primary production, others an increase (references in Moore et al., 2013). This study is thus aiming at looking into the response of surface water DIC on biological production and it's seasonality, as well as the physical factors controlling both. To get a better estimate of biological carbon uptake in remote and challenging regions of the polar oceans, a reliable method of transforming surface ocean glider pCO_2 measurements covering vast extends of the SO into net community production, is essential.

The Southern Ocean Carbon and Climate Observatory (SOCCO), the institute leading this SO glider experiment, is currently planning large-scale surface glider operations over vast areas of the Subantarctic Zone SAZ. At present, methods to derive NCP from DIC or TCO_2 data, as described by, for example, Merlivat et al. (2014) or Munro et al. (2015), require knowledge of vertical and horizontal gradients and assume a constant profile over depth, both which is not provided for in single surface glider experiments. The second Southern Ocean Seasonal Cycle Experiment (SOSCEx II) provides a unique dataset of two gliders coupled to sample biological data from the ocean interior and data on CO_2 dynamics at the ocean's surface and therefor the opportunity to directly link upper ocean diurnal changes in DIC concentration to biological consumption. This allows for an optimization in modeling net community production from DIC data that matches the seasonal cycle of NCP derived with chlorophyll data. The aim of my thesis is thus twofold: firstly, to compare the seasonal development as well as the magnitude of NCP and daily DIC fluxes, hypothesizing that they are of comparable magnitude and follow the same pattern the majority of the sampled time; and secondly, to assess the physical mechanisms that are driving chlorophyll dynamics and NCP fluxes, as well as daily DIC fluxes in the spring/summer season in the SAZ, hypothesizing that the daily DIC flux is underlaying the same physical controls as the chlorophyll-modeled NCP.

2 Background

2.1 Phytoplankton and marine primary production

Phytoplankton forms the base of the food web in marine pelagic systems, transforming inorganic components into new organic compounds during the process of photosynthesis. Photosynthesis, in the water as well as on land, is governed by the energy of light. The spectrum of light that can be used by the plant is the photosynthetically active radiation (PAR) at wavelength between 400 and 700 nm. With increasing amounts of light the amount of carbon that can be fixed increases linearly up to a point (P_{max}) where a maximum photosynthetic rate is reached and further increase in radiation does not increase production. In some plants a further increase in radiation can even damage the cells or proteins within and production will decrease due to photoinhibition. The slope (α) of the linear part of the photosynthesis-irradiance-curve (PI-curve) is a plant's response to light conditions that provoke physiological changes in the photosynthetic biochemistry (the light dependent reactions in the cells). It can be different between plant types and even within species individuals acclimatize according to the site where the plant is growing or respond to changing light conditions during the day. The P_{max} value of a plant is determined by environmental factors, such as nutrient availability and temperature (positive correlation). A plant can change its pigment content within the cells and thus acclimate to light conditions, which results in plants adapted to low light conditions having less chlorophyll a pigments per cell than those acclimated to high light levels (MacIntyre et al., 2002; Raven and Geider, 2003). The same accounts for nutrient limitation and low temperatures.

The abundance of phytoplankton in the open ocean is limited, most importantly by light and micronutrients. Their growth is restricted to the upper part of the ocean, the euphotic zone, where light levels are high enough to provide the algae to compensate for its respiratory losses. Here, the rate of carbon assimilation is higher than the rate of autotrophic respiration. The light level where respiratory carbon losses are exactly compensated for by assimilation is called the compensation irradiance (Ic), occurring at a specific water depth, the compensation depth

(zc).The net primary production here is zero. The compensation depth marks the bottom of the euphotic zone (euphotic depth ED).

As the incoming solar radiation is scattered, absorbed and reflected by particles in the water and also the water molecules themselves, it exponentially decreases with depth. How deep it penetrates is dependent on the amount of suspended matter in the water column. Already at a depth of 1 m 65% of the incoming radiation is absorbed (Pinet, 2006). Different types of algae and bacteria have different photosynthetic pigments that absorb different wavelength and they can package those pigments into their cells depending on depth and light conditions (Stuart et al., 1998).

Since phytoplankton is moving constantly with the water it is living in, it will, depending on the water depth, also be carried out of the euphotic zone deeper than the compensation depth. The depth until the water column is no longer evenly mixed is called the mixed layer depth (MLD). The part of the water column that is well mixed (above the MLD) will have different properties (i.e. temperature, salinity) and thus a different density than the waterbody underneath, which makes the MLD a natural barrier between the water masses.

At the critical depth (zcr), daily integrated water column gross photosynthesis is equal to integrated water column respiration in a way that the community is carrying out net production. The production is integrated over the whole water column until the mixed layer depth over day and night, including net gains and losses in C fixation. The respiration term is considering autotrophic as well as heterotrophic respiration and assumed to be constant over depth (Sverdrup, 1953). As long as phytoplankton can be transported to depth lower than the critical depth by mixing, no net growth of the plankton community can occur below it. On this assumption, Sverdrup based his "Critical Depth Hypothesis" in 1953, claiming that net phytoplankton growth can only occur if the mixing depth is shoaling above the critical depth.

Physically, phytoplankton growth is controlled by two factors. The amount of light and the supply of inorganic nutrients, in the open ocean mainly provided by the mixing of nutrient poor top and nutrient rich deep waters. These two factors are crucial for marine productivity and determine how much and which species of phytoplankton, as well as species represented at higher trophic levels, occur. In line with these two factors, two counteracting attributes can be considered of importance for a bloom: stratification, allowing algal growth in surface waters, and mixing, adding new nutrients to depleted surface waters. Provided the condition that neither light nor nutrients are limiting, phytoplankton can grow rapidly. The growth can be disproportionally large compared to losses through sinking and grazing. Picoplankton can divide at very high rates, producing 3 generations per day, and larger plankton produces 0.3 to 1 generation per day (Kaiser et al., 2005). This phenomenon, the rapid net growth of algae populations, is considered a bloom.

The amount of chlorophyll, and phytoplankton accordingly, can increase either due to increased cell devision rates (due to abiotic factors such as light intensity and nutrient availability) (Sverdrup, 1953) or due to reduced grazing pressure during food-web shifts (biotic factor) (Behrenfeld and Boss, 2014), and which factors are ultimately controlling a bloom are controversial (Behrenfeld and Boss, 2014). This rapid population increase can be seen in temperate to arctic waters in the spring (and in temperate waters once more in the autumn), when increasing solar radiation provide for thermal stratification which traps the algae in the upper water column

and hinders mixing into deep waters, i.e. raising the mixing depth. According to Sverdrup (1953), this fulfills one of the requirements for a spring bloom. Since the water is mixed deeply in the winter (due to strong winds in the winter as well as low angles of the sun, i.e. high reflectance and accordingly low incoming light levels into the water, preventing stratification), plenty of nutrients are available in the eutrophic layer. During the summer, when irradiance levels continue to be high and the thermocline stabilizes, nutrients become limiting and growth rates decrease. According to Sverdrup's critical depth hypothesis (Sverdrup, 1953) a bloom can develop as soon as the MLD shoals above the critical depth. Today, there exists a variety of alternative theories explaining the development of a bloom, incorporation explanations for appearance of a bloom earlier in the season when the Sverdrup criterion is not met (see for example Mahadevan et al., 2012; Taylor and Ferrari, 2011; Behrenfeld and Boss, 2014).

The pelagic part of the ocean is a highly dynamic and heterogeneous environment whose inhabitants are free to move in all three dimensions of the water column following their physiological limits. Heterogeneity in temperature, salinity, eddies and nutrient availability promotes different kinds of habitats with various amounts of species, biomass and productivity. These patches can change over an area, over depth and also over time. It is a central part in climate and productivity modeling to understand how the physical forcings affect the biology of the oceans. Especially phytoplankton life is subject to small-scale vertical mixing (Martin, 2003), due to being short-lived and unable of locomotion on a larger scale. Sommer et al., (2002) showed the direct positive correlation of phytoplankton production to nekton production, meaning that plankton ecology and abundance will influence the whole ecosystem. Due to physical conditions, productivity can be distributed in patches of varying ecosystems over the pelagic, and the understanding of these physical and biophysical interactions is topic of ongoing research.

2.2 Dissolved inorganic carbon

The transfer of CO_2 from the atmospheric reservoir into the ocean reservoir, its solubility and finally fate in the global ocean circulation system, is governed by three major processes: the solubility pump, physical circulation and mixing and biological uptake and remineralization. The biological incorporation can either be into soft tissue or carbonate shells, which are not further discussed in this thesis. These three factors control the partial pressure of CO_2 (pCO_2) in the surface water, and it is the gradient between this and the partial pressure of CO_2 in the overlaying atmosphere that is driving a flux.

Inorganic carbon in seawater is present as one of the following carbonate species: dissolved CO_2, carbonic acid H_2CO_3 (only a transition form), bicarbonate HCO_3^- and carbonate ion CO_3^{2-}. The proportion of species present is dependent on temperature, pressure and pH. The sum of all carbonate species is called dissolved inorganic carbon (DIC). CO_2 from the atmosphere is able to enter the oceans if the partial pressure of CO_2 between the two systems is in disequilibrium. A flux is created (FCO_2). Uptake or release of CO_2 from/to the atmosphere will result in transition between the carbonate species, specifically from carbonate ions to bicarbonate with increasing CO_2 concentrations, as they are a buffering system attempting to keep a constant pH.

The biological pump is able to remove carbon from this cycle, as phytoplankton is taking up the inorganic carbon, transform it into organic carbon via photosynthesis, and transport it out of the surface ocean into the deep waters when dying and sinking. A major proportion

of this debris is remineralized either within or underneath the mixed layer and brought back to the surface waters via upwelling or vertical mixing, where it will re-enter the cycle. Only 5-10% of the organic carbon produced in the surface water eventually gets out of this cycle and reaches the deep water (Chester, 2000).

Biotic and abiotic factors are strongly correlated and constantly evolve and influence each other. Biological production on land as well as in the water shape the chemical composition of the atmosphere and the global climate, in equal measure do atmosphere and climate shape biological production in the oceans. This can happen directly, by controlling the amount and wavelength spectra of the incoming radiation, but also indirectly, by providing heating and stratification, as well as the necessary weathering and transport processes for the distribution of minerals of terrigenous origin. Arising from great concern about the human's role in present elevated greenhouse gas concentrations in the atmosphere and resulting possible changes in global climate, is the striving for a broader understanding of interactions between physical dynamics and the oceanic biosphere.

2.3 Modelling marine primary production

Some estimates of global marine primary production rely on information gained by satellite images of plant pigments and bio-optical algorithms that detect the radiance leaving the water surface and use it to derive surface water chlorophyll concentrations (Behrenfeld et al., 2002). The information on surface water chlorophyll distribution can, together with empirically derived photosynthesis parameters, be used in models to calculate primary production (Behrenfeld et al., 2002). While remotely sensed approaches using satellite images (as used for example in Munro et al., 2015) require assumptions on the depth-distribution of phytoplankton cells (Behrenfeld et al., 2002), are autonomous diving platforms such as floats or gliders (as used in this study and for example in Thomalla et al., 2015 and Swart et al., 2014) able to take optical measurements and resolve of the upper 1000 m of the ocean's water column. These models based on optical methods are able to cover fast spatial and temporal scales (Behrenfeld et al., 2002). Others estimates of productivity are based on the difference in budgets of proxies that are consumed or produced in a constant ratio to the amount of C taken up during photosynthesis and thus allow for drawing a direct link to biological uptake (as used for example in Munro et al., 2015 and Huang et al., 2012). Lastly, some studies use the incorporation of a certain detectable marker like ^{14}C into the biomass as a measure of inorganic C uptake and productivity (this method was invented by Steemann Nielsen in 1952).

In this study, the bio-optical data sampled by the buoyancy glider was used to calculate NCP. This bio-optical, chlorophyll-based, method was compared to a budget-based approach of DIC consumption/addition during the course of a day.

2.3.1 Bio-optical measurements

Bio-optical measurements are based on resolving different wave-lengths and coupling these to empirical parameters of time- and depth-dependent changes in photosynthesis-irradiance relationships (Behrenfeld et al., 2002) to get information about plankton content and biological production. The amount of phytoplankton cells in a water body are seldom measured in a direct way. A convenient proxy for phytoplankton biomass is the quantity of Chlorophyll *a* (Chl *a*). Chlorophyll *a* is an major pigment for photosynthesis that absorbs the energy of

photons and is located in the plants thylakoid membrane. Other accessory pigments, which absorb different wavelengths, can be present and increase the ability of the phytoplankton's light absorbance (Sathyendranath et al., 1987) and thus carbon fixation. In this thesis, every time I use the expression "Chl" or "chlorophyll" I am talking about chlorophyll *a*. Since the accessory pigments are in a relatively constant ratio to Chl *a* within a taxon (Goericke and Montoya, 1998; MacInyre et al., 2002) (except during e.g. cyanobacterial blooms), the amount of Chl *a* is still a valid proxy for C fixation. Even though Chl *a* concentration is a widely accepted proxy for phytoplankton biomass, the amount of Chl *a* in a cell is subject to nutrient and irradiance levels, which are not permanently constant and might even change during a day (Marra, 1997). The chlorophyll *a* pigment is the only one that is abundant in all types of phytoplankton (Kaiser et al., 2005) and can easily be quantified by fluorescence.

The phenomenon where a photon is emitted by an electron, element or molecule during its return from an excited state to the ground state and re-emitted at a longer wavelength is called fluorescence. It can be observed in various processes in nature, one of them being light absorbed by Chlorophyll *a* in photoautotrophic cells. I included a more detailed information about the processes concerning radiation within the chlorophyll in the appendix.

Optical backscattering and fluorescence are both modes of optically measuring phytoplankton concentrations in the ocean. Fluorescence can give information about the Chlorophyll *a* concentration in the water column, which is correlated to phytoplankton abundance. A disadvantage when using this method is the appearance of non-photochemical quenching and the fact that fluorescence yield and chlorophyll packaging can change with taxa, light conditions and nutrient status (MacIntyre et al., 2002). In the SO however, chlorophyll *a* and phytoplankton biomass are well correlated (Behrenfeld et al., 2005). Optical backscattering is correlated to carbon particle concentrations in the water (Babin et al., 2003), and in the open ocean, where inorganic particles are minimum, it can provide a measure of phytoplankton carbon biomass. The advantages of this approach are that it is not subject to light dependent quenching and neither to intracellular changes in pigment concentrations (Behrenfeld and Boss, 2006).

However, the correlation of backscattering to phytoplankton carbon biomass bears uncertainties. Firstly, because of the difficulty to distinguish between C_{phyto} and other carbon particles (Eppley et al., 1992; Oubelkheir et al., 2005) and secondly, due to the variations of particulate organic carbon (POC) towards backscattering (Cetinic et al., 2012). In the Southern Ocean, both aspects bear very low uncertainties (correlation between POC und bbp has an R^2¿0.92 found by Stramski et al., 1999). Both approaches are complimenting each other, as the backscattering data can serve to correct daytime fluorescence quenching, and the ratio of both (Chl *a*: Cphyto) can give information on the chlorophyll packaging of the plankton cells.

Measuring chlorophyll fluorescence in situ has the advantage that the phytoplankton can stay in their natural surroundings and, importantly, in their natural light field, as changes in ambient light conditions can change physiological properties within the cells (MacIntyre et al., 2002). Various other optically active particles in the water column (for example CDOM, coloured dissolved organic matter) can either add or subtract light of the same wavelength into the detector, which is unavoidable. The amount of CDOM is largest in coastal and estuarine water though, but can be significant even in the open ocean during a bloom (Nelson et al., 2007), which is why a dark correction with depth between 300-400 m was applied in this study. After the chlorophyll data is obtained, it needs to be set in relation to production and respiration rates.

In this study, I used empirical equations for productivity calculations in the water column and assumptions based on the Sverdrup Hypothesis, which was explained earlier.

Respiration in the euphotic zone of the ocean plays an important role for the efficiency of the biological pump, as it counteracts biological carbon sequestration (Robinson and Williams, 2005).The respiration rates calculated with the Sverdrup model are assumed to be constant over depth. Some studies disagree and point out, that phytoplankton respiration is a function of available light (growth respiration) or light and nutrients (maintenance respiration) (Smetacek and Passow, 1990). Respiratory rates in this study are the sum of heterotrophic and autotrophic respiration. The autotrophic portion accounts for ∼50% (Siegel et al., 2002), bacterial respiration for 42 +- 10% and zooplankton 10 +- 8.5% (Robinson and Williams, 2005). Community respiration was found to be the two thirds power of photosynthesis (Del Giorgio et al., 1997) when comparing volumetric rates, so the respiration was found to be a more or less constant ratio of photosynthesis (Robinsons and Williams, 2005). If this was the case, respiration would not be constant over depth. Robinson and Williams (2005) also found that, when comparing depth integrated rates, the relationship did not show a significant correlation anymore and they argue that respiration is not necessarily an immediate response to photosynthesis, but more a transient time integrated measure of production. However, keeping in mind all these arguments against the respiration being constant over depth, to model autotrophic respiration over depth sufficient information might be available, but heterotrophic respiration and distribution over depth, even though being correlated to autotrophic respiration, is more difficult to model and would probably be a study on its own, which is why the Sverdrup approach is used.

The exact mechanisms controlling phytoplankton phenology and leading to a bloom (Smayda, 1997b), are up to today not completely understood (Lavigne et al., 2013). Some studies find evidence supporting the in 1953 by Sverdrup proclaimed condition of the depth of mixing controlling the bloom (Sverdrup, 1953), while others find disagreements with that theory and provide other possible explanations. Sverdrup's model assumes that the bloom starts if the MLD is higher than the z_{cr} in a well-mixed layer, but various recent studies report the beginning of a bloom when mixed layers are still deep (Townsend et al., 1992; Taylor and Ferrari, 2011; Ferrari et al., 2014). Nevertheless, an alternative valid and robust explanation until today still has not been found, but efforts are being made to explain the beginning of the bloom either by biological (Behrenfeld, 2010; Banse, 1992), physical (Taylor and Ferrari, 2011; Chiswell, 2011) or a combination of multiple drivers (Lindemann and St. John, 2014). Contrary to the findings by the previously named authors, there are also a lot of studies that do find agreements with Sverdrup's model. For instance Lavigne et al. (2013) found a strong coupling of the bloom towards the mixed layer depth in the Mediterranean, as did Wilson and Coles (2005) for the sub-polar latitudes reviewing satellite data and Cassar et al. (2010) comparing MLD and NCP in the SAZ.

2.3.2 Proxy-based budget approaches

Budget-based approaches rely on the dynamics of a proxy that is directly proportional to biological carbon fixation. This proxy can be a nutrient concentration (phosphate or nitrate), oxygen or carbon. In the lab, there are other experimental methods based on the uptake and incorporation of a certain proxy, like the incorporation of radioactively labeled aminoacids Leucine or Thymidine during protein synthesis (applied and described in for example in Mulholland et al., 2011). For larger scale open ocean experiments however, nutrient-, oxygen- or

carbon budgets are the ones most commonly used. Contrary to the more recently developed bio-optical methods, this approach has a historical significance (Eppley, 1989) and techniques for DIC analysis are existing since the 1980s. An advantage of this approach over experimental incubation experiments is that, like with bio-optics, the data can be taken in-situ. Furthermore, the NCP is averaged and integrated over time and the sampling-bias is smaller (Ishii et al., 1997). While Munro et al. (2015) compared the budgets between October and April to derive a seasonal budget, Ishii et al. (1997) looked at the budgets of DIC concentration between the current measurements and concentrations in the winter mixed layer. Budget data is often used as validation and for parameterization of satellite and glider derived data (Munro et al., 2015).

Budget-based approaches of DIC are based on the assumption that, after subtracting or adding the amount of C that is removed from the water via air-sea flux, the net amount of inorganic carbon that is consumed during a time period is equivalent to the net amount of organic carbon that is generated. Hence, this budget is directly showing the amount of carbon, which is nowadays the factor of highest public intrest, that is removed from surface waters or the atmosphere into the deeper oceans. Nutrient-based budget calculations first need to be converted via Redfield stochometry into carbon equivalents, which is known to vary between different taxa and different nutrient scenarios (e.g. Karl et al. 1990, Ishii et al., 1997). The exchange of C with the atmosphere can add to the uncertainies when modeling NCP from DIC data if no data on pCO_2 or air-sea fluxes is available (Ishii et al., 1997). The solubility effect for CO_2 uptake by the water can be normalized to temperature, salinity and total alkalinity by deriving a linear equation with solubility values under standard conditions and the measured values, as applied in for example Thomas (2002). Furthermore, not incorporating lateral processes, gas exchange and MLD entrainment can lead to an underestimation of the DIC budget of 35% (Munro et al., 2015), so that correctly quantifying these fluxes is essential.

When using the budgets of nutrients, Redfield (Redfield et al., 1663) stochometry is assumed, meaning that the C, N and P consumed are in constant ratio to each other as well as to the O_2 produced. Since the development of Redfields theory, newer studies have found that the stochiometry of C to nutrient ratios is not constant for all regions and taxa (references in Thomas, 2002), neither with depth (references in Thomas, 2002). This is a drawback when using budget-based approaches. Budget based approaches using the utilization of phosphate can be biased by the preferential remineralization of phosphate during summer, which could lead to an underestimation of the phosphate budget (Rubin, 2003).

Approaches based on budgets of oxygen are comparing O_2 supersaturation with Argon supersaturation. By comparison with the ratio in air saturation values information about the net community O_2 productivity, which is after being multiplied with the photosynthetic quotient (PQ) the same as NCP, can be obtained. Both Ar and O_2 have similar solubilities, but contrary to O_2, Ar is conservative regarding biological processes and can serve to correct for physical processes that can alter the O_2 concentration in the water.

Various satellite based NCP estimates observe NCP peaks in summer (Munro et al., 2015; Weeding and Trull, 2014), whereas budget based approaches generally seem to observe the peak earlier in the season in October and most of the NCP accumulation by November (Weeding and Trull, 2014; Wang et al., 2001; Munro et al., 2015), likely due to the effect of episodic entrainment in spring (Weeding and Trull, 2014; Wang et al., 2001; Munro et al., 2015). Carranza and Gille (2015) found the difference in maximum chlorophyll concentrations based on

the longitudinal location, with a peak chlorophyll concentration observed in spring north of the Antarctic Circumpolar Current.

2.4 The Southern Ocean

The Southern Ocean (SO) is the fourth largest of the world's oceans surrounding and circling eastwards around Antarctica. The circumpolar current system connects the Atlantic, Pacific and Indian Ocean and is one of the two parts in the world's ocean where deep water is formed. It has no land-masses as boundaries to the north, and therefore no clearly defined borders. The Southern Ocean has a very narrow and steep shelf area and an average depth between 4000 and 5000 m, which has implications on it's biology. It is governed by strong winds and deep mixing length scales in winter (Wang and Matear, 2001) and strong seasonality with a sea ice extend reaching further north than 60°S (Chapman and Walsh, 1993). As there are no land masses interfering with the current direction (except for peninsulas of Antarctica), there are no upwelling areas and no input of fluvial or aeolian matter. This is the reason the Southern Ocean is classified as an HNLC (High Nutrient Low Chlorophyll) region, having high concentrations of nitrogen and phosphorous but low productivity, which is due to limitation of iron. Productivity is thus limited by light the majority of the year and by iron towards the end of summer (Peloquin and Smith, 2007).

The Southern Ocean consists of several rings of frontal systems, each with distinct zones of water masses and concurring properties in-between. Wind at the water surface does not only create horizontal, but also vertical movements of water masses, depending on whether two wind directions converge or diverge. Two water bodies that meet result in sinking water masses. In the opposite case, when the wind stress is driving two water masses apart, deeper water masses move up to replace them. The surface water of the world's oceans is moving in complex patterns, and movements of convergence and divergence can take place in large oceanic gyres as well as small scale Langmuir circulations. Typically, high concentrations of biomass and high productivity can be observed along oceanic fronts, caused by the presence of two dissimilar (in temperature, salinity etc) water bodies.

Fronts can develop if two water bodies have different speeds or different directions. In the Southern Ocean, there are three major fronts with the Polar Front (PF) being furthest south, the Subantarctic Front (SAF) and the Subtropical Front (STF) to the north. The polar frontal zone (PFZ) and the subantarctic zone (SAZ) are situated between those fronts. The different physical conditions provide for competitive differentiation between the different plankton taxa, so that different dominating groups can be found in the different locations (Knox, 2007). This study is set in the SAZ, where the STF sets the boundary of warm, salty, surface waters of the South Atlantic subtropical gyre coming from the north, while the SAF sets a boundary for the colder, fresher Polar Frontal Zone water masses coming from the south. The upwelling in the Arctic Convergence, situated between the eastward flowing Antarctic Circumpolar Current (ACC) and the westward flowing Polar Current (PC) has one of the world's largest open ocean area of productivity (Brown et al., 2001).

Next to larger circulation patterns, smaller rotating eddies are altering parameters of the water (Temperature, nutrient levels). Mesoscale eddies are comparable to the weather systems in the atmosphere, they develop as small rotatory currents that move a few kilometers per day and are between 50-200 km big with a lifespan of a few month. They often develop close to frontal

currents, since those slope and are over a long term unstable (Brown et al., 2001). They are also known to cause stratification and favor bloom conditions (Mahadevan et al., 2012).

2.5 Ocean gliders

Fluctuations in the ocean have been observed not only between season and between the climatic zones, but also to considerable extend on much smaller scales. The mesoscale fluctuations include time spans of 10 and 100 days and length scales of 100 km, whereas the sub-mesoscale distinguishes even smaller scales in the range of 10 km and 1 to 10 days. Variations on small scales have been observed for circulation patterns and eddies (Le Traon, 1991; Stammer, 1997), as well as for Chl *a* fields (Gower et al., 1980). Mesoscale and submesoscale processes can contribute to enriching nutrient depleted surface waters with new nutrients, i.e. by uplifting isopycnals (eddie pumping), vertical mixing or frontal processes (Lewis, 2002). They can also be responsible for lateral movements of dissimilar water masses, creating stratification (Mahadevan et al., 2012). Understanding the dynamics and causes behind mesoscale processes is crucial for the estimation of nutrient fluxes and stratification levels and depth, necessary parameters to correctly estimate global primary production and global climate models.

Autonomous ocean gliders are able to resolve and sample at fine temporal and special scales, the mesoscale (10-200 km) as well as the submesoscale (1-10 km). This allows the glider to provide important information about processes that are not being captured by other modes of observations. As ocean gliders are more cost effective than ship based measurements and moorings, it allows the measurements to be carried out over an extended amount of time. Furthermore, gliders are able to sample more frequent and regular in both space and time than ship measurements.

The gliders are usually operating in pairs, a surface glider is sampling the surface waters in an octagonal shape of $\sim$25km^2 while a profiling glider is diving at the same spot. The gliders can be either be programmed to sample along a transect or to stay at the same location to record seasonal developments. Surface wave gliders are measuring CO_2 partial pressure in the surface waters and in the overlaying air. Ocean interior buoyancy gliders are able to dive to depth to 1000 m and sample the upper ocean physical properties between 4 to 6 times a day. The collected data of both glider types is transmitted via satellite to the database (after reaching the surface after each dive, in case of the buoyancy glider). Being equipped with battery packs and solar collectors, the gliders are able to collect data over a period of 6 month continuously, while a GPS sensor controls the sampling track. One dive cycle of the glider takes between 2.5 and 5 h (SOSCExII, this dataset and SOSCEx the previous year) to complete while it covers a horizontal distance of 2.8 km on average SOSCEx, see Swart et al., 2014 for further information).

3 Methods

For this thesis work and my time in Cape Town, raw physical data of the glider measurements was provided to me by the Southern Ocean Carbon and Climate Observatory (SOCCO). All the processing steps described below, including the programming that was necessary, was carried out by myself, the glider data from this experiment had not been worked with so far (except for the FCO_2 data)). I was not part of the glider deployment and cross calibration via ship based measurements. The methodology was partly taken from previously existing literature

and studies as referenced, and the methodology for quenching correction and daily DIC fluxes had to be invented by myself and my supervisors, as, to my knowledge, no method that would deliver reasonable results existed or was considered robust enough.

The processing of bio-optical measurements as they were sampled and provided by the ocean gliders for this experiment towards the process of biological production requires, contrary to budget-based approaches, the utilization of empirical equations that transform bio-optical data to production and respiration rates. The empirical equations by Platt et al. (1980) and Platt and Sathyendranath (1993) and the Sverdrup (1953) approach were chosen to model PP, R and NCP and the method was previously applied by for example Thomalla et al. (2015). The methodology to model NCP was taken from the previously named references, but all the calculation steps presented here and the modeling in matlab was carried out by myself. The methodology used to model diurnal changes in DIC concentrations had to be invented by myself and my supervisors, as other approaches require the utilization of data that was not available for this study.

3.1 Experimental set up and glider deployment

The glider data was obtained during the second Southern Ocean Seasonal Cycle Experiment (SOSCEx II), which took place over a 4 month period during summer 2013/14 in the Sub-Antarctic Zone of the South Atlantic Ocean, which is situated between the Sub-Antarctic and the Sub-Tropical Front.

A Liquid Robotics Wave Glider and a Profiling Buoyancy Glider were sampling simultaneously. The wave glider described a circular sampling pattern 16 km in diameter, in whose center the seaglider was diving and taking measurements about 5 times a day. The gliders were deployed on the 13th of October 2013 at 41°S, 9.5°E, approximately 1300 km southwest of Cape Town. The gliders were navigated to their permanent sampling place, which was centered at 43°S, 8.5°E, where they were sampling continuously for 83 days, from the 17th of November 2013 to the 8 February 2014 (119 days from deployment until retrieval). The Liquid Robotics Carbon Wave Glider was equipped with a surface CO_2 sensor which was modified from MAPCO2 technology (Sutton et al., 2014) and measured in situ air and sea pCO_2, as well as temperature and salinity, which are used to derive gas solubility and concentrations of dissolved inorganic carbon (DIC). The buoyancy glider measured conductivity, temperature, pressure, dissolved oxygen, optical backscattering (at 470 nm and 700 nm), fluorescence and photosynthetically active radiation (PAR) with a temporal resolution of 1.5 hours per average per profile.

Complementary to the glider measurements, ship-based Conductivity Temperature Depth (CTD) samples of salinity, dissolved oxygen, chlorophyll a, total alkalinity and other parameters were taken at deployment and retrieval sites of the gliders as calibration and quality checks of the data from the glider sensors. These CTD samples were taken as a profile over depth with one data point every meter, and simultaneously by capturing water samples in bottles, which were analyzed for chlorophyll a, dissolved oxygen and salinity on board. This way, the glider chlorophyll a data was calibrated with y=4.12x-0.21 (r^2=0.66) (see Swart et al., (2014) for detailed information about the calibration), which provides a conversion specific to the Southern Ocean instead of just the manufacturers conversion factor. The deployment and retrieval match ups of glider data and ship based data for SOSCExII were the same as in the previous

year for SOSCEx, thus calibration data and the linear regression was obtained from Swart et al. (2014). The irregularly spaced datasets were interpolated to a 6 hourly grid, from which midday and midnight profiles could be identified.

3.2 Modelling Net Community Production

Net community production was calculated using the empirical equations by Platt et al. (1980) and Platt and Sathyendranath (1993) which are mainly based on surface chlorophyll concentration and surface PAR, following the Sverdrup hypothesis (1953).For these calculations, the raw physical data sampled by the buoyancy glider needed to be transformed into biological and physical parameters. The following are the steps necessary to obtain data that was needed as input for the NCP model, which is presented afterwards. As argued in section 2.3.1, the Sverdrup Hypothesis nowadays appears controversial. I am aware that the Sverdrup critical depth model, and thus the calculations of NCP, might be flawed, but could not find strong enough evidence of the validity of any of the newer arisen theories to base this study on.

3.2.1 Physical parameters

The mixed layer depth (MLD) was set as the depth where the temperature varied more than 0.2°C from the reference temperature at 10 m after the method by de BoyerMontégut (2004).

Values of PAR were multiplied with a scaling factor to convert from V to μE cm^{-2} s^{-1} after being corrected with the instrument specific dark correction factor. An additional dark correction was conducted by subtracting the average PAR in the nighttime. Since not all PAR profiles had data points in the surface water due to wavy conditions, an exponential curve was fitted from the lowest depth of all profiles where a PAR measurement was available (5 m) to 55 m (so the top 50m of the watercolumn where measurments were available for every profile). In every midday profile this exponential fit was extrapolated from 5m depth upwards to the surface, assuming an exponential decrease of irradiance in the watercolumn. This simultaneously generated the light attenuation coefficient in the water column kd, which is needed lateron to model the decrease of biological production in the watercolumn.

3.2.2 Optical Backscattering

Optical backscattering was used to correct the fluorescence data for non photochemical quenching, which is necessary to convert fluorescence to chlorophyll. To obtain particulate backscattering data, raw digital counts measured at two wavelength, 470 nm and 700 nm, had to be converted according to Eq. (1):

$$bbp = 2\pi\chi_p[S(c - D) - \beta_{SW}] \tag{1}$$

This leaves the backscattering in unit of volts instead of digital counts. χ_p is the value of 1.1 to convert backscattering from an angle of 117 to backscattering from all directions. S is the scaling factor specific for the instrument, C are digital counts for 470 nm and 700 nm respectivly, D is the instrument specific dark counts, β_{SW} is the scattering of pure water. I applied this method after Thomalla et al. (2015) and references therin. Suspicously high values were rejected if bbp in 200 m was larger than 0.001 V. An additional dark correction was applied by subtracting the average backscatter in a depth between 300 and 400 m from all profiles. The rejection of flawed profiles resulted in gaps in the dataset. Those gaps were interpolated, over the time series as well as over the depth of the profile. In cases where more than 3 days

of data were missing (a gap of more than 12 profiles), the interpolated part was set as NaNs, because the interpolation over a long period of time might not be correct and conditions and phytoplankton abundance might change.

Particulate backscatter (bbp) is a measure of phytoplankton biomass in the open ocean (Behrenfeld and Boss, 2003) and a linear relationship between backscatter and particulate organic carbon in the open ocean was found by Stramski et al. (1999).

$$POC = 32057 * bbp + 2.6 \tag{2}$$

Eq. (2) sets the amount of particulate organic carbon (POC) in relation to the backscatter counts at either bbp 700 or bbp 470. This linear relationship was found by Thomalla et al. (2016a, manuscript submitted for publication) by a conjunction of 221 POC samples from 3 different cruises with co-located bbp measurements from the SAZ of the SO, and I used it to convert the backscattering data provided by the glider to convert to POC.

I used Eq. (3) in this study to estimate phytoplankton carbon biomass (C_{phyto}) with

$$C_{phyto} = (39418 * bbp - 13) * 0.3 \tag{3}$$

Where $32057 * bbp + 2.6$ represents the linear relationship between optical backscatter and particulate organic carbon the SAZ of the SO and 0.3 is the fraction of phytoplankton carbon of total POC (Behrenfeld and Boss, 2005). In this paper they compared different studies and found the fraction of C_{phyto} to vary between 19% and 49% in different regions of the oceans, so that 30% used here and in Thomalla et al. (2016a, manuscript submitted for publication) represents an average over different regions. The POC and C_{phyto} were calculated with the bbp 700 values (POC_{700}, $C_{phyto700}$) and also with the bbp 470 values (POC_{470}, $C_{phyto470}$).

3.2.3 Fluorescence

Glider measurements of fluorescence were used to obtain chlorophyll *a* data. The raw fluorescense measurements were freed from spikes and bad profiles via a deep mean (300-400 m) treshold of 70 rfu. The data was multiplied by the instrument's scaling factor to convert to chlorophyll units and subtracted by the instruments dark count. Additionally, subtracting the mean fluorescence value of all profiles between 300 and 400 m gave a second, for this case specific, correction. Conversion to chlorophyll was optimized by applying a linear function found and described by Swart et al. (2014), which is representative of phytoplankton properties within the Southern Ocean. Missing values in the upper meters of the water column due to instrument malfunction were replaced by adding the mean difference between the meter bins of the top 10 m to the uppermost available fluorescence value, continuing until the surface was reached.

As the occurrence of non-photochemical quenching was visible for daytime profiles in the upper water column, those profiles were quenching corrected through comparison with the nighttime chlorophyll values. Non photochemical quenching was still visible until 2 hours after sunset, so the correction was applied to profiles from sunrise to sunset plus 2 hours. Particulate organic carbon, which was derived from optical backscattering data and thus not affected by the quenching phenomenon, was multiplied from the depth where quenching started occurring to the surface upwards with a correction factor. The correction factor was derived by averaging the ratio of chlorophyll to POC between surface and MLD in the following night. In cases where MLD was not available, which was the case in the beginning of the time series at the

beginning of spring, MLD was set as 80 m, as the average depth in the following week was 82 m. In the second week of December the mixed layer was only a few, and sometimes only 1, meters deep, which does not provide for a reasonable average. In these cases (if the MLD was shallower than 10 m), MLD was set as 20 m, which is in agreement with MLD averages before and after this phase. The correction was done with the POC_{470} values, and on profiles where optical backscatter counts from 470 nm where missing, the 700 nm counts were used. In cases where neither backscattering for 700 nm nor for 470 nm was available, the chlorophyll value at the lowest quenching-affected depth was extrapolated to the surface. The depth until which fluorescence measurements were still affected by non-photochemical quenching was determined as the depth where PAR=0.08 $\mu Em^{-2}s^{-1}$, which is 4,8% of the average surface PAR. This threshold was determined empirically by minimizing the standard deviation of the difference between nighttime chlorophyll values and daytime chlorophyll values under varying depth of the starting point of the correction. The value of 0.08 $\mu Em^{-2}s^{-1}$ (800 μmol photons$^{-2}s^{-1}$) is slightly higher but in the same order of magnitude with findings from other studies, where the amount of light were non-photochemical quenching was still visible was found to be 400-500μmol photons$^{-2}s^{-1}$ (Marra, 1997), 300μmol photons$^{-2}s^{-1}$ (Perkins et al., 2006), 450 μmol photons$^{-2}s^{-1}$ (Olaizola et al., 1994) and 100 μmol photons$^{-2}s^{-1}$ (Demers et al., 1991), which is equivalent to 1.3-2.7% of mean surface PAR.

Correctly solving how to correct for daytime quenching is very important for one of the main products in this thesis, NCP, as the midday surface chlorophyll concentration is one of the most essential input parameters for the model. Hence, I included a description of the non-photochemical quenching phenomenon in the appendix, together with an uncorrected chlorophyll profile and a correlation analysis showing that daytime and nighttime values are now similar.

To obtain information about the amount of chlorophyll in the mixed layer, Chlorophyll values were integrated between the surface and MLD with the trapezoidal method. This data was used for the bloom detection methods (see the appendix).

3.2.4 Primary Production, Respiration and Net Community Production

The net production of a community (NCP) can show whether a community is net autotropic, fixing more carbon than is consumed, or heterotrophic, where respiration is exceeding production. It is defined as the autotrophic production minus the autotrophic and heterotrophic respiration within the community.

Primary production was calculated according to the empirical equations by Platt et al. (1980) and Platt and Sathyendranath (1993). Phytoplanktonic primary production can be derived from two variables, irradiance and autotrophic biomass (pigment concentration) and varies as a function of two photosynthesis parameters. In the surface waters, Primary Production (PP_0) can thus be described with these two parameters as a function of available light (Eq. 4).

$$PP_0 = P_{max} * (1 - e^{-\alpha I_0^m / P_{max}}) \tag{4}$$

I_0^m is the daily PAR at the surface of the water column. The PAR data derived from the glider are midday values. As the results of PP, R and NCP are supposed to be expressed as a rate over the whole day and not only in the middle of the day where PAR values are highest, a time factor needed to be incorporated into the equation. Midday PAR was extrapolated for

the remaining part of the day by assuming a sinusoidal increase and decrease of radiation from midday towards sunset and sunrise, where PAR was assumed to be zero (as suggested in Evans and Parslow (1985)). This way, midday PAR was integrated over the daylength ([hours]) from sunrise over the peak at midday to sunset. The parameter α ([(mgC / m^3)/(μE / m^2 s)]) represents the slope of the Production-Irradiance curve (PI curve) near the origin (initial slope) and the second parameter, P_{max} ([mgC / m^3]), is the assimilation number, which is the production rate at optimal light intensity (Platt et al., 1980). Power law regression functions gave the relationship between P_{max} and chlorophyll concentration (Chl) (Pmax=0.8183$*$Chl^0.8615 R^2: 0.83) and α and chlorophyll (alpha=0.0222$*$Chl^0.7971 R^2: 0.76) (Thomalla et al., 2016b, manuscript submitted for publication). These functions were obtained through various measurements of PI-curve incubation experiments in the Southern Ocean and the derived functions are a compilation by Thomalla et al. (2016b, manuscript submitted for publication) of studies by Dower and Lucas, (1993), Hiscock, (2004) and data from their study. All experiments are set in the Southern Ocean and in the spring/summer period, thus incorporating factors that might play an influencing role in phytoplankton assimilation rate, such as temperature and nutrient status, specific for the Southern Ocean and the season. As previously mentioned, the SO is highly variable which makes a generalization of phytoplankton specific parameters difficult, but this study (Thomalla et al., 2016b, manuscript submitted for publication) makes an effort to incorporate all data on PI curve experiments that is available for the area up to date, and I used their equations for my calculations.

The ratio between P_{max} and α is the light adaptation parameter (Ik) and was calculated according to Eq. (5):

$$Ik = \frac{P_{max}}{\alpha} \tag{5}$$

Eq. (5) was used to normalize the surface irradiance. We now got the normalized daily surface irradiance (I_*^m) (Eq. 6):

$$I_*^m = \frac{I_0^m}{I_k} \tag{6}$$

The production within the watercolumn will be a function of this dimensionless factor, as it contains information about the shape of the PI curve.

The solution of this dimensionless function I_*^m was found by Platt et al.,1980 and accounts for the variability in primary production contributed by the forcing parameters (Eq. 7). The values of the analytic solution were tabulated by Platt and Sathyhendranath (1993) (for the range 0,2$<f(I_*^m)<$20, see their table A1)

$$f(I^*m) = 0.7576 ln I_*^m + 0.5256 \tag{7}$$

As production is dependent on the amount of PAR, it will decrease with decreasing levels of irradiance and increasing depth in the watercolumn. It can be described as the fraction of the initial production at the water surface, whos irradiance (within $f(I_*^m)$) is reduced by the light attenuation coefficient (kd). I thus calculated the decrease over the water depth with (Eq. 8):

$$PP_{wc} = PP_0 * \frac{f(I_*^m)}{kd} \tag{8}$$

PP_{wc} ([mg C m^{-2} d^{-1}]) is the production integrated over the whole watercolumn.

The production within the mixed layer (PP_{mld}) was determined by calculating Eq. (1) (I0,Istarm,fIstarm) for the irradiance and thus production at the depth of the MLD. The production was then integrated from the mixed layer depth to the bottom and subsequently subtracted from PP_{wc} (Eq. 9).

$$PP_{mldintegr} = PP_{wc} - PP_{mld} \tag{9}$$

The calculation of primary production is possible with the knowledge of incoming PAR and its attenuation in the watercolumn, surface chlorophyll concentration and photosynthesis-irradiance parameters. Community respiration on the other hand, necessary to derive net community production, is harder to obtain since the heterotrophic respiration can not be directly derived from autotrophic production. Solving the Sverdrup critical depth model (Sverdrup, 1953) will allow to set respiration equal to production at the compensation depth (see detailed explanation of the hypothesis in the background 2.1). The determination of the compensation depth requires knowledge about the date of bloom initiation, as, according to Sverdrup's hypothesis, it is the day when the MLD has the same depth as the compensation depth where production and respiration are equal. Bloom initiation dates were calculated using 8 different approaches, and the date that produced an NCP identical with the mean NCP of all dates (the 8th of November) was chosen as the "final" bloom initiation date. A detailed description of the bloom initiation date detection methods and their results can be found in the appendix.

The Irradiance decreasing exponentially within the watercolumn was calculated as (Eq. 10):

$$I(z) = I_0 * e^{-kdz} \tag{10}$$

$I(z)$ is the irradiance at a certain depth z, I_0 is the surface irradiance and kd is the light attenuation coefficient. Since a linear relationship between production and PAR can be assumed at the beginning of the bloom (Sverdrup, 1953; Platt et al., 1990), PP at depth z ($PP(z)$) was calculated as

$$PP(z) = \alpha I(z) = \alpha I_0 e^{-kdz} = PP_0 e^{-kdz} \tag{11}$$

Eq. (11) describes the exponential decease of PP with depth. Respiration in an aquatic community on the other hand, is according to Sverdrup's hypothesis not dependent on depth and light and is assumed to remain constant throughout the watercolumn (Sverdrup, 1953), so I calculated it as (Eq. 12):

$$R(z) = R_0 \tag{12}$$

$R(z)$ is the respiration at depth z and is equal to the respiration at the surface (R_0).

The compensation depth zc is the depth where production equals respiration (Eq. 13).

$$R_0 = PP_0 e^{-kdzc} \tag{13}$$

A certain level of irradiance at the compensation depth is needed to provide for this condition, this irradiance level is called the compensation irradiance Ic (Eq. 14).

$$I_c = I_0 e^{-kdzc} \tag{14}$$

So with rearranging Eq. (13), I_c can as well be written as Eq. (15):

$$Ic = \frac{I_0 * R_0}{PP_0} \tag{15}$$

To calculate net community production, the values of production and respiration within the mixed layer depth are essential, because the equations and assumptions are based on a thoroughly mixed water column. The primary production integrated over the MLD (PP_{MLD}) was derived from Eq. (16):

$$PP_{MLD} = PP_0 \int_0^z e^{-kdz} \mathrm{d}z = \frac{PP_0}{kd}(1 - e^{-kdz_{MLD}}) \tag{16}$$

where z is z_{MLD}. The mixed layer integrated respiration (R_{MLD}) I calculated with Eq. (17) (as respiration is assumed to be constant over depth):

$$R_{MLD} = R_0 \int_0^z \mathrm{d}z = R_0 z_{MLD} \tag{17}$$

Sverdrup's assumption is that on the day the spring bloom starts, the critical depth (where integrated production = integrated respiration) is equal to the mixed layer depth. Which means on the day identified as the start of the bloom, we can use the MLD as zcr, which also means that PP_{mld}=PP_{zcr}=R_{zcr}=R_0 (as R is constant over the watercolumn) and I rearranged Eq.(16) to Eq. (18):

$$\frac{R_0}{PP_0} = \frac{1}{kdz_{cr}}(1 - e^{-kdz_{cr}}) \tag{18}$$

To calculate respiration, I needed the compensation irradiance. Combining Eq.(15) and Eq.(18) we can calculate I_c ([μE cm^{-2} s^{-1}]) with Eq. (19):

$$I_c = I_0 * \frac{1 - e^{-kdz_{cr}}}{kdz_{cr}} \tag{19}$$

Now all the variables are available to solve Eq. (13) and Eq. (15) to calculate R_0 (Eq. 20).

$$R_0 = \frac{I_c PP_0}{I_0} \tag{20}$$

and Eq.(17) to calculated MLD integrated respiration accordingly. Respiration was now calculated for the whole time series under the assumption that the compensation irradiance stays constant over the sampling time.

As in Eq.(16) and Eq.(17) mixed layer integrated production and respiration are now defined. I calculated net community production (NCP) as the difference of both:

$$NCP = PP_{MLD} - R_{MLD} \tag{21}$$

The error going into the calculations of NCP is difficult to quantify, as only one single data value is available per time step. The error going into the calculations due to instrument and sensor specific uncertainties is considered neglectable compared to the magnitude of NCP.

3.3 Modelling diurnal changes in surface water DIC concentrations

To calculate the changes in the carbon content of the surface water occuring over the course of a day that are controlled by biological processes, surface water DIC concentrations as well as data or proxies on carbon fluxes in and out of the sampling area are needed. For these calculations, the raw physical data sampled by the surface wave glider needed to be transformed into DIC concentrations. In the following, I present the steps that are necessary to convert the glider data into DIC concentrations and afterwards the steps necessary to derive DIC fluxes over a day. Those are then comparable and in the same unit as the NCP calculated with the method presented previously.

3.3.1 Dissolved Inorganic Carbon

Wave glider measurements of surface temperature (SST) and surface salinity (SSS) were used to calculate total alkalinity (TA) of the surface waters. The calculation was performed after the equation by Lee et al. (2006), which is an empirically derived relationship between SST, SSS and TA specific from measurements and samples taken at different latitudes and ocean basins. The following which was used in this study (Eq. 22) is specific for the Southern Ocean (30°S-70°S) and a SSS range between 33 – 36 and SSTs of below 20°C:

$$TA = 2305 + 52.48 * (SSS - 35) + 2.85 * (SSS - 35)^2$$
$$-0.49 * (SST - 20) + 0.086 * (SST - 20)^2 \quad (22)$$

The values derived from the polynomial equation by Lee et al. (2006) were validated with ship based measurements of temperature, salinity and alkalinity.

DIC concentrations in the surface waters were calculated with total alkalinity and pCO_2 values in the surface water. Dissolved inorganic carbon is defined as the sum of all carbonate species in the water (Eq. 23):

$$DIC = [CO_2]_{aq} + [H_2CO_3] + [HCO_2-] + [CO_3^{2-}] \quad (23)$$

H_2CO_3 and CO_2aq are usually combined as CO_2aq is three orders of magnitude bigger.

The concentration of CO_2 in solution can be derived from measurements of the partial pressure of CO_2 in the water. pCO_2 is defined as the partial pressure CO_2 in the water would have if it was in equilibrium with the overlaying gas phase. With measurements of temperature (T) and pressure (p) (partial pressure of CO_2 in this case) from the surface glider, the amount of CO_2 per volume can be derived according to the ideal gas law

$$pV = nRT \quad (24)$$

where R is the universal gas constant. To have all variables in Eq. (23) in the same unit, Eq. (24) is multiplied with the density of seawater and the concentration of CO_2 in the water can be calculated with Eq. (25):

$$[CO_2] = \frac{pCO_2}{R * T} * 1.025 \quad (25)$$

The remaining terms in the equation are captured by the term of the total alkalinity, which is the sum of all concentrations of the ion-species that accept protons. In seawater these are $TA = [HCO_2-] + [CO_3^{2-}] + [B(OH)_4-]$+other weak acid ions. The contribution of borate to the total alkalinity is 4% and other ions are neglectable, which allows the assumption that TA consists of mostly carbonate species.

3.3.2 Daily DIC fluxes

The concentration of DIC in a certain part of the ocean is driven by fluxes in and out of this area by different processes. These are vertical Ekman transport, MLD entertainment and loss, horizontal diffusion, air-sea CO_2 exchange and biological production and respiration. As it is the aim of this study to identify biological drawdown of DIC, all the other factors need to be measured or estimated.

Scatterometer winds were obtained from (http://podaac.jpl.nasa.gov) to derive gas exchange rates. CO_2 fluxes were then calculated according to Nightingale et al., 2000.

The DIC entrainment term through deepening of the MLD is difficult to quantify without direct measurements and might contribute a large proportion of DIC to the above-MLD stock (Munro et al., 2015). The episodic entrainment term is especially large in spring (Munro et al., 2015). Vertical mixing can be responsible for bringing deep water masses enriched in DIC into the surface water within just a few days (Merlivat et al., 2005). To reduce the impact of entrainment and advection, the signal from entrainment is removed by normalizing the DIC to a fixed salinity. The same approach was used by for example (Granfors et al., 2013), who normalized volatile organic compounds and chlorophyll *a* in melted sea ice water and brine to seawater salinity with an equivalent to Eq.x to find the proportion of volatile organic compounds and chlorophyll *a* that is formed by biological production in the sea ice. Entrainment and advection are physical processes which have a signature in the salinity (Johnson and Lyman, 2015), the salinity itself is independent from biological processes. The salinity normalized DIC concentration is calculated as

$$\text{normalisedDIC} = \frac{\text{surf.DIC}}{\text{surf.salinity}} * \text{meansurf.salinity} \tag{26}$$

Afterwards, the air-sea exchange of CO_2 is subtracted from the normalized DIC.

To derive a DIC consumption/ production rate over a day, the difference between the average DIC concentration measurements from sunset -3 h and sunrise +3 h was calculated.

The observed changes in DIC in-between days might be caused by entrainment from MLD deepening, lateral advection, air-sea exchange carbonate production/ dissolution and biological production/ respiration. By looking at the changes in DIC concentrations between the morning and the evening with ∼6 h in between, the main part of MLD entrainment should be excluded, assuming that most mixing takes part in the night when thermal stratification decreases. Generally, the input of heat from the sun causes the MLD to shoal and stabilize during the daytime, while during the nighttime cooling and increased winds cause it to deepen and MLD entrainment is largest (Woods, 1980). This way, and by normalizing to salinity and subtracting air-sea exchange, the changes of DIC concentrations during the day are assumed to be mainly caused by biological drawdown.

Solely the surface water DIC concentrations are provided by the glider measurements. However, for being able to compare DIC fluxes to ED integrated NCP, a vertical profile of DIC concentrations and fluxes has to be integrated. As neither direct nor proxy data is available, assumptions about the depth distribution of DIC fluxes have to be made. The DIC flux was integrated over the euphotic depth assuming an exponential decrease with the same attenuation coefficient that was used in Eq.x in the NCP calculations. The assumption is that if firstly, the biological production decreases exponentially with depth (Kaiser et al., 2005), secondly, normalizing with the salinity removes the lateral input (Johnson and Lyman, 2015) and thirdly, only calculating the flux during the daytime is excluding the majority of MLD entrainment (Woods, 1980), between sunrise and sunset the DIC concentration is only changed by air-sea exchange and biological production. Hence, after subtracting the air-sea flux, the DIC flux should also exponentially decrease with depth, in the same way biological production does. Studies investigating vertical profiles of DIC concentrations have found different results, showing (Beaupre and Aluwihare 2010) or calculating with (Merlivat et al., 2014) constant concentrations over depth, while other

found increasing concentrations (Grifith et al., 2012; Dore, 2009) over the upper few hundred meters of the water column. The approach of calculating decreasing DIC fluxes over depth in the same way that production decreases is, to my knowledge, a new approach that was suggested by my supervisors.

The usage of the just mentioned methodological assumptions brings errors into the calculations of the DIC fluxes. However, how much error exactly each of the assumptions, for example the salinity normalization, is adding is considered as impossible to quantify at the current state of the project, as a whole new experiment would have to be carried out, which would be beyond the scope of this thesis project. The quantification of the error of these assumptions could improve the interpretation of the results and be helpful when discussing and comnparing the DIC flux and NCP time series, as the here presented values of DIC fluxes might not be the true value but more so vary within a range of values depending on the error.

A 7 day running mean filter was applied to smooth the time series and allow for detecting trends that can be compared to the NCP timeseries instead of daily fluctuations.

3.4 Analysis of the factors influencing NCP and DIC

To study which factors are influencing the biological production rates and the daily changes in DIC and to see whether the same drivers are controlling both fluxes, single variable linear regressions with a least square fit were carried out. The coefficient of determination (R^2) and p value of the regression assuming normal distribution were determined. Factors considered as being of importance are mixed layer depth, surface Temperature, net heat flux, surface wind stress, surface PAR, daily change in MLD.

Wind data was derived via SeaWinds (Zhang et al., 2006, ftp://eclipse.ncdc. noaa.gov/pub/seawinds/), which is a combination of different sea surface wind measurements by satellite radiometers and scatterometers. The data is gridded at 6 hourly time steps and 0.25° spatial resolution and was collocated with the gilder sampling area. Windspeed was converted to windstress with the method of Large and Pond (1981).

Heat flux data was derived from the NCEP/DOE AMIP-II Reanalysis-2 model at 6 hourly temporal resolution and collocated with the glider sampling area. The net heat flux (Qnet) is the downwards heat flux minus the (net upwards + latent + sensible heat flux).

To smooth the time series and allow for interpreting trends without small scale daily fluctuations, and to incorporate appropriate response times, 3 day or 5 day running averages were applied. Whether a 3 day or 5 day running mean was used for the correlation analysis is reasoned in the discussion part 5.4.1. All correlation analyses were carried out with both the running mean data as well as the the actual data. As, firstly, the correlation coefficients were generally lower with the actual data and, secondly, it was furthermore reasoned that applying a running mean for the correlation is more reasonable due to the time lag between cause and response (see Discussion part 5.4.1), results from the running mean data is presented in the results part.

The MLD was considered as a main controlling factor for NCP (as found by i.e. Huang et al., 2012), so that the NCP was divided into a fraction controlled by MLD, and the remaining

fraction (residual NCP) which is controlled by other processes. This way, the variation and effect the MLD causes on NCP is removed and the variations caused by the remaining factors can be addressed. Otherwise it would be difficult to separate the parameters and to determine which of the influencing factors is actually driving the variability. A residual analysis is a common way to remove the essential part of the variation of the dependent variable and assess the remaining variation by plotting the residual against other variables. It has been used in a variety of studies, for example by de la Fuente et al. (2014) to remove the effect of salinity and temperature to find the effect of biological activity on apparent oxygen utilization and humic-like fluorescent dissolved organic matter. A linear regression function was derived from the correlation of MLD and NCP datapoints, and the residual NCP was determined by subtracting an NCP calculated with the regression equation from the actual NCP. This residual NCP is concluded to be influenced by other factors than the MLD and contains the influences of other controlling properties like for example temperature and light that are not caused by the MLD. The residual NCP is thus used for further correlation analysis with the remaining physical factors.

In the same way, a residual DIC was calculated by subtracting a DIC flux derived from a linear regression equation of NCP and DIC from the actual DIC flux. This way, the variability and control on the daily DIC fluxes that is caused through autotrophic production and respiration is subtracted from the data and it can be analyzed whether the remaining part shows any correlation or particular pattern to any other possible drivers like for example wind. The residual DIC is the fraction of the DIC flux that is assumed to be influenced by other factors than the biology. Correlation analysis were used to test the influence of physical factors on the daily DIC flux.

4 Results

4.1 The seasonal development of NCP

4.1.1 Chlorophyll *a* and C_{phyto}

Chlorophyll concentration in the water column was one of the main input variables for the model used in this study to calculate NCP. The changes in chlorophyll concentration and phytoplankton carbon biomass are both responding to and reflecting biological production (with limitations, discussed in 5.1.1) and are suitable to visualize the seasonal development of the phytoplankton abundance.

The seasonal development of Chlorophyll *a* in the upper ocean showed a clear maximum of Chlorophyll in early summer (end of November until end of January) (Fig. 1). This maximum could also be seen in the phytoplankton C biomass. Before this phase, in spring, Chl*a* concentrations showed a more temporarily heterogenous pattern, where multiple short-lived patchy mini-blooms were present.

In the beginning of the time series, phases with higher ($\sim$0.5 mg m^{-3}) and lower ($\sim$0.15 mg m^{-3}) Chlorophyll concentrations were alternating. In the end of October, the beginning of November and the middle of November there were three events with a duration of about 3 days each, where the amount of Chlorophyll appeared to be slightly elevated (>0.6 mg m^{-3}) compared to the days before and after ($\sim$0.2-0.3 mg m^{-3}). In the end of October and the

beginning of November, the Chl concentrations were higher just underneath the MLD between 20-40 m than above. Chlorophyll concentrations in the surface waters above the MLD declined after the middle of November, but continued to be high below a depth of 60m for another 10 days. The patchy alternating pattern that was occurring until the middle of November could also be seen in the C_{phyto} data (<20 mg m^{-3} and patches with up to 40 mg m^{-3}), although not as promoted. Only in the end of October the C_{phyto} seemed to have higher values below the MLD than above (below: >35 mg m^{-3}, above: ∼22 mg m^{-3}). Chlorophyll concentrations started rising on the 25th of November to values of ∼0.5 mg m^{-3} and stay at these levels for one week, until Chlorophyll values reached their phase of maximum concentrations. This phase with Chl levels between 0.5 and 3 mg m^{-3} (∼1 mg m^{-3} on average) lasted for 3 weeks, until they sunk again to <0.4 mg m^{-3}. During the following 2 weeks chlorophyll values were slightly higher below the MLD (∼40 m) (0.4-0.5 mg m^{-3}) than above (0.2-0.3 mg m^{-3}).

The time series of C_{phyto} values showed a similar pattern, with a range between 15 to 180 mg m^{-3} and an average of ∼30 mg m^{-3} for the peak period and concentrations of <15 mg m^{-3} afterwards (Fig. 1). Chl *a* concentrations started increasing again at the 4th of January, and they increased to higher values underneath the MLD than below. The situation remained like this until the end of the time series with values of ∼0.3-0.4 mg m^{-3} above the MLD and ∼0.5-0.6 mg m^{-3} underneath. The pattern of phytoplankton carbon biomass after the peak period looked different than the Chl *a* pattern. Firstly, a phase of elevated C concentration (∼20 mg m^{-3}) between the 30th of December and the 4th of January in a depth between 80 and 120 m became visible, which was not seen in the Chl data. After this, the C_{phyto} concentrations showed a more vertical homogenous pattern. Values of C_{phyto} were constant over the depth of the watercolumn with an exception between the 23rd and 25th of January, where the concentration was 10-15 mg m^{-3}above and 25 mg m^{-3} below the MLD.

Regarding the ratio of Chl *a* to Cphyto there were fairly constant ratios (<0.03) over the whole time series, with two exceptions between the 6th and 13th of January and between the 22nd of January until the end of the time series on the 9th of February (Fig. 1). During these two events, chlorophyll concentrations were in a higher relative proportion to phytoplankton carbon biomass (average: 0.1) than during the rest of the time, where the Chl:C_{phyto} ratio was mostly around 0.02.

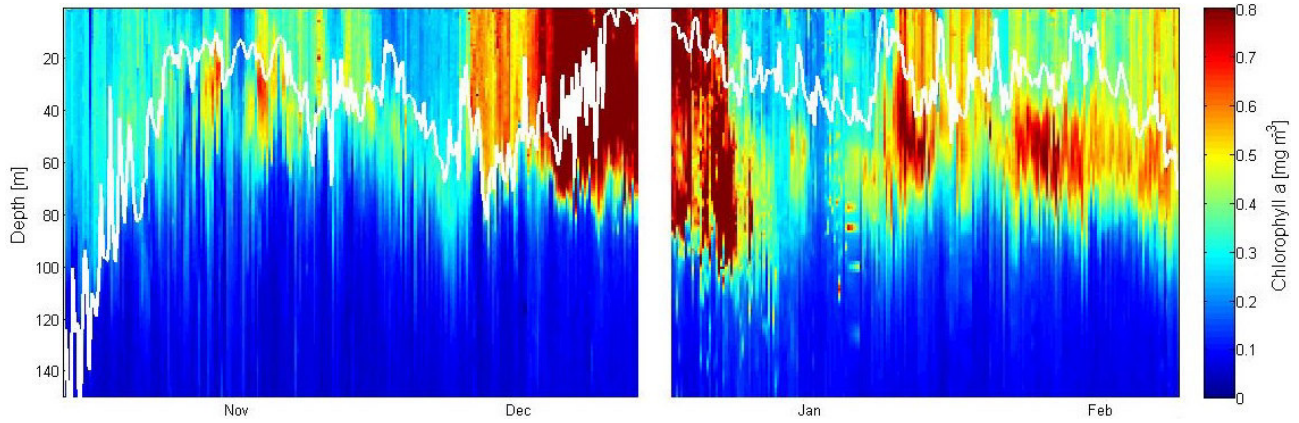

(a)

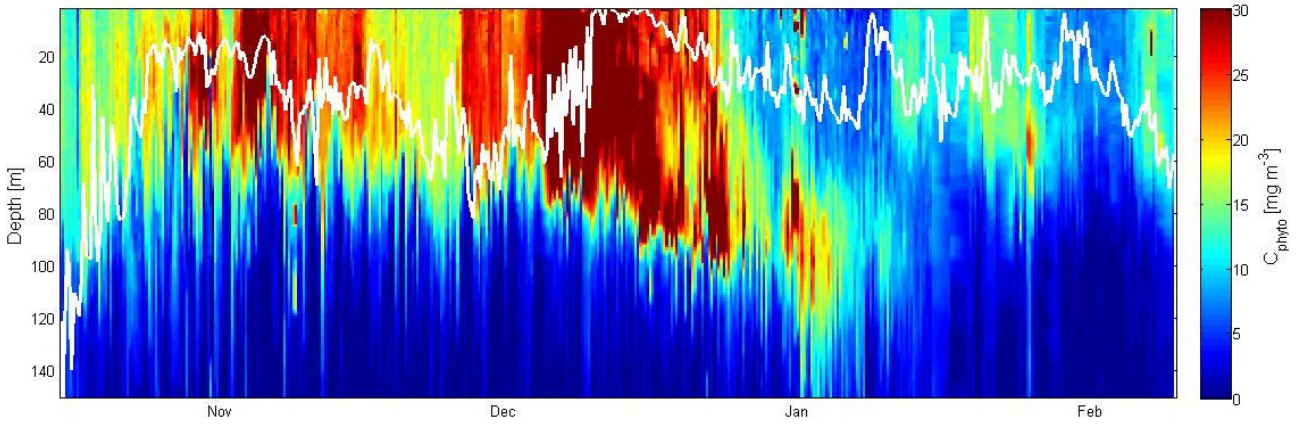

(b)

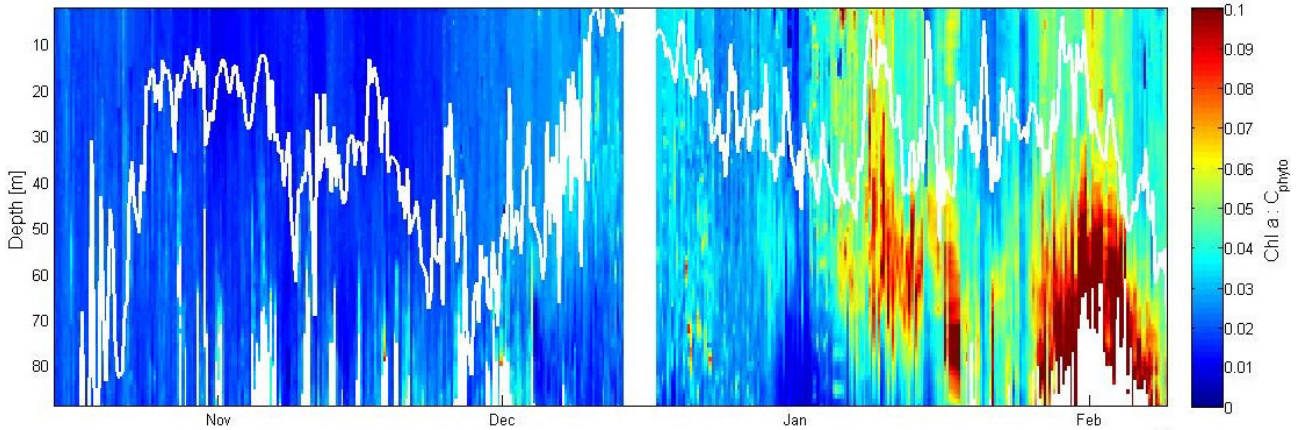

(c)

Figure 1: Concentrations of Chl *a* (a), phytoplankton carbon biomass (C_{phyto}) (b) and the ratio of Chl:C in the upper ocean over the sampling period. The MLD is plotted on top (white line)

4.1.2 Primary Production, Respiration and Net Community Production

Production, respiration and net community production were calculated for the water surface and integrated over two depths, the mixed layer depth and the euphotic depth. The mixed layer is the part of the watercolumn that is evenly mixed, and the euphotic depth is depth of the lowest light limit until which photosynthesis is still possible (1% of surface PAR).

Mixing depths were very shallow at the beginning of December, and integration over the MLD resulted in very small integrated production and respiration rates (see Fig. 23 in the appendix). Thus, I will present the ED integrated results of PP, R and NCP here and discuss this choice in section 5.1.2. Due to lack in backscattering data from both wavelength over a time period that was thought to be too long for interpolation, no chlorophyll data, and thus no PP, R and NCP, was available between the 14th – 16th of December.

The ED integrated PP varied between ∼80 mg m^{-2} d^{-1} in the beginning of the time series and over 500 mg m^{-2} d^{-1} at the peak of the productive season (Fig. 2). Biological production rates were low (between 81 mg m^{-2} d^{-1} and 243 mg m^{-2} d^{-1}, average: 152 mg m^{-2} d^{-1}) until the 24th of November, when PP values started increasing until the peak at the 12th of December (538 mg m^{-2} d^{-1}). The production stayed at these high rates (356 mgm^{-2} d^{-1} on average) for about 1 month in total (24th November until 22nd of December). After this time period, PP fluctuated for the rest of the season with 271 mg m^{-2} d^{-1} on average.

The ED integrated respiration calculated with bloom initiation date on the 8th of November did not show a seasonal pattern as the PP did (Fig. 2). R values fluctuated between ∼30 mgm^{-2} d^{-1} and 566 mg m^{-2} d^{-1} over the entire season, although fluctuations appeared to be of lower magnitude between the 17th of November and the 1st of January, which covers the period of highest production. The average R over the whole time series was 129 mg m^{-2} d^{-1}.

The NCP, as the difference of PP and R, followed the same season pattern as PP but with larger fluctuations, which coincided with the fluctuations in respiration rates. The beginning of the time series is defined by a period where NCP fluctuated above and below zero between -485 mg m^{-2} d^{-1} and ∼130 mg m^{-2} d^{-1} with 13 mg m^{-2} d^{-1} on average (Fig. 2). After the 17th of November NCP stayed positive until the end of the production peak. This first period of fluctuation NCP above and below zero generated an integrated production of the community of 527 mg m^{-2} until the 24th of November, from where on NCP started increasing. From the 25th of November NCP values started increasing to a maximum of 390 mg m^{-2} d^{-1} on the 20th of December, after which community production rates were decreasing again. During this peak period that lasted for almost a month (25th of November until 20th of December), the community generated a net of 5500 mg m^{-2}. From the 21st of December onwards, NCP values were highly variable again with fluctuations to negative values (between mg -268m^{-2} d^{-1} and 319 mgm^{-2} d^{-1}), but with a higher average (150 mg m^{-2} d^{-1}) than the period in the beginning of the time series before the production peak. The net production during this time (∼1.5 month) was 7600 mg m^{-2}. The overall NCP integrated over the whole time series between the 13h of October until the 9th of February (120 days) was 1.37 $*10^4$ mg m^{-2} and the average was 118 mg m^{-2} d^{-1}.

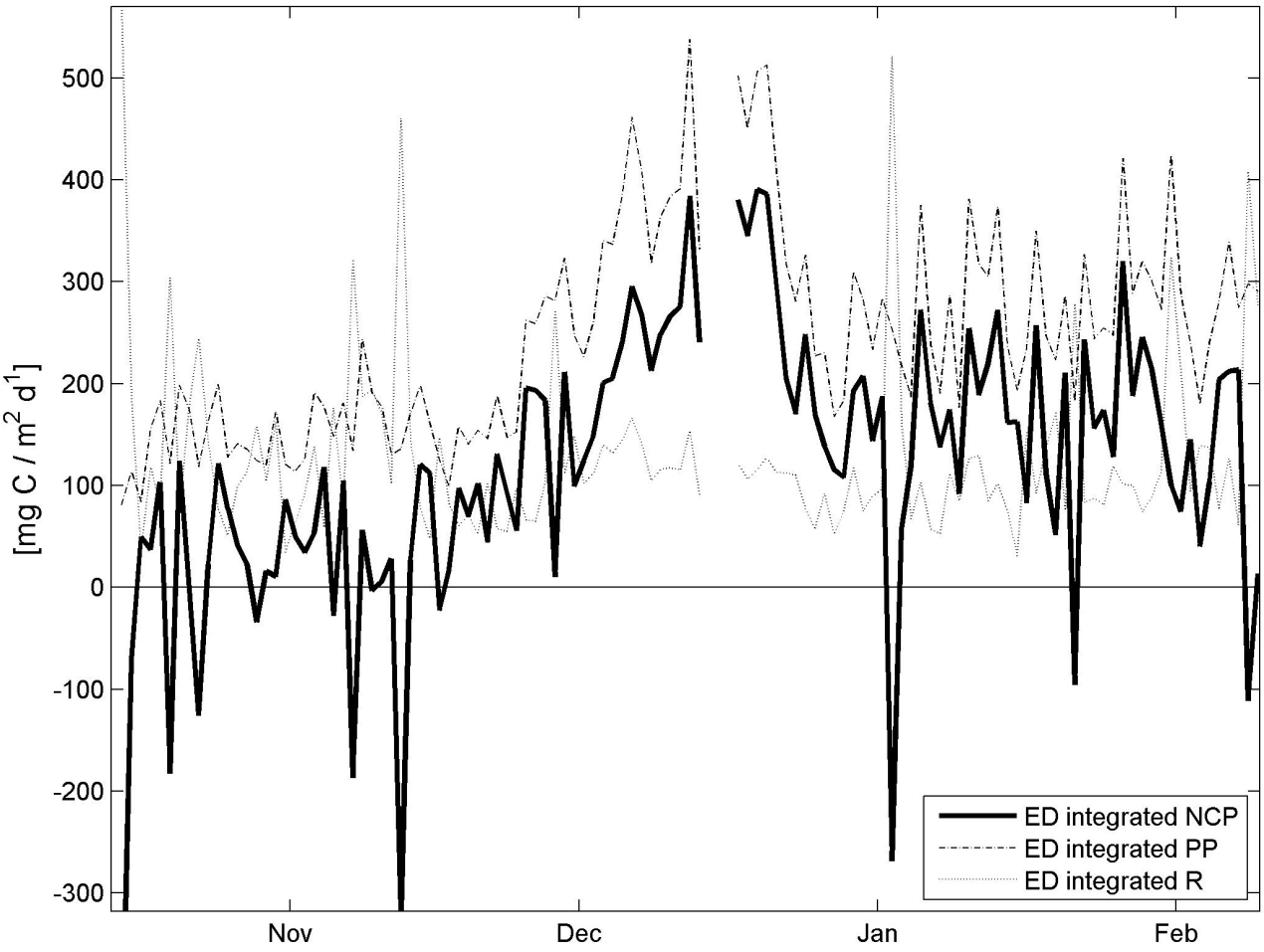

Figure 2: Seasonal development of euphotic depth integrated primary production (PP) (dotted line), respiration (R) (grey line) and net community production (NCP) (black line) modeled with chlorophyll data

The magnitude of NCP is dependent on the date that is chosen as the start of the phytoplankton spring bloom (Fig. 3). It can vary significantly between the dates suggested by the different bloom initiation methods (see appendix), which should be kept in mind when comparing the NCP to the DIC flux lateron.

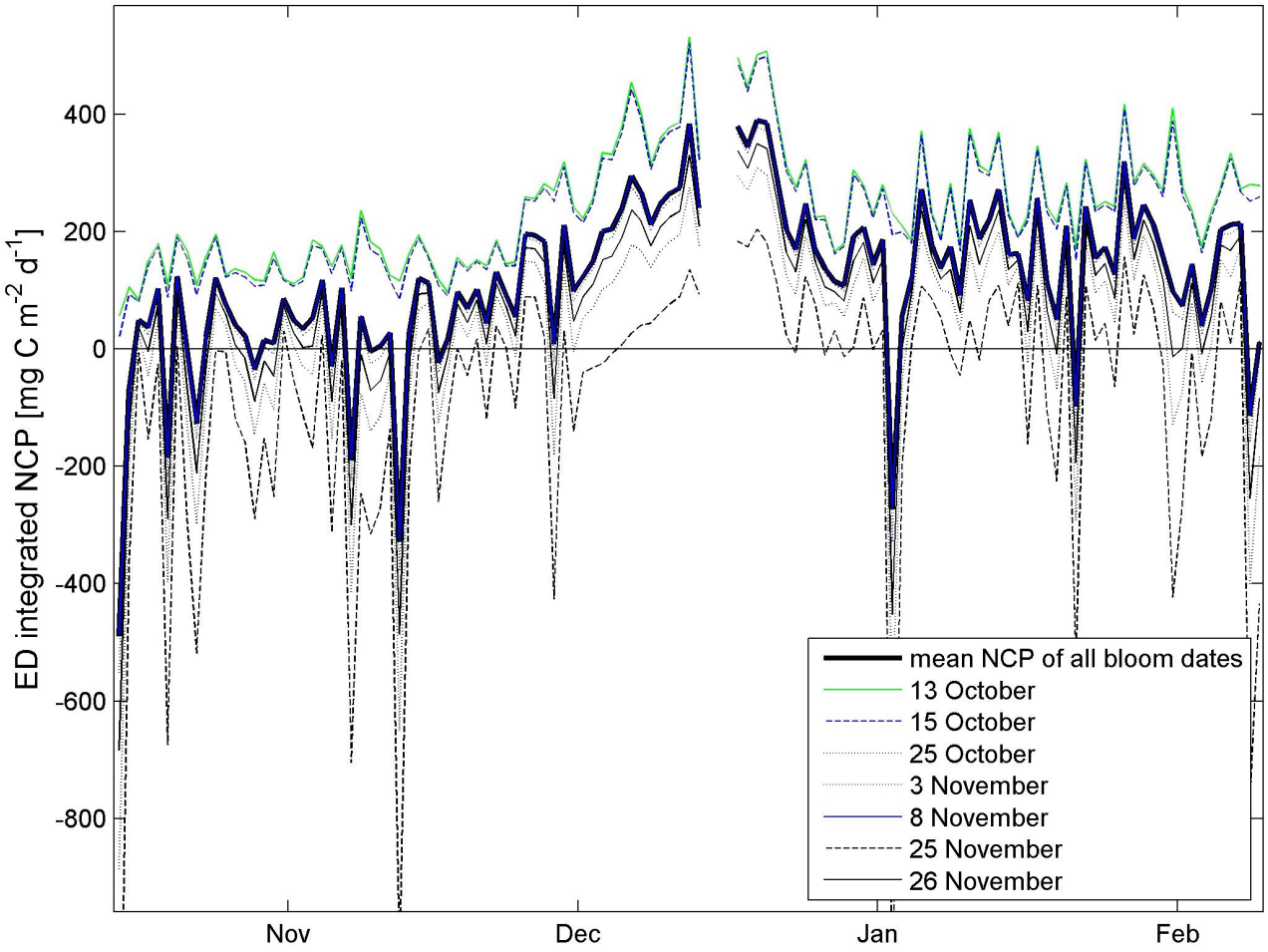

Figure 3: Seasonal development of euphotic depth integrated net community production (NCP) modeled with the 7 different bloom initiation dates found by the 8 different calculation approaches. The mean NCP of all dates (thick black line) is identical with the NCP calculated with the bloom initiation date set to the 8th of November

4.2 The seasonal development of daily DIC fluxes

The DIC concentration in the surface water is responding to different drawback and replenishment mechanisms and shows how the amount of carbon dissolved in the ocean changes over the season. The air-sea CO_2 flux is showing whether, or when, the ocean is releasing or taking up CO_2 from the atmosphere. Both parameters were used in this study to derive daily changes in DIC concentrations but are, by themselves, not controlled by the biology alone. Nevertheless, showing their seasonal pattern here helps to visualize and understand the Southern Ocean's carbon uptake and exchange capacity, as well as to a small extend the magnitude of the daily DIC fluxes.

Looking at the time series of DIC concentrations, it can be seen that there was a big drop in the first half of December from $2.47*10^4$ to $2.42*10^4$ mmol m^{-3} (average of these datapoints), which slightly increased again after two weeks (Fig. 4). From the last week of October until the middle of November the variability in-between the data points was especially high (the maximum is 248 mmol m^{-3}, whereas the maximum difference during the rest of the time was 92 mmol m^{-3}).

The air-sea CO_2 flux data (FCO_2) showed that the majority of the time there was a flux of CO_2 into the ocean (Fig. 4). Only over shorter time periods was the flux going out of the water (last week of October until November, last week of January until February) or was around zero (2nd and 3rd week of November, 2nd week of December, 1st week of January).

The daily DIC fluxes mainly showed a high daily variability, which is why a 7 day running mean filter was applied. The daily variability was especially high until the 16th of November, when DIC fluxes were varying between up to $-1.7*10^3$ and $3.3 *10^3$ two days later (Fig. 4). During this time, a third of the days showed positive DIC rates and the average DIC rate was -117 mg m^{-2} d^{-1}. Looking at the 7 day filter data allowed to see a drop in DIC rates to negative values that lasts for 2 weeks until the 1st of November which was followed by 2.5 weeks of mainly positive DIC fluxes. After the middle of November the amplitude of daily variability was not as high and the rates are mostly negative with a 2 time periods where DIC rates varied between negative and positive values (between the 21st of December and the 3rd of January and after the 20th of January). The average DIC rate during this time was -285 mg m^{-2} d^{-1}, and it was -235 mg m^{-2} d^{-1} over the whole time series.

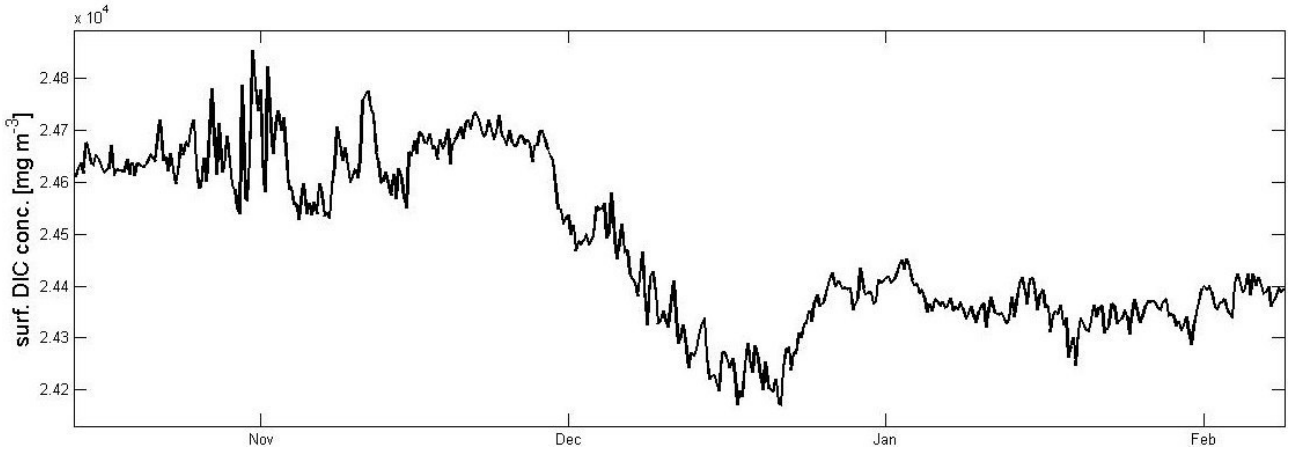

(a)

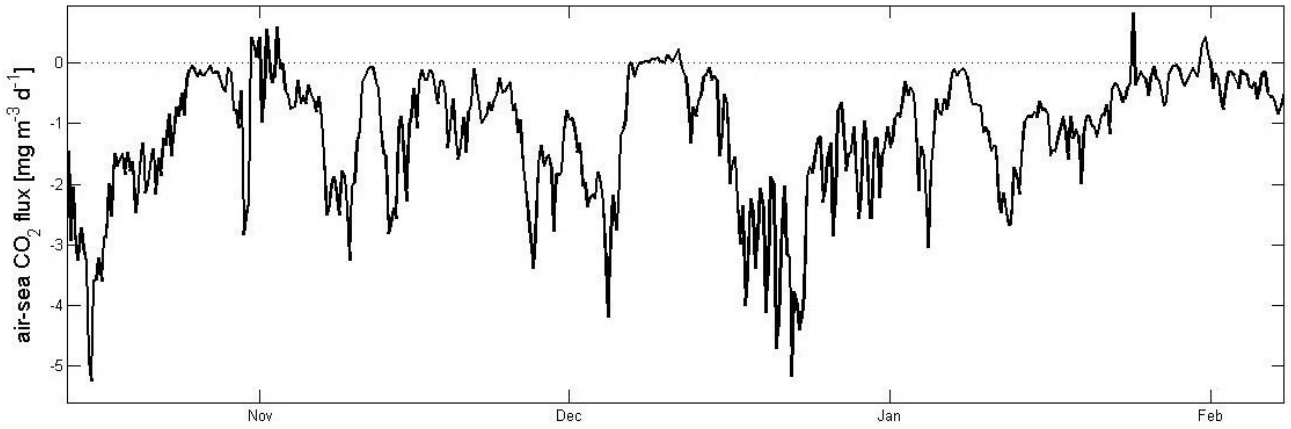

(b)

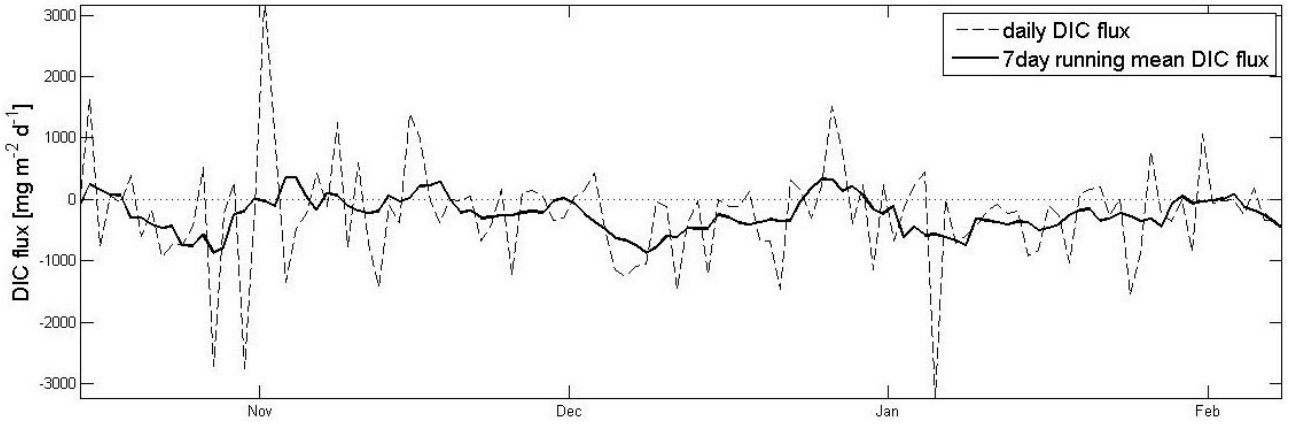

(c)

Figure 4: Seasonal development of surface water DIC concentration (a), air-sea CO_2 flux (a negative value represents a flux from the atmosphere into the water)(b) and the diurnal changes in ED integrated DIC concentrations (c), where the dotted line represents the actual data and the solid line the data smoothed with a 7 day running mean filter

4.3 Comparison of the NCP and DIC flux time series

As it was the aim of this study to compare the seasonal development of both NCP and DIC fluxes and to investigate whether both of them are behaving the same way and follow the same seasonal pattern, the time series of NCP and daily DIC flux are plotted in Fig. (5).

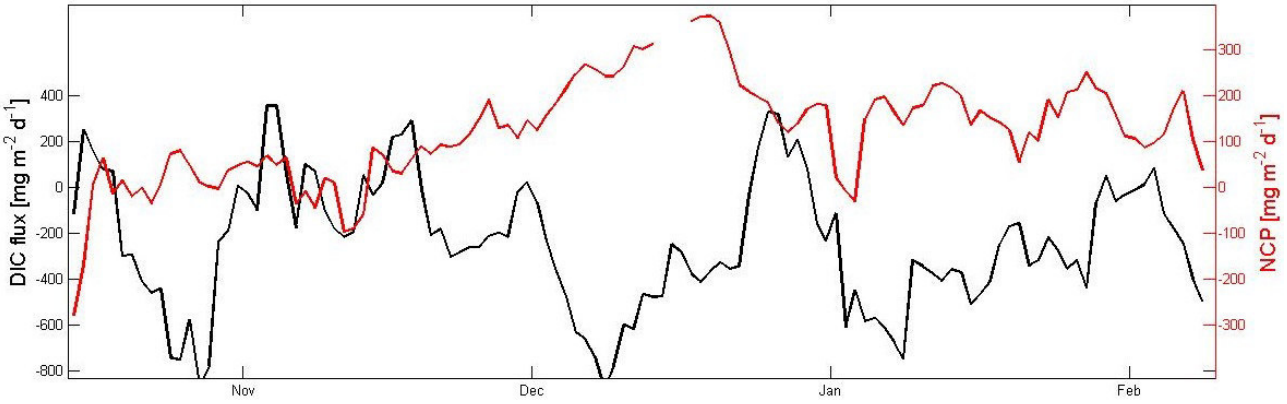

Figure 5: Seasonal development of NCP modeled with chlorophyll data (red line) smoothed with a 3 day running mean filter and the seasonal development of the daily DIC fluxes (black line) smoothed with a 7 day running mean filter

Looking at the 7 day running mean instead of the actual daily values gave a better overview over the seasonal development of DIC fluxes. As the amplitude of daily fluctuations was not as big in the NCP data, this time series did not require such a high filter since it would have removed almost all variability between the days, so that a 3 day running mean was applied.

Looking at the time series of NCP and DIC rates showed that the majority of the time they behaved inversely, but that the DIC time series varied with greater amplitude between days (Fig. 5). Over the whole season, the average fluxes were at a similar range, especially when regarding the maximum and minimum NCP calculated with all the different bloom initiation dates. The DIC flux was -235 mg m^{-2} d^{-1} on average and the NCP between -90 and 242 mg m^{-2} d^{-1} (mean: 118 mg m^{-2} d^{-1}). Note that a negative DIC flux means that DIC was consumed/decreased over the course of a day. This would correspond to a positive NCP value, when assuming that the observed changes in DIC are mainly caused by biological drawdown.

For the majority of the time, NCP was positive when DIC was negative. In the beginning of the time series, when the MLD was deeper than 80m, for a few days NCP rates were negative and DIC rates positive. After the 18th of October NCP was positive for the first time and on the same day DIC rates dropped to negative values. DIC values stayed below zero for 2 weeks with up to -800 mg m^{-2} d^{-1}, and NCP values were positive with up to 100 mg m^{-2} d^{-1}. While DIC experienced a drop that was short-lived but high in magnitude, NCP fluctuated at constantly low values and continued to do so when DIC rates increased to positive values on the 1st of November. For the following two weeks NCP and DIC fluctuated between positive and negative values and the fluctuations in the DIC data were of much greater magnitude. From the 20th of November onwards, NCP rates started increasing while DIC rates started to decrease, and both developments were interrupted for 3 days from the 27th until the 30th of November, after which both rates developed their peak. The DIC rates peaked already 1 week after this, whereas NCP rates did so 1 week later. For this whole time there seems to be a time lag between DIC and NCP rates of 1 week, which starts with a steeper increase in

DIC rates. From the first week of January onwards, NCP and DIC showed an inverse pattern of phases where one of them was positive and the other one negative. Looking at the actual data without running mean filter, not much agreement can be seen between the two time series.

The negative correlation of NCP and DIC fluxes can also be seen when looking at the correlation of the two (Fig. 6), although it was weak and not statistically significant when looking at the actual data without running mean (R^2: 0.02, p value: 0.12). The days that can not be explained well by the regression line can mainly be found before the middle of November (Fig.x, days before the 15th of November overlaid in red) and the largest spread in the data points was during these days. Excluding these days from the regression analysis resulted in a statistically significant negative relationship with a higher but still low R^2 (R^2: 0.08, p value: 0.02). Correlating the time series of 3 day running mean filtered NCP and 7 day running mean filtered DIC resulted in a statistically significant weak negative correlation (R^2: 0.1, p value: <<0.01).

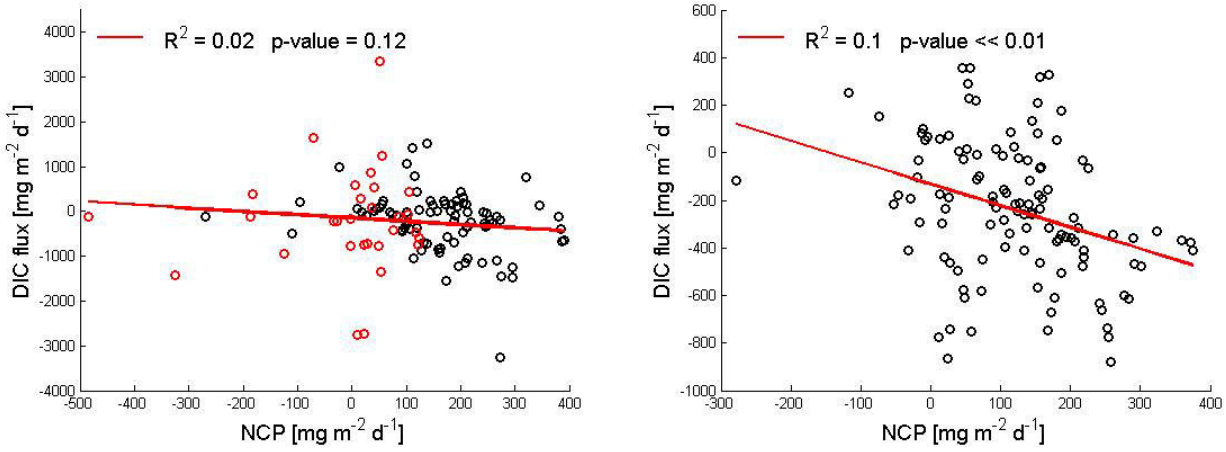

(a) (b)

Figure 6: Correlation analysis of the daily DIC fluxes and NCP using the actual data (no correlation, R^2: 0.02, p value: 0.12) (a), the datapoints furthest away from the regression line can be found before the middle of November and are overlaid in red. The correlation using the 3 day running mean filtered NCP and the 7 day running mean filtered DIC flux is statistically significant and negative (R^2: 0.1, p value: <<0.01).The linear regression equation (y=-0.8x-141) derived from this relationship was used to calculate a residual DIC flux which is believed to be controlled by other factors than biological ones

4.4 Drivers controlling biological production and carbon dynamics

The buoyancy glider was resolving physical properties (Temperature, salinity, PAR) of the upper 400 m of the ocean at fine temporal and spatial scales, which is necessary to fully understand the biology in the water body. Other physical forcing mechanisms from satellite data (surface wind stress, surface heat flux (note that a positive value means a flux into the ocean)) were consulted to get a better understanding of the factors influencing the ocean properties and to examine their role as drivers of NCP and DIC fluxes.

Fig 8. shows the time series over the sampling period of the physical factors considered as being of importance for the magnitude of NCP and daily DIC fluxes.

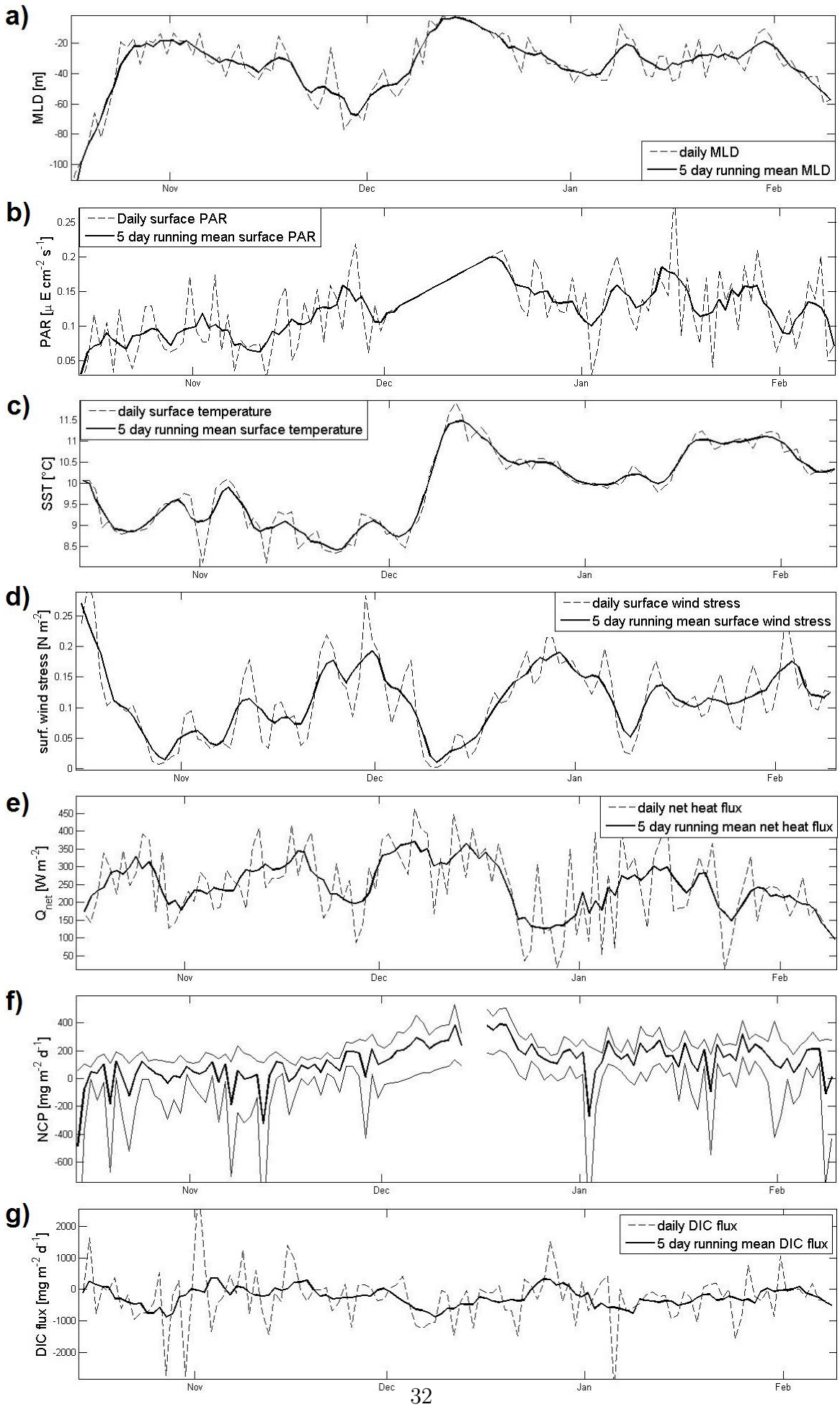
a)
MLD [m]
-20
-40
-60
-80
-100
daily MLD
5 day running mean MLD
Nov
Dec
Jan
Feb
b)
PAR [μ E cm^{-2} s^{-1}]
0.25
0.2
0.15
0.1
0.05
Daily surface PAR
5 day running mean surface PAR
Nov
Dec
Jan
Feb
c)
SST [°C]
11.5
11
10.5
10
9.5
9
8.5
daily surface temperature
5 day running mean surface temperature
Nov
Dec
Jan
Feb
d)
surf. wind stress [N m^{-2}]
0.25
0.2
0.15
0.1
0.05
0
daily surface wind stress
5 day running mean surface wind stress
Nov
Dec
Jan
Feb
e)
Q_{net} [W m^{-2}]
450
400
350
300
250
200
150
100
50
daily net heat flux
5 day running mean net heat flux
Nov
Dec
Jan
Feb
f)
NCP [mg m^{-2} d^{-1}]
400
200
0
-200
-400
-600
Nov
Dec
Jan
Feb
g)
DIC flux [mg m^{-2} d^{-1}]
2000
1000
0
-1000
-2000
daily DIC flux
5 day running mean DIC flux
Nov
Dec
Jan
Feb

Figure 8: Seasonal development of the physical properties that are considered of importance in influencing NCP and daily DIC fluxes. The mixed layer depth (a), amount of PAR (b) and the surface temperature (c) were sampled by the buoyancy glider, the surface windstress (d) and net heat flux (a positive value represents a flux into the ocean) (e) were derived via satellite data. Those factors are compared with the time series of NCP (max., min. and mean of all bloom dates) (f) and DIC fluxes (7 day running mean) (g)

The mixed layer depth was calculated with the glider's temperature measurements. It can be seen that it varied a lot between the beginning of the time series in October and the rest of the spring and summer season (Fig. 8). From the beginning of the time series (13th of October) until the 18th of October, surface wind stress was very high and reached it's maximum value during the sampling period (0.42 N m^{-2}) (Fig. 8). This resulted in very deep mixing depth of between 170 and 68 m. After this 5 day storm event the wind stress decreased, and with a short time lag the MLD shoaled to a depth of around 20 m one week later, which was possible since it became almost wind still during this time (<0.01 N m^{-2}). The net heat flux was rising, as were the surface temperatures.

Before this shoaling event, during which the mixed layer stayed at fairly stable depth (average 20m), mixed layer depths were highly variable and varied up to 51 m per day. The MLD stayed at this shallow depth until the 6th of November, when the winds were getting slightly stronger again and surface temperatures dropped. Surface PAR values on the other hand, were high (0.14 μE cm^{-3} s^{-1} on average as compared to 0.08 μE cm^{-3} s^{-1} on average before this time). The wind stress, and the MLD accordingly, were now in a phase where they fluctuated between periods where the MLD was as shallow as 13 m (0.03 N m^{-2} wind stress) and a phase where wind stresses were high (∼0.3 N m^{-2}) where the MLD deepened to 82 m (end of November). After this, during the beginning of summer, the MLD was slowly shoaling again until the wind stress became almost 0 at the 9th of December, which made the MLD shoal up to the surface (between 1 and 8m, average: 3.5m) where it stayed for 4 days. During this time, the surface T and Q_{net} reached their maximum values (Q_{net}: 463 W m^{-2}, T: 11.9∘C). Surface PAR measurements are missing for this period (5th until 16th of December) and the values between the two days of existing measurements had to be interpolated so that the peak of highest surface PAR can be seen a few days after the peak in all the other physical parameters (17th of December).

After the MLD shoaling event to the surface, the wind stress increased again, whereas surface T, Q_{net} and the MLD were decreasing. Generally, surface temperatures stayed at higher levels after the MLD shoaling (average 10.5∘C) than before (average 9.2∘C), as did surface PAR (average before: 0.1 μE cm^{-3} s^{-1}, average after: 0.14μE cm^{-3} s^{-1}). The mixed layer was not deepening as much as during spring, even though the wind stress was almost as high as in the beginning of the time series (maximum: 0.4 N m^{-2}, average: 0.15 N m^{-2}).

On the 8th and 9th of January there was another windless day (0.005 N m^{-2}) with high heat flux values (∼400 W m^{-2}) and the MLD rose to the surface (3m) once more. From this day onwards, mixed layer depth, Surface T, surface wind stress stayed at fairly constant levels with minor fluctuations (MLD between 4 and 53 m, average 28m. T between 9.8 and 11.2∘C, average 10.5∘C. Wind stress between 0.01 and 0.3 N m^{-2}, average 0.1 N m^{-2}) until the beginning of autumn and the end of this time series, where the MLD started deepening

to 70m. From the 30th of January onwards, Q_{net} and surface temperatures were steadily decreasing.

4.4.1 Physical factors influencing NCP

Single variable linear regressions were carried out to determine to what extend the various physical forcings were controlling the net community production in the South Atlantic sector of the Southern Ocean. As integration over the euphotic depth was chosen for PP and R, the mixed layer depth is not involved in the NCP calculations. For the correlation analysis, a 3 day running mean filter was applied. Looking at the time series of MLD and NCP it can be seen that phases of deep MLDs coincided with phases of low NCPs, particularly when looking at a general trend and not at exact dates. A phase where this does not apply, is between the 20th of November until the 1st of December, where the MLD was getting deeper but NCP was increasing. In the last third of the time series, the NCP was fluctuating more than the MLD.

The correlation of NCP towards MLD showed a statistically significant negative correlation (R^2: 0.32, p value: <<0.01) (Fig. 9). The datapoints furthest away from the regression line can be found at shallow MLDs and slightly negative or close to zero NCPs. As the NCP was negative together with shallow MLDs mainly in the beginning of the time series (from last week of October until ∼20th of November), this is the time when the magnitude of NCP was not well explained by the MLD (the datapoints during this time 10-37 are overlaid in red, R^2: 0.67).

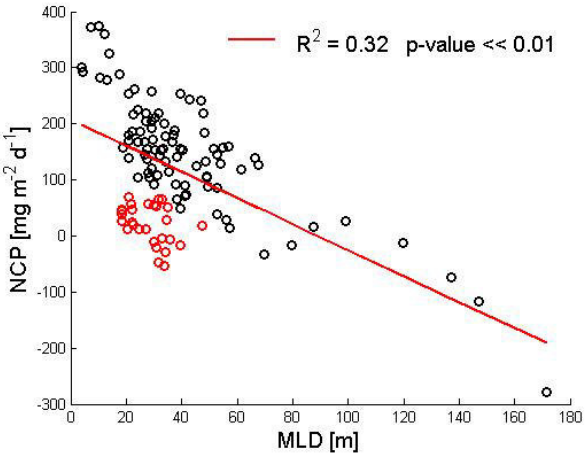

Figure 9: Regression analysis of NCP and MLD showing a statistically significant negative correlation (R^2: 0.32, p value: <<0.01). A 3 day running mean filter was applied for both datasets. The datapoints between the last week of October until the 20th of November, which are furthest away from the regression line are overlaid in red. The linear regression equation (y=-2.2x+203) derived from this relationship was used to calculate a residual NCP term which is believed to be controlled by other factors than the MLD

The residual NCP during this time was negative, meaning that the actual NCP was lower than expected by the prevailing MLD conditions. For the rest of the time series, the residual NCP was mainly positive (Fig. 10).

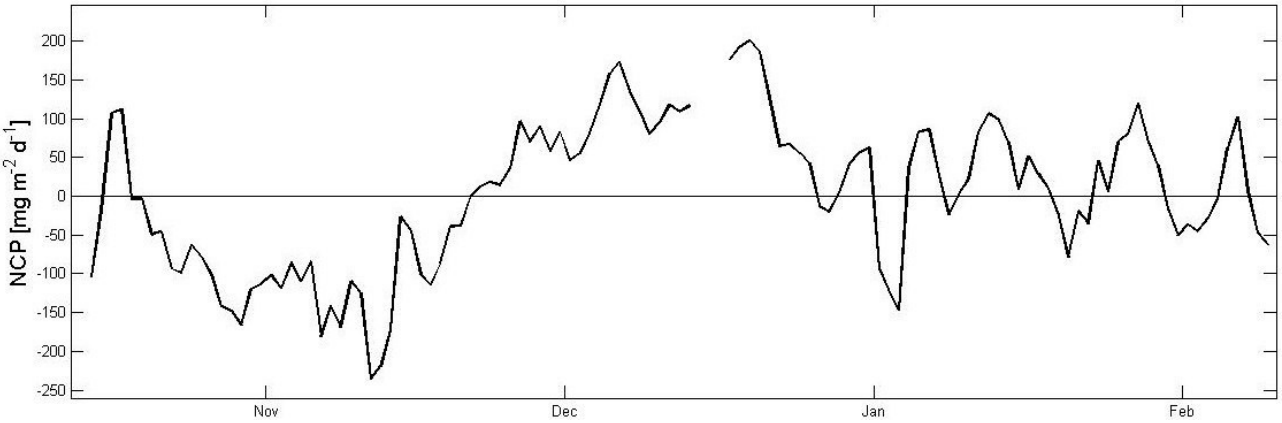

Figure 10: The residual NCP is the part of the variation in DIC data that can not be explained by the MLD and was derived from the linear regression equation (y=-2.2x+202) between NCP and MLD

There was no correlation between NCP and windstress (R^2: <0.1, p value: 0.49) or Qnet (R^2: 0.03, p value: 0.08), but a statistically significant positive correlation between NCP and surface temperature (R^2: 0.3, p value: <<0.01) (Fig. 11).

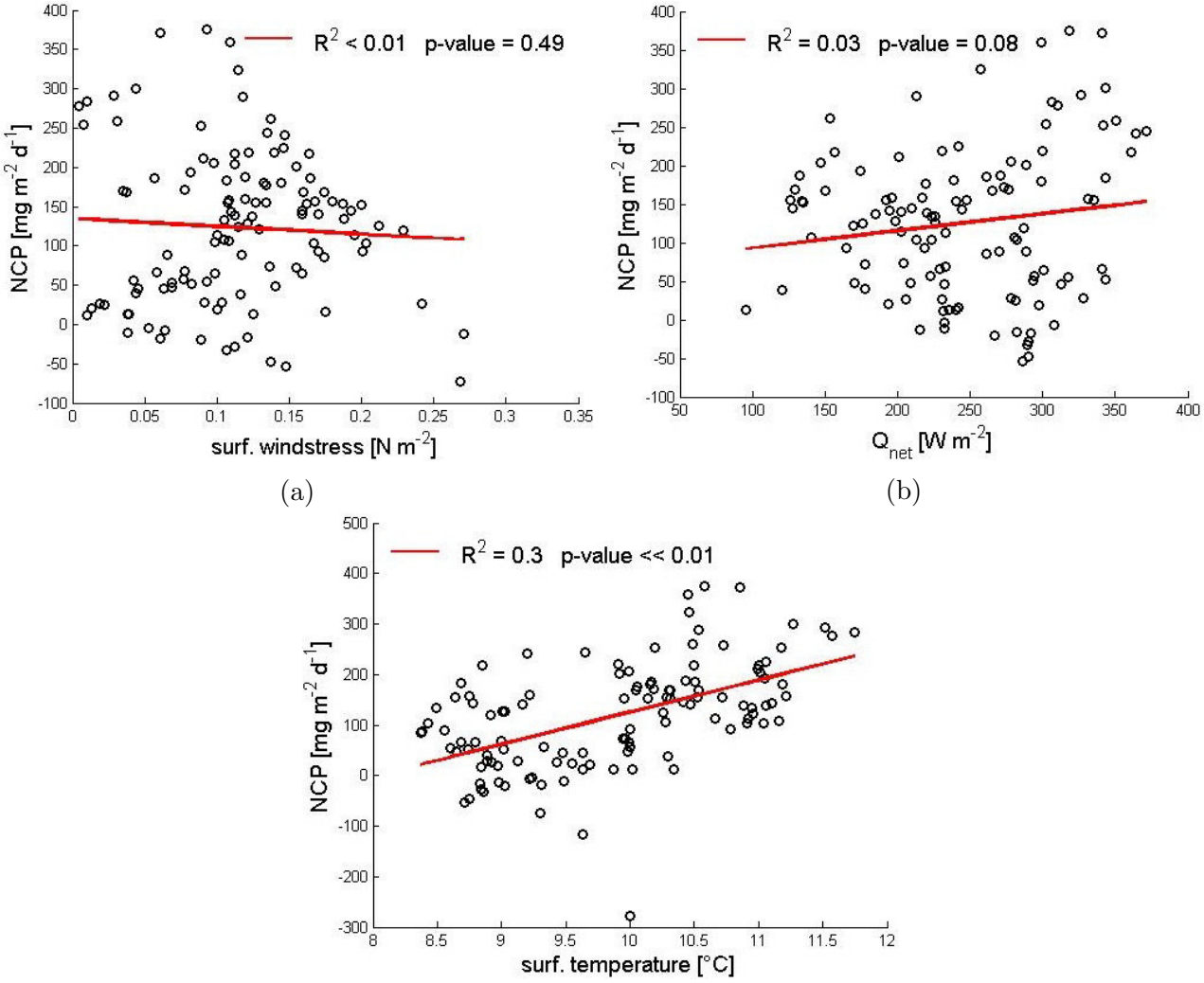

Figure 11: Correlation analysis of NCP with surface windstress (no correlation, R^2: <0.1, p value: 0.49) (a), Qnet (no correlation, R^2: 0.03, p value: 0.08) (b) and surface temperature (positive correlation, R^2: 0.3, p value: <<0.01) (c). For this analysis, 3 day running mean filters were applied to the datasets

Factors considered important for controlling the depth of the mixed layer are windstress and solar heat flux, so that the effect of those on NCP should express itself through the depth of the mixed layer. As the water body properties are changed at larger time scales, 5 day running averages were used for this analysis. There was a statistically significant positive correlation between MLD and wind stress (R^2: 0.47, p value: <<0.01) (Fig. 12). The relationship was weakest (datapoints furthest away from the regression line) during a time when wind was strong but the MLD shallow, which was mainly in the end of December (datapoints for this time 70-86 overlaid in red). This shows that, even though a direct correlation of NCP and windstress was not significant, it has an indirect impact on NCP through regulating the MLD. The heat flux was not statistically significantly correlated to MLD (R^2: 0.03, p value: 0.09), but a tendency can be seen for the MLD to be shallower when the heat flux was lower. There was a statistically significant negative correlation between MLD and surface T (R^2: 0.18, p value: <<0.01). The datapoints furthest away from the regression line were the first four days of the time series

where MLDs were very deep (datapoints overlaid in red), excluding these days resulted in a statistically significant correlation with a higher R^2 (R^2: 0.34, p-value: <<0.01).

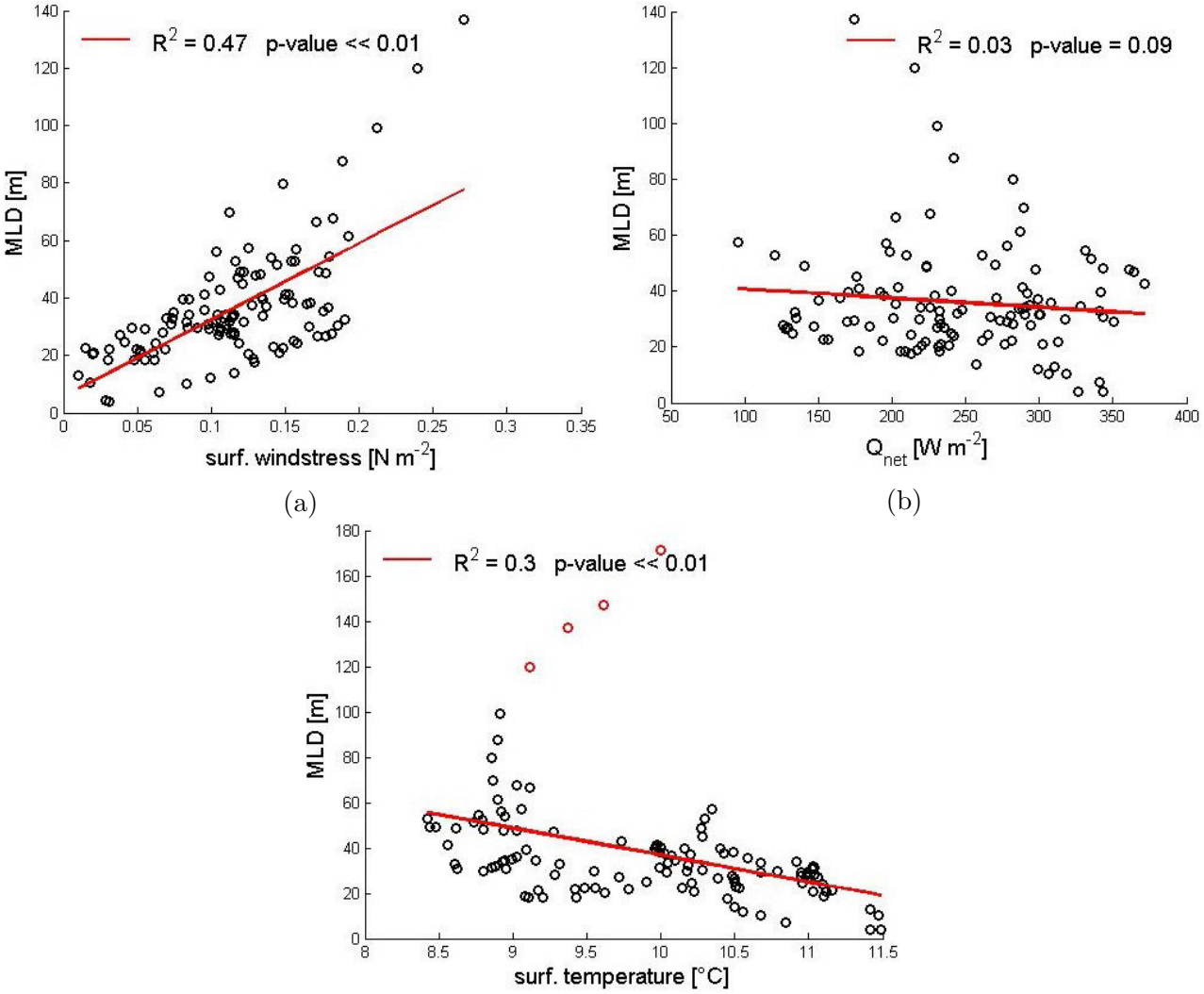

Figure 12: Correlation analysis of the MLD with surface windstress (positive correlation, R^2: 0.47, p value: <<0.01) (a), the datapoints furthest away from the regression line can be found during the end of December and are overlaid in red. There is no correlation of MLD and Qnet (R^2: 0.03, p value: 0.09) (b) and a positive correlation with surface temperature (R^2: 0.3, p value: <<0.01), the datapoints furthest away from the regression line are the first 4 days of the time series and are overlaid in red. For this analysis, 5 day running mean filters were applied to the datasets

To get a better understanding of the importance of each of the drivers on NCP, the time series was divided into 3 phases: The pre-bloom, from the 23rd of October until the 24th of November (the first 9 days of the time series were left out because no sign of elevated Chl concentrations was evident during this time and the MLD was deeper than 90m), the peak of the bloom until the 24th of December and the rest of the bloom until the end of the time series. The residual NCP term showed strongest correlation with surface PAR (R^2: 0.56, p value: <<0.01) (Fig. 13). Most of the negative residual NCP (NCP was lower than would be expected by the mixing depth) was situated in the pre-bloom phase and correlated with low light levels.

High light levels during the bloom peak correlated with high positive residual NCP. There was a statistically significant but weak positive relationship between the residual NCP and T (R^2: 0.15, p value: 0.01), and wind (R^2: 0.07, p value: <<0.01). There was no clear relationship between residual NCP and MLD deepening in the whole dataset (R^2: 0.03, p value: 0.14), but considering only the last third after the main bloom peak a weak negative correlation could be seen (R^2: 0.18, p value: 0.05) (datapoints for this time overlaid in red). All correlation tests were done with the 3 day running mean filter.

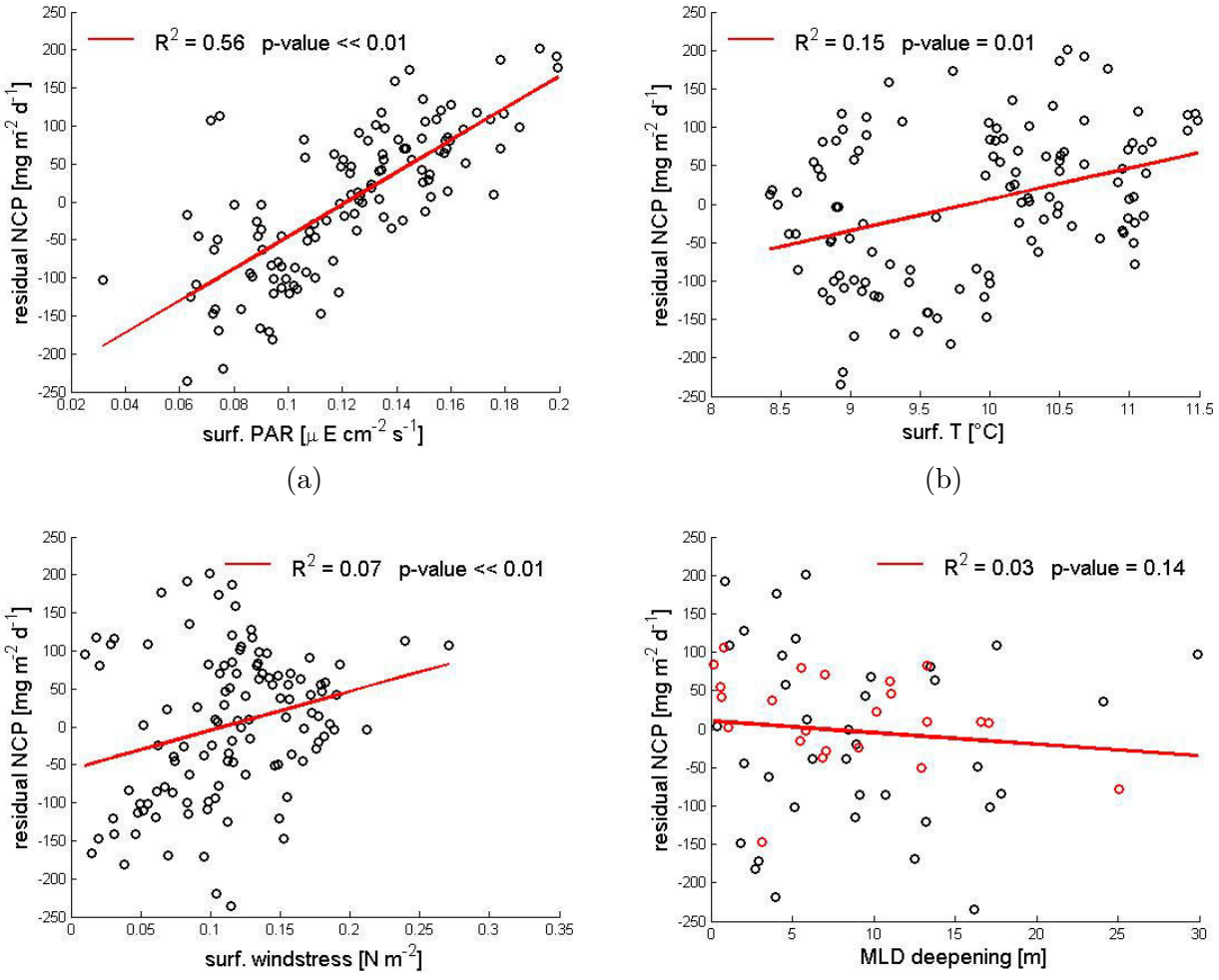

Figure 13: Correlation analysis of the residual NCP with surface PAR (positive correlation, R^2: 0.56, p value: <<0.01) (a), surface T (positive correlation, R^2: 0.15, p value: 0.01) (b), surface windstress (very weak positive correlation, R^2: 0.07, p value: <<0.01) and MLD deepening (no correlation, R^2: 0.03, p value: 0.14), datapoints closest to the regression line during the last third of the time series overlaid in red. For this analysis, 3 day running mean filters were applied to the datasets

4.4.2 Physical factors influencing DIC fluxes

Considering the running mean time series, a similar (inverse) pattern could be seen for the seasonal development of NCP and DIC fluxes for a large amount of the experimental period, which allows to believe that the DIC fluxes are largely and primarily controlled by the biology. With the regression equation derived from the correlation of NCP and DIC fluxes, a residual

DIC flux was calculated, which is assumed to be controlled by other factors than biological consumption. Fig. 14 shows the DIC flux together with the residual DIC flux, where it can be seen that the difference between the two graphs is smallest before the middle of November and in the end of December.

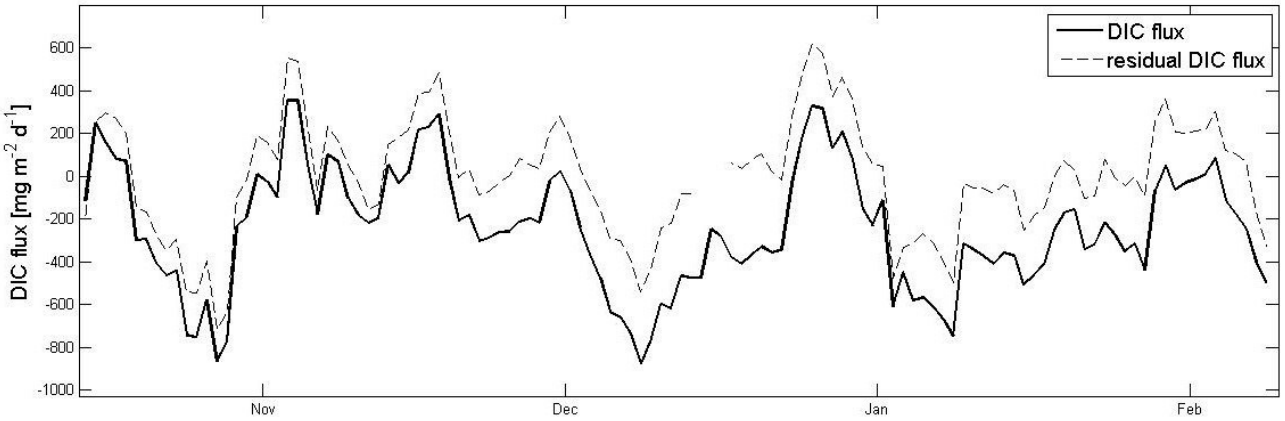

Figure 14: The residual DIC flux (dotted line) is the part of the variation in DIC data that can not be explained by the biology and was derived from the linear regression equation (y=-0.8x-141) between DIC flux (solid line) and NCP

30 days were identified where the NCP and DIC fluxes did not have the same sign (either both positive or both negative) and looking at the time series, there are mainly 5 phases when these occured: 1. between the 14th and 23rd of October, 2. 29th of October until 18th of November, 3. 24th until 29th of December, 4. 2nd and 3rd of January and 5. 29th of January until 3rd of February (Fig. 15).

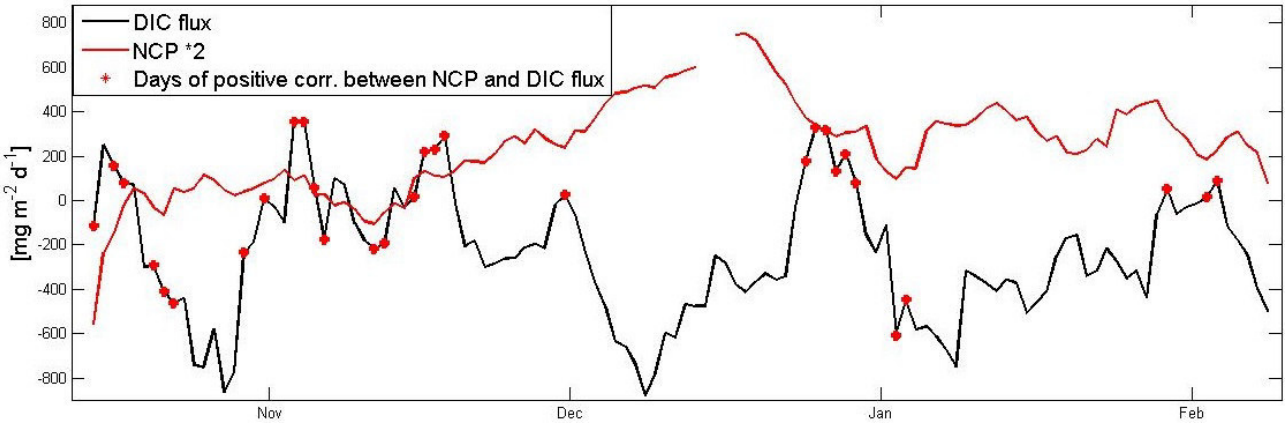

Figure 15: Time series of DIC flux (7 day running mean, black line) and NCP (3 day running mean, red line) with the days where DIC flux and NCP have the same sign (either both positive values or both negative values) marked with red stars

Fig.(15) visualizes once more that these were phases that could not well be described with the NCP, as during these days the difference between actual DIC and residual DIC was smaller than the rest of the time (i.e. the residual DIC was almost as big as the actual DIC).

Correlation analysis with single variable linear regressions where carried out to find the physical forcings responsible for the changes in DIC rates over the course of a day. As described and reasoned in the methods 3.3.2, the DIC flux present is caused by mostly biological processes. To test whether the DIC fluxes were controlled by the same mechanisms that were identified as important to control the biology, the correlation between DIC and MLD, Qnet, windstress, SST and PAR was tested (the 5 day running mean data was used). These are the factors that were also considered of importance for NCP. There was no correlation between DIC flux and MLD (R^2: 0.02, p value: 0.1) (Fig. 16). The datapoints furthest away from the regression line were the days where MLDs were shallow and DIC fluxes positive, between the 30th of October and the 17th of November and the 24th until 28th of December. There was no correlation between DIC flux and SST (R^2: 0.03, p value: 0.08) and very weak but statistically significant correlations with Qnet (R^2: 0.09, p value: $<<0.01$), windtress (R^2: 0.07, p value: $<<0.01$) and PAR (R^2: 0.08, p value: $<<0{,}01$). When using the actual data instead of the running mean data, no correlation with any of the factors was evident.

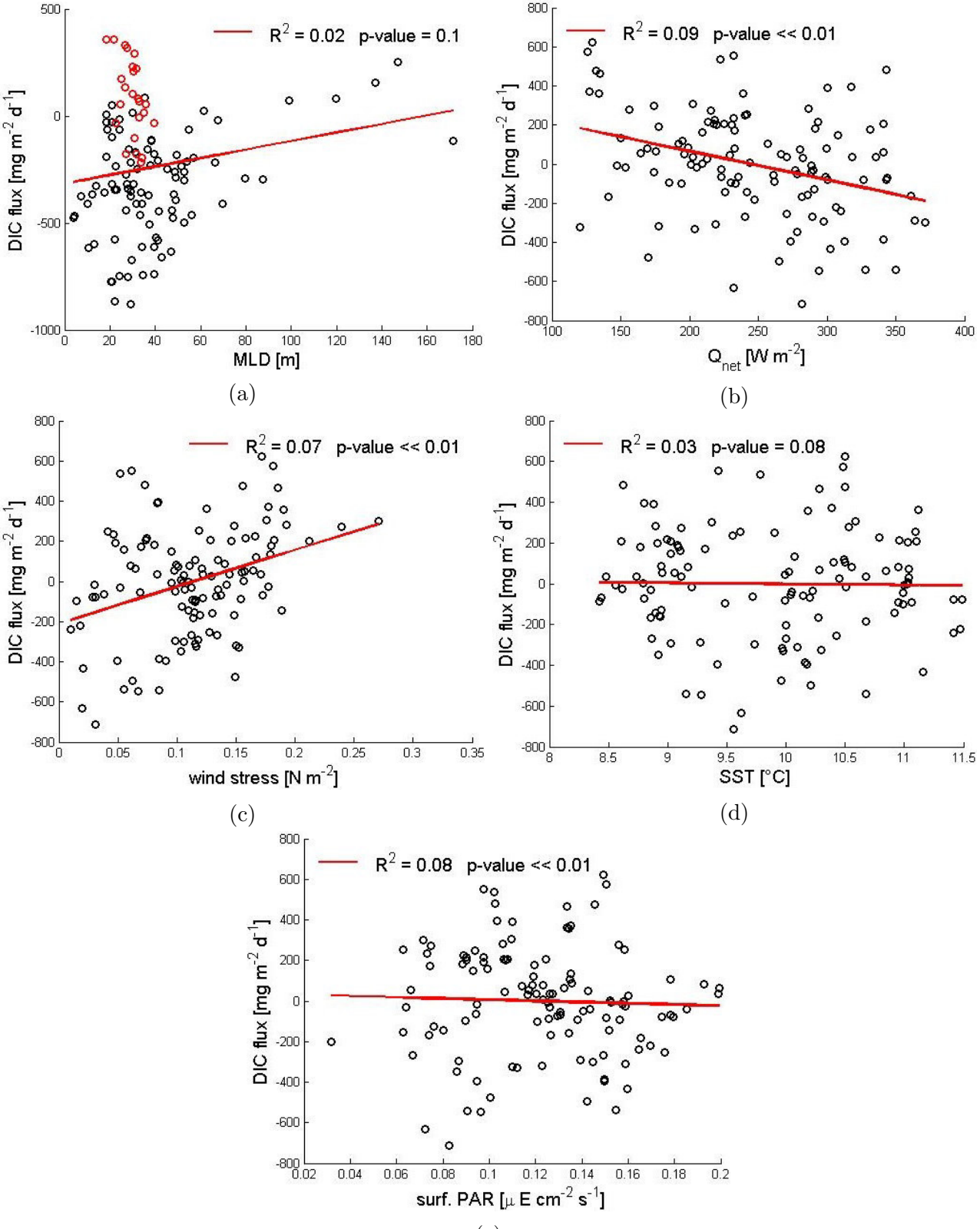

Figure 16: Correlation analysis of DIC with the MLD (no correlation, R^2: 0.02, p value: 0.1)(datapoints furthest away from the regression line between the 30th of October and the 17th of November and the 24th until 28th of December overlaid in red) (a), Qnet (weak negative correlation, R^2: 0.09, p value: <<0.01) (b), surface windstress (weak positive correlation, R^2: 0.07, p value: <<0.01) (c), surface temperatures (no correlation, R^2: 0.03, p value: 0.08)(d) and surface PAR (weak negative correlation, R^2: 0.08, p value: <<0,01)(e). For this analysis, 5 day running mean filters were applied to the datasets

A residual DIC was calculated for the proportion of DIC flux that can not be described by the biology (Fig 14). Correlation analysis were carried out between residual DIC and MLD, wind, SST and MLD entrainment. There was a statistically significant but weak positive correlation between wind stress and residual DIC (R^2: 0.1, p value: <0.01) (Fig. 17). There was no statistically significant correlation between residual DIC and any of the other factors, neither with the actual data nor with the data when a 5 day running mean was applied. The residual DIC was not influenced by temperature (R^2: <0.01, p value: 0.95) the MLD (R^2: <0.01, p value: 0.87) or MLD deepening (R^2: =0.02, p value: 0.3). The data points furthest away from the regression line of residual DIC towards MLD were the days with shallow MLDs and high DIC rates, which could be found during the first two weeks of November and again in the last week of December (datapoints overlaid in red), which was also the time where NCP and DIC were not negatively correlated.

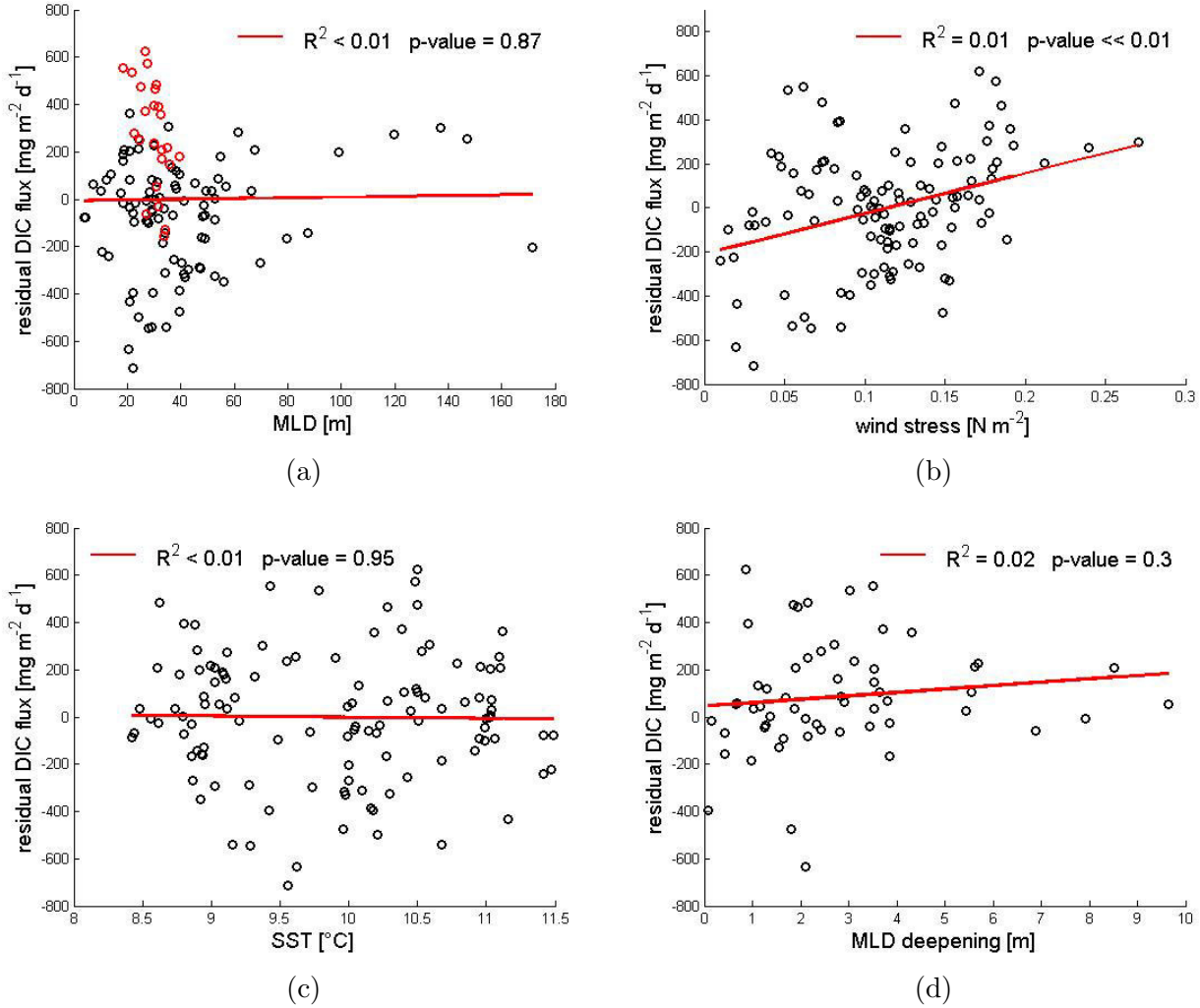

Figure 17: Correlation analysis of NCP with the MLD (no correlation, R^2: <0.01, p value: 0.87)(datapoints furthest away from the regression line between the 30th of October and the 17th of November and the 24th until 28th of December overlaid in red) (a), surface windstress (positive correlation, R^2: 0.1, p value: <0.01) (b), surface temperatures (no correlation, R^2: <0.01, p value: 0.95)(c) and MLD deepening (no correlation, R^2: 0.01, p value: 0.4). For this analysis, 5 day running mean filters were applied to the datasets

Looking solely at the days where DIC and NCP have the same sign, the highest correlations (but weak nevertheless) were found between residual DIC and T (positive correlation, R^2: 0.09, p value: 0.11) and residual DIC and MLD relationship (negative correlation, R^2: 0.09, p value: 0.09), although both were not statistically significant (Fig. (26) in the appendix). During the first week the MLD and temperatures were decreasing and so was the residual DIC. Until the middle of November the residual DIC varied between positive and negative values and the temperature varied between 9 and 10 degrees, for the first week they fluctuated inversely, the second week in phase. During the first week the MLD was generally shallow and the residual DIC was high, during the second week the MLD was deeper and the residual DIC was just as high. For the remaining days with the same sign, the temperature was not significantly different from the days before and after, and the MLD was generally deepening. Looking at only negative and positive residual DIC values separately, the only slightly relevant, but very weak, correlation was between residual DIC and windstress (R^2: 0.08, p value: 0.03) (Fig. (26) in the appendix).

The MLD entrainment is another term that can alter DIC concentrations in the surface waters, but there was no statistically significant correlation between the two, neither with the whole dataset (R^2: 0.01, p value: 0.4), nor with only the days of the same sign (R^2: 0.04, p value: 0.46) (the 5 day running mean MLD was used). Looking at Fig. (18) however, one can see that there are 4 timeperiods when the days where DIC and NCP have the same sign coincided with days of MLD deepening: the first 2 weeks of November, 24th until 29th of December, 2nd and 3rd of January and 2nd to 3rd of February. From the 24th until 29th of December and the 2nd to 3rd of February the residual DIC was positive, which means that the diurnal flux of DIC was higher than expected by the biology alone. Between the 2nd and 3rd of January it was negative, which means the DIC was lower than ecpected from NCP. During the first 2 weeks of November it was half positive and half negative.

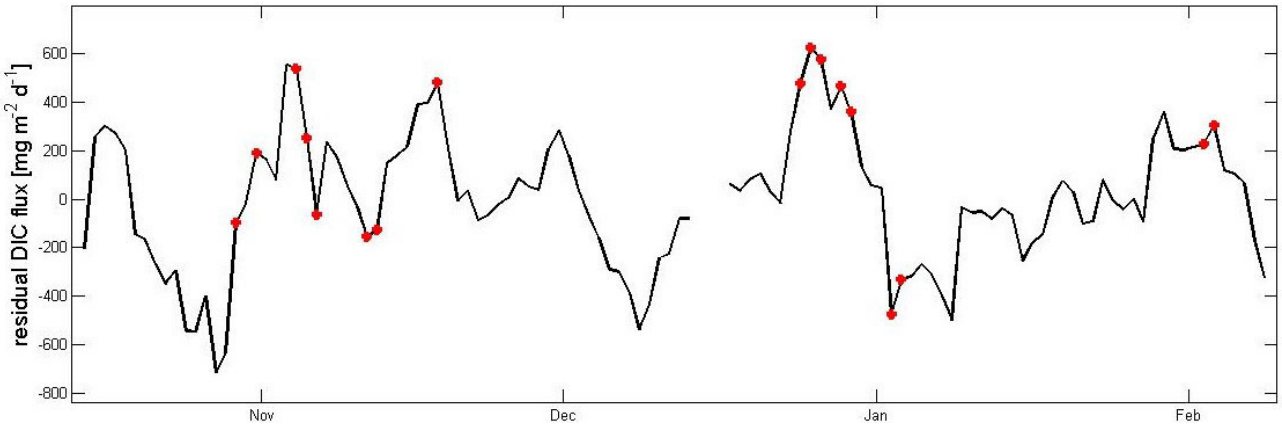

Figure 18: Time series of the residual DIC flux (7 day running mean, black line) with the days where DIC flux and NCP have the same sign (either both positive values or both negative values) and furthermore the MLD is deepening marked with red stars

5 Discussion

Carbon is stored and exchanged in the different reservoirs of this planet: the atmosphere, the hydrosphere and the lithosphere. Understanding the storage capacities and the fluxes in-between the reservoirs is of great value when estimating the future fate of the currently

emitted carbon by fossil fuels into the atmosphere. The importance of the oceanic reservoir and it's uptake capacity in this cycle has been recognized (Takahashi et al., 2009; Schimel et al., 1994), but a lot of further information and understanding of the factors that drive and control carbon fluxes and storage conditions is needed to fully estimate the future of climate change. Concerning the ocean, there are three processes controlling the flux between water and air: physical forcings, the solubility pump and the biological pump (Volk and Hoffert, 1985). In the Southern Ocean (between 30° and 50° S), a combination of all three factors is controlling the high rates of CO_2 uptake, strong winds, cooling of water masses flowing southwards and high biological production rates (Takahashi et al., 2012). This study is aiming at revealing the relationship between the biological community production and daily changes in DIC concentrations and investigating to what extend the biological production controls carbon fluxes in the Subantarctic zone of the Southern Ocean.

I will begin with discussing the glider data and the modeled net community production and reason about limitations, assumptions and possible sources of error in the data as well as in the method. The same will be done for the DIC data. Lastly, I will compare and discuss the seasonal development of both time series, which were hypothesized to follow the same pattern, and look into the driving mechanisms of both fluxes, which were hypothesized of underlaying the same drivers which would allow for the usage of the here developed method to derive NCP from DIC datasets.

5.1 Modelling Net Community Production

5.1.1 The seasonal development of Chl *a* and C_{phyto}

During spring, chlorophyll concentrations were elevated for the first time a few days after the MLD shoaled to a depth of 20 m and short-lived intermitted patches of high Chl were present (Fig. 1). During this time, wind stress was low (Fig. 8), which can result into stratification of the upper water layer and keep the phytoplankton from being mixed out of the euphotic zone (Huismann et al., 1999). Accordingly, Mahedevan et al. (2012) found these patchy pre-blooms to be driven by small scale eddies that stratify the water and trap plankton during a time when it is otherwise light limited.

The amount of light available for photosynthesis (surface PAR) during spring (before the 1st of December) was lower (average 0.096 μE cm^{-3} s^{-1}) than during the rest of the time series (average 0.14 μE cm^{-3} s^{-1}) and could be as low as $\sim$0.04-0.06μE cm^{-3} s^{-1}, whereas during summer the lowest light levels were around 0.09-0.1 μE cm^{-3} s^{-1}. The compensation irradiance, which was calculated with the Sverdrup model, was found to be 0.034μE cm^{-3} s^{-1} with the bloom initiation date on the 8th of November and ranged between 0.0015 and 0.09 μE cm^{-3} s^{-1} over the range of bloom initiation dates. Considering the range of Ics, the lowest light levels in spring might be below the compensation irradiance so that respiration exceeds production. Considering the mean Ic of all bloom dates, light levels during spring are already high enough to support net growth, and most of the bloom initiation detection methods detect the beginning of the bloom during this period.

As the wind stress became 0 in the second week of December, mixing almost stopped and the mixing depth diminished to the uppermost meters of the water column. This lead to the phytoplankton masses that previously had been hold in the surface waters by the MLD to sink out into deeper waters, as they had to stratification holding them near the surface

anymore. The subsurface resolution of the glider allowed us to see that production is likely not only taking place within the mixed layer, but that high chlorophyll concentrations can be seen as well underneath. From the second week of January onwards, the glider data revealed the presence of a deep chlorophyll maximum (DCM) underneath the MLD, which is likely the same phytoplankton that has previously been washed out of the mixed layer (Parslow et al., 2001).

Chl *a* and C_{phyto} concentrations in the water column showed very similar patterns over the course of the study period with the only difference being the time after the first week of January, where Chl *a* concentrations were clearly elevated underneath the MLD compared to above, and C_{phyto} concentrations were not. The ratio of both revealed a period where chlorophyll packaging per amount of carbon biomass was not constant anymore. The ratio of Chl to C_{phyto} is an indicator of firstly: the light and nutrient environment the plankton community is living in (MacIntyre et al., 2002) and secondly: the taxonomic type of phytoplankton present (Yacobi and Zohary, 2010). Fig. (1) shows, that Chl:C ratios were five times higher in the deep chlorophyll maximum than anywhere else during the time series (0.1 on average as compared to 0.02 on average the rest of the time). Kaiser et al. (2005) suggests using ratios between 0.01 and 0.05 or 0.02 on average. This lead to the conclusion that the phytoplankton community present was incorporating more chlorophyll into their cells and thus adapting to the low light environment. As this phytoplankton community was trapped below the MLD, it had to incorporate more chlorophyll into their cells for being able to synthesize enough ATP. This also means that they had not died after sinking out of the mixed layer and that they were still photosynthesizing and allocating their biomass into higher chlorophyll ratios. It is also possible that a different taxonomic group took over the community structure, as some taxa have genrally higher Chl:C ratios than others (Yacobi and Zohari, 2010).

During spring and early summer, chlorophyll concentrations responded to MLD deepening or shoaling, in the way that shallower MLDs provided greater light exposure and thus higher growth rates and deeper MLDs diluting chlorophyll biomass, part of the time (for example 17th, 23rd, 28th of October). After the main bloom event from the middle of December onwards, this almost never happened (Exception: 18th – 22nd of January). Chlorophyll concentrations seemed to either not respond to MLD shoaling or deepening (for example between the 24th of January and 5th of February), or increased slightly as MLDs are gradually deepening (10th of January, 6th of February). This could show, that during spring phytoplankton growth was rather light limited, causing elevated chlorophyll concentrations when the MLD held the cells in high light environments, and that during summer, the growth was rather nutrient limited, leading to elevated Chl concentrations when new nutrients from underneath the MLD become available.

5.1.2 The seasonal development of net community production

As seen from satellite data, the annual surface Chl *a* concentrations was found to be 16% lower than the one seen during this time series (see in the appendix under "Bloom initiation dates"), so the annual average NCP should as well be at least 16% lower. Probably even lower than 16%, as the light levels in autumn and winter are a lot lower and the days shorter. Additionally, the wind stress is stronger, which will increase mixing depth and critical depth, and prevent stratification. Generally speaking though, the Southern Ocean is known as being a net sink of atmospheric carbon because of its fixation as biomass and export via the biological pump to the deep ocean (Takahashi et al., 2009). Table (1) shows a range of calculated NCPs in the

Southern Ocean by various authors. Comparing the mean NCP of this study to other studies, it can be seen: firstly, that there is a whole range of NCP values reported and secondly, that the average value found here lies in the middle.

Author	NCP [mg/m^{2}d^1]	Region (all in the SO)	Season	Method
This study	-90 - 242	South Atlantic SAZ	spr./sum.	Sverdrup
Cassar et al., 2011	327	Australian SAZ	summer	O_2/Argon
Munro et al., 2015	39.5 $\pm$ 23	Drake Passage	whole year	PO_4^{3-}
Munro et al., 2015	52.6 $\pm$ 13.2	Drake Passage	whole year	TCO_2
Merlivat et al., 2014	336 - 1728	Atlantic + Indian SAZ	spr./sum.	DIC
Huang et al., 2012	-25 - 650	West Ant. Peninsula	summer	O_2/Argon
Thomalla et al., 2015	-357 - 198	South Atlantic SAZ	spring	Sverdrup
Thomalla et al., 2015	-369 - 361	South Atlantic SAZ	summer	Sverdrup
Thomalla et al., 2011	62 - 81	South Indian SAZ	late summer	^{15}N

Table 1: Comparison of NCP values found by other studies in the Southern Ocean

The maximum NCP value found in this study is rather low, compared with other findings. This is the case even though the NCP was integrated over a greater depth than the mixed layer depth, which is more commonly used (for example in Munro et al., 2015, Merlivat et al., 2014, Thomalla et al., 2015). Integrating over the MLD would have resulted in even lower mean and maximum NCP. The maximum in this study was 390 mg m^{-2} d^{-1}, whereas for example Cassar et al. (2011) found maximum NCP rates of 1286 mg m^{-2} d^{-1} and Merlivat et al. (2014) found values of 1726 mg m^{-2} d^{-1} sampling in late summer/ early autumn along the STF and the PF. They argue that these especially high NCP values can be expected and have previously been reported by Taylor and Ferrari (2011) along fronts due to restratification that prevents mixing. Some studies show that NCP values calculated and averaged for the whole year (Munro et al., 2015), including the low productive part of the year, are likely to be lower compared to this study's NCP of the spring and summer, and values for only summer (Cassar et al., 2011), considering only the most productive season of the year, are likely to be higher. A direct comparison with findings from other projects is difficult, as a lot of different methods were used, different seasons were sampled, different regions, and also different integration depths. Nevertheless, the comparison with other studies proves the here calculated NCP to be in the same order of magnitude as reported from other studies and therefor makes it eligible for comparisons to the daily DIC fluxes.

Primary production and respiration were calculated with chlorophyll, PAR and light extinction, MLD and z_{cr} as input parameters, and the net production of the community is the difference of both. The results are highly dependent on only these few input parameters.The calculated photosynthetic rates are directly related to surface chlorophyll concentration, so that the relative daily and seasonal development of PP rates is reflected in the amount of chlorophyll present. This shows the importance of correctly calculating and modeling chlorophyll concentrations with appropriate conversions (from backscatter to C_{phyto}, from fluorescence to chlorophyll and the P-I curve parameters) for this specific area and time of the season and a suitable quenching correction method. Chlorophyll and PAR values used for calculations are solely the surface values. This assumes a homogenous mixing until a certain depth above which all production takes place. As the glider data is resolving also the depth

of the water column, discrepancies between assumptions and realities, consistency between surface and deeper chlorophyll values, mixing depth and production depth, can be detected.

The Sverdrup method assumes productivity to take place in a homogenously mixed layer, over which all production and respiration is integrated. Integrating over the MLD lead to very low values of NCP after the 9th of December, since this was the time when the MLD shoaled almost up to the surface which made the integration depth only a few meters (between 1 and 8 m). It is clearly visible from both Chl *a* and also C_{phyto} data, that large amounts of biomass were still present and still photosynthesizing and respiring underneath the shallow MLD, which made NCP in reality bigger than the MLD integration would lead on. This is why, in the case of this study, the euphotic depth integrated NCP is to be preferred. MLD and ED were never the same or similar over the whole time series (Fig.(23) appendix) and the MLD was on average 54% of the ED. Without mixing, phytoplankton will slowly sink out of the euphotic layer and light levels will be too low for production to exceed respiration and the heterotrophic respiration would not be constant with depth. These are limitations the integration over the euphotic depth brings, but not incorporation 50% of the seasonal NCP when integrating over only the uppermost few meters of the watercolumn, when much likely there is more actively photosynthesizing phytoplankton biomass underneath, seems to be the greater loss.

The main period where ED integrated NCP and MLD integrated NCP were very different from each other was when the MLD was shoaling to the surface in the middle of December (between 9th and 19th of December the mean ED integrated NCP was 316 mg m^{-2} d^{-1} and the MLD integrated NCP was 65 mg m^{-2} d^{-1}). Over the whole season, this is equivalent to a difference of $1.4*10^4$ (ED integrated) towards $6{,}7*10^3$ mg m^{-2} (MLD integrated). In the time period after the bloom, integration over the ED was incorporating the deep chlorophyll maximum that was occurring in January and February, whereas the MLD integration did not, as this maximum was underneath the MLD (Fig.(23) appendix). This shows, that the only time it did not apply that the integration depth over the watercolumn was homogenously mixed, was the time with a deep chlorophyll maximum (DCM) in January and February. I included some more background information on DCMs in the appendix.

The DCM can contribute to a large proportion of the WC productivity (Richardson et al., 2000). For this study, the method used is calculating PP with the surface values only and assumes a homogenously mixed watercolumn, which leaves the actual production and NCP in this DCM unknown. It is another limitation of this method, that changes in chlorophyll and possibly production can not be included in the calculations for NCP. Although, dark adapted cells that have a high amount of chlorophyll, do not have higher total PP rates, as the assimilation number for each individual Chl molecule is smaller than for the light adapted cells (Kaiser et al., 2005). Furthermore, as phytoplankton cells in deeper water masses are likely to be equipped with higher amounts of other accessory pigments than Chl *a* (Sathyendranath et al., 1987), the actual PP and NCP might be even higher as when calculating PP solely with Chl *a* concentrations. This should be kept in might for the comparison with DIC data.

To conclude, integrating net community production over the euphotic depth instead of the mixed layer brings the advantage that all the NCP is captured during the peak of production where MLDs lay a fewer meters underneath the surface. A disadvantage is that

the method used here assumes a homogenously mixed depth of integration, which is not the case, as chlorophyll concentrations are higher at depth than at the surface in the end of the time series but also to a smaller degree in the beginning. This would mean that during these periods the production does not exponentially decrease with depth and that the real NCP is likely higher than the one modeled.

5.2 Modelling daily DIC fluxes

The physical factors influencing the concentration of dissolved inorganic carbon are the entertainment from below the mixed layer, flux between sea and atmosphere and lateral advection. The flux between the ocean and the atmosphere is what appears to be the most relevant factor, as we are interested in whether or not the world's oceans are able to take up the anthropogenically emitted large quantities of CO_2. However, the flux into the ocean is controlled by the previously named factors, as well as by the biology.

The air-sea CO_2 flux is dependent on differences in the partial pressure of CO_2 (pCO_2) between the surface water and the overlaying atmosphere (Takahashi et al, 2002). Since the spatial variability in atmospheric pCO_2 is not very big (Takahashi et al., 2002), it is mostly the spatial and temporal variability in surface ocean pCO_2 that is driving the flux (Marinov et al. 2008; Cadule et al. 2010). The amount of CO_2 that can dissolve in the water is dependent on temperature, total CO_2 concentration and alkalinity (Takahashi et al., 2002), these factors will change with ocean mixing (Jiang et al., 2014). While the SST is controlled by heat flux, wind and the mixed layer depth, the other two factors are controlled by biological processes, such as production, autotrophic and heterotrophic respiration and calcification (Takahashi et al., 2002). There is no data available to detect the development of calcite shells, but the formation is considered unlikely in being of major importance for observed changes in DIC concentrations (Karl et al., 1991). Changes in alkalinity were found to be not important for controlling the CO_2 flux in the SAZ (McNeil et al., 2007). Furthermore, total CO_2 concentration and alkalinity can be changed by upwelling of deep water masses and MLD deepening (Takahashi et al., 2002). A strong link and causal relationship between biological production and DIC concentrations was reported by Weiss et al. (1979), Karl et al. (1991) and Ishii et al. (1997). Karl et al. (1991) highlights that the amount of CO_2 entering the water via gas exchange is small compared to the amount consumed by biological production.

When looking at the time series of the DIC flux as it is presented here (Fig. 5), corrected for vertical and horizontal fluxes by normalizing with salinity and subtracting the air-sea CO_2 flux, and comparing that time series to the ones without those corrections (Fig. (24) in the appendix) it could be seen that the difference between those calculated fluxes was minor except for a few selected days. There was no clear trend on whether the salinity normalization or the FCO_2 was adding or subtracting from the DIC fluxes, on some days the daily flux became bigger by adding one of the two factors, on some days it got smaller. The salinity normalization, and thus the change in DIC concentration by vertical transport processes and below MLD entrainment, seemed to have a slightly bigger impact on daily DIC fluxes than the air-sea flux (the difference between the blue line and the red line seems to be bigger than the difference between the red and the black line). In the study by Munro et al. (2015) they found in their evaluation of processes that add variability to their calculated mass budgets of PO_4^{3-} and TCO_2 that the input of C from the atmosphere accounts for only a small proportion to the NCP calculations (only applicable for the TCO_2 budget) and that the input

by lateral advection and entrainment is of greater importance (their Table 1). Altogether, those three processes can bias their budget based NCPs by 35%.

5.3 Comparison of the NCP and DIC flux time series

One of the aims of this study was to determine the seasonal pattern of net community production and daily DIC fluxes and compare them with each other, hypothesizing that they largely follow the same trends and are thus of similar magnitude.The hypothesis would be met if an inverse pattern and a negative correlation can be seen for both time series for the majority of the time frame and if the magnitude of seasonal average DIC flux was within the range of NCPs with the different bloom initiation methods.

Looking at the seasonal development of NCP and daily DIC fluxes, it could be seen that both of them followed the same, inverse, trend for the majority of the time. This relationship only became visible when looking at the smoothed running mean time series, the daily variability in the DIC data was very high and didn't allow to instantly identify seasonal trends. Looking at the daily patterns without filter, no trend or similarity becomes evident (data not shown). As DIC fluctuated with a higher amplitude towards both positive as well as negative values, the average DIC rate over the seasonal was still in the same range as NCP. As discussed in 5.1.2, the values of NCP depend strongly on the choice of bloom initiation date, and choosing a bloom initiation date on a day when MLDs are very deep (on the 13th of October the MLD is 173m) that generates a deep critical depth resulted in the highest seasonal NCP. As mentioned (see part 2.3.1), a lot of more recent studies than the one by Sverdrup report that blooms can occur early in the season when MLDs are still deep, which would suggest that the NCP generated with the early bloom initiation date and deep critical depth (average seasonal NCP: 242 mg m^{-2} d^{-1}) is closer to being correct than the one with the bloom initiation date at the end of November with a critical depth of 23 m (average: -90 mg m^{-2} d^{-1}). Furthermore, a seasonal average NCP of 118 mg m^{-2} d^{-1}), as calculated with the mean of all bloom initiation dates, is rather in the lower range compared with other studies in the Southern Ocean (see Table 1). Especially the results found by Merlivat et al. (2014), who used a method most similar to mine among the ones I chose for comparison here (also using DIC data) are among the highest within this comparison. Munro et al. (2015) compare in their study their, and other, budget based NCP estimates with chlorophyll based estimates, and find that budget based estimates are generally higher. This makes the seasonal average NCP and DIC fluxes comparable, even though, as mentioned, the amplitude of the seasonal pattern and the daily variability in the DIC data is bigger.

The finding by Munro et al. (2015) that budget based NCP estimates tend to peak earlier in the season than chlorophyll or satellite based estimates, is supported by our data, however not very promoted (see Fig.(25) in the appendix). When looking at the cumulative sum of the chlorophyll modeled NCP and the DIC budget calculations, both cumulative sums have a similar slope, the DIC flux peak is reached slightly ($\sim$1.5 weeks) before the NCP (the NCP cumulative sum is increasing and does not peak until the end of the measurements), which means that the slope of the cumulative sum of DIC flux time series is slightly steeper than the one of NCP. As already mentioned, the total DIC rate was higher than the NCP.

The whole concept of identifying a bloom by elevated concentrations of chlorophyll is problematic altogether, since, as Platt and Sathyendranath (1991) and Behrenfeld (2010)

explain, growth rates can be high but not get detected if the dilution by storms is large. The choice of bloom initiation date can have a big influence in community production, as it is used to calculate compensation irradiance (Ic) and respiration. Fig.(3) visualizes the spread in magnitude of NCP when it is calculated with different bloom initiation dates. Average NCP over the time series can vary between 242 mg m^{-2} d^{-1} when calculated with bloom date on the 13th of October, and -90 mg m^{-2} d^{-1} when calculated with the 25th of November. This is due to the critical depth, which is equivalent with the MLD on the day of bloom initiation, which is 173 m on the 13th of October and 23 m on the 25th of November. Therefore, a variety of different detection methods was applied and a date was chosen that is representative of the mean of all methods, assuring not to base this study on an either low or high extreme. This comparison shows that it is very important to compare the outcome of different bloom detection methods.

Thus, the actual magnitude of NCP modeled with the approach I used here is highly variable even within one method (because of the different bloom initiation methods) and also the literature shows such a great variety in the magnitudes of NCP data (however they were found in different regions), that I still consider that the NCP modeled here with chlorophyll and the daily DIC fluxes are of comparable magnitude. Especially, and most importantly, since they are following a similar pattern over the season. This seasonality can only be seen in the smoothed dataset, the daily variability is overshadowing the seasonal pattern. It would highly improve the method, if a way was found to reduce the influence of entrainment from below the MLD and lateral fluxes into the sampling area. The daily variability was especially large until the middle November. One could speculate that this might be caused by the fact that during this time the gilder is moving more than during the rest of the sampling period, when it stayed in one spot and moved in a circle. Alternatively, the reason could be that during this time it is still spring, when processes like episodical MLD entrainment are large (Munro et al., 2015). This would lead to the conclusion that the daily DIC flux method should most importantly get improved for the springtime, or that the method should during spring only be used with caution. Preferably, the glider should stay in one location permanently, to avoid crossing vertical gradients that could add DIC that is not controlled by the biology. This could also mean that, if the larger scale surface glider experiments were to move over larger distances, a good proxy for MLD entrainment and advection needs to be found, or the approach with salinity normalization I used here needs to be optimized, otherwise the movement of the glider could incorporate too large errors.

5.4 Drivers controlling biological production and carbon dynamics

Phytoplanktonic primary production in the Southern Ocean is governed by complex interactions of different factors that can support growth, and the conditions that are controlling productivity and chlorophyll dynamics are up to date still being under debate. Furthermore, the high variability at very small spatial and temporal scales has been recognized (Thomalla et al., 2011) and can lead to highly heterogenous conditions and phytoplankton responses in the upper water column. The physical conditions in the ocean that are controlling the phytoplankton and zooplankton community growth can have different effects, depending on the season and the region in the world. In this study, the effects on biological production and upper ocean carbon dynamics are studied over the spring/ summer period in the Subantarctic Zone of the Southern Ocean. In addition to the factors that might also play a role in controlling the amount of chlorophyll that was used to model NCP, surface water DIC concentrations

can be changed by additional factors that have either no or a significantly smaller influence on the biology, such as the solubility of CO_2 in the water and entrainment from below the MLD.

In the following, all factors that might be relevant for having an impact on the biological production as well as the carbon dynamics are discussed and evaluated.

5.4.1 Physical factors influencing NCP

A major part of the influences on net community production express themselves through controlling the MLD, which will, in turn, influence NCP. The mixed layer depth controls the phytoplankton's exposure to sunlight and is thus important for phytoplankton growth (Sverdrup, 1953). The NCP used in this study was integrated over the euphotic depth and not the mixing depth, thus all the calculations for NCP are independent from the MLD. To clarify, wind stress, Qnet and T have a component that directly influences the phytoplankton physiology (for example nutrient entrainment, physiological temperature response) and another, that directly influences the MLD, which will directly influence the NCP. I will begin to first discuss the components and importance of the MLD that can explain the magnitude of NCP, and afterwards discuss possible explanations for the residual term of NCP that might be driven by factors other than the MLD.

The depth of the mixed layer is controlled by mainly two processes: wind stress, which is the force that is necessary to drive mixing, and solar heat flux, which is necessary to heat up the water and increase its buoyancy. Surface warming, induced by solar radiation, salinity gradients and reduced surface wind stress can lead to stratification and shoaling of the MLD (Swart et al., 2014). Thomalla et al. (2015) highlights the importance stratification plays for NCP and export production accordingly. Huang et al. (2012) found NCP inversely related to MLD (R^2: 0.21, p value: < 0.002) with MLD stratification being the most important driver of NCP in shelf regions, and Vernet et al. (2008) reports PP to be higher where MLDs are shallower. The study of Huang et al (2012) explains that the statistically significant relationship could not be seen in offshore areas, however chlorophyll concentrations there were very low in general. The mixed layer depth is controlled by wind and buoyancy forcings on timescales of days to weeks (Carranza and Gille, 2015). This means, a certain condition of wind strength or incoming heat might not show themselves in a response of the MLD immediately on the same day as it occurs. For this reason a 5 day running mean filter was applied to MLD, Qnet, T and wind stress data, which smooth the time series and allows to detect general trends during a time period instead of immediate responses, as, as mentioned, the responses might not be immediate.

There was a statistically significant correlation of wind and MLD (R^2: 0.47, p value: $<<0.01$) (Fig.16). This is in agreement with the findings of (Carranza and Gille, 2015). Swart et al (2014) found a stronger correlation of wind and MLD during the summer than during the spring (summer: R: > 0.4, p value: $<< 0.01$, spring: R: 0.23, p value: 0.01). In this study, the opposite is the case, as a much stronger correlation could be seen during spring (p value: $<<0.01$, R^2: 0.83) than in summer (p value: $<<0.01$, R^2: 0.39).

The relationship between Qnet and MLD was not as clearly correlated (Fig.16). Carranza and Gille (2015) found that surface cooling deepens the MLD, but with weaker correlation than the wind (21.8% of MLD variance is explained by wind, 16.7% by Qnet) and they conclude that winds have a stronger influence on the MLD in summer than Qnet. Also Swart et al. (2014) concludes that wind is the main driver of the MLD in the South Atlantic

SAZ, as the variability of wind (storms) and the variability of the MLDs are at the same time scales (∼5-7 days). According to Swart et al. (2014) heat flux in the SAZ in spring is too weak to result in the observed stratification. They also observed, that during periods of increasing stratification surface T remain unchanged, and conclude that a change in salinity is responsible for limiting and controlling the MLD up to the depth of the halocline, whereas in summer, temperatures and the thermocline are a more important factor to limit the MLD lower boundary. In spring, the MLD is controlled by wind, eddy driven stratification and salinity, in summer by heat flux. A similar pattern could be seen in the data of this study, after the main bloom event the correlation of MLD and Qnet was much stronger than before in spring (pre bloom phase: R^2: 0.04, p value: 0.2, after the bloom peak: R^2: 0.14, p value $<<$0.01). During summer, the MLD did not deepen as much as during spring, even though the wind stress had similar magnitudes. This can be explained by the larger amounts of incoming solar radiation (positive solar heat flux) that come with the beginning of summer which increased the buoyancy of the water.

Due to the previous period of warming, the mixed layer was not as affected by wind forcing. The same observation was made by Wang et al. (2001) for the PFZ.

The SST can help to explain the depth of the mixed layer. Contrary to Qnet and wind, temperature is not a cause but a result of the MLD: Surface temperatures are controlled by the amount of incoming solar radiation and the rate of mixing with colder, deeper water masses. Carranza and Gille (2015) showed, that SSTs are more importantly controlled by oceanic processed than by atmospheric ones. This makes the SST mainly but not solely controlled by the MLD. Simultaneously, are SSTs able to influence the wind in the marine atmospheric boundary layer (Wallace et al., 1989) and alter Qnet (Carranza and Gille, 2015). The correlation of wind speed to surface T is generally negative (Kahru et al., 2010). Carranza and Gille (2015) found for the SAZ high chlorophyll concentrations when surface Ts were high, which suggests that in the SAZ shallow MLDs with warm waters are more important for phytoplankton growth than MLD entrainment.

Winds have been reported to influence production and surface water chlorophyll concentrations in two ways: in a positive way through nutrient entrainment (discussed later) in areas with shallow MLDs (Kahru et al., 2010), or in a negative way, which seems generally more the case for the SO with generally deep MLDs (Kahru et al., 2010), by carrying phytoplankton cells into deeper waters out of the euphotic zone. This reflects the main limiting factors for phytoplankton growth (previously discussed in background 2.1), light or nutrients (Kahru et al., 2010). A seasonal switch from positive to negative correlations of wind and Chl is reported by Kahru et al. (2010) for the north Atlantic and north Pacific when MLDs get shallower than 70m during summer, not for the SO though. In regions with deep spring MLDs, the water underneath the MLD has low stratification and if the winds are strong in summer, the MLD can easily deepen and lower chlorophyll concentrations (Kahru et al., 2010).

The mixed layer depth does not only determine the light exposure, it's deepening also provides nutrients from deeper water masses which can promote phytoplankton growth (Carranza and Gille, 2015; Swart et al., 2014). Production in the Southern Ocean, being a HNLC region, is limited by iron (Martin et al., 1990b; Boyd, 2002; de Baar et al., 2005). Nevertheless, phytoplankton blooms occur in the spring and sustain throughout the summer

(Blain et al., 2007), which means that the surface waters have to get re-supplied with iron. Iron can deposit as dust, or the surface waters get re-supplied with nutrients by MLD entrainment (Carranza and Gille, 2015; Swart et al., 2014). In the summer, even nitrogen might be limiting (Pollard et al., 2002). Nutrient entrainment from below the MLD occurs on days when the MLD is deepening. Underneath the MLD, nutrient concentrations are higher than above, as there is typically low productivity (unless there is a DCM). So the deepening of the MLD will bring proportionally more nutrients than an additional volume of water would bring if the concentration over depth was constant. Nutrients could also be re-supplied to the area by Ekman-induced upwelling, eddie circulations or horizontal advection (Carranza and Gille, 2015) (all induced by wind), but no data on these terms is available for this study. Furthermore, according to the dilution-recoupling-hypothesis of Behrenfeld (2010), increased mixing depths will dilute the phytoplankton as well as their predators, reducing predator-prey-interactions and thus releasing the grazing pressure so that net phytoplankton growth can occur. Both of these arguments would counteract the previously named effect of shallow MLDs providing sunlight exposure and higher production rates.

As nutrient entrainment through MLD deepening occurs with a short time lag of only several hours (Carranza and Gille, 2015) and phytoplankton can double their cells more than once a day (Carranza and Gille, 2015), as can zooplankton (Carranza and Gille, 2015), an almost immediate response of increased windstress and MLD deepening should be seen in the chlorophyll data in the time scale of a day. For this reason, a three day running mean filter was used, which makes it possible to detect correlations that follow a day before or after an event.

The data of this study supports rather the findings by Kahru et al. (2010), as community productivity is negatively correlated with MLD deepening. The suggestion by Swart et al. (2014) or Carranza and Gille (2015) that MLD entrainment is necessary to fuel productivity, is not evident from the data presented here.

Another way how the wind could influence productivity is by nutrient input by dust. Due to the fact that the solubility of iron deposited with dust is low (Luo et al., 2005; Boyd et al., 2010; Baker and Croot, 2010) and that iron is mostly deposited as minerals (Boyd and Ellwood, 2010), whereas phytoplankton take up dissolved iron (Sunda and Huntsman, 1995), dust is assumed to be a minor source of iron for the Southern Ocean (Meskhidze et al., 2007; Wagener et al., 2008). Dust from Africa typically gets deposited east of 40° East (Piketh et al., 2000) and deposition from southern America only plays a minor role (Swart et al., 2014). Therefore, it can be assumed that wind does not supply the area with iron by other means than the one expressed in the MLD entrainment term. This is supported by our data, as no correlation existed between wind and the residual NCP.

Strong winds could also impact surface water productivity and chlorophyll concentrations in a way that they mix phytoplankton from the deep chlorophyll maximum to the surface waters (Carranza and Gille, 2015). This could be the case in the second week of January, but otherwise seems to be unlikely for this study, as the DCM is situated ∼10-20 m below the MLD (the correlation results in a very low R^2 and high p value, data not shown).

In the study by Huang et al. (2012), a positive correlation of NCP and surface temperature was evident (R^2: 0.36, p value: <0.001), and the same was reported by Carranza and

Gille (2015) for Chl *a* and T (at weekly time scales). By regarding the residual NCP which is not explained by the mixing depth, the factor that colder SSTs represent MLD deepening and nutrient entrainment is already eliminated, so that the now discussed changes are physiological responses of phytoplankton to the surrounding temperatures. Reay et al. (2001) report that phytoplankton growth rates in the Southern Ocean increase when ambient temperatures increase. It was found by Eppley in 1972 that an increase in 10°C would almost double cell division rates, and Banse (1991) confirmed the same relationship for Antarctic diatoms. Raven and Geider (1988) dedicated a whole study to temperature effects on cellular processes in phytoplankton (overview in their Table 1) and also discuss that the effect of temperatures on growth rates is different depending on nutrient status, light levels and taxa. Here, there was no correlation between residual NCP and T, for neither of the bloom phases. Possibly, the changes in temperature are too low to result in a significant effect, as they only vary between 8.1 and 11.3°C over the whole study period.

Huang et al. (2012) also found a strong correlation of NCP towards community composition, but data on the prevailing species is not available in this study. Furthermore, correlations of NCP and nutrient availability have been reported (Pollard et al., 2009), but no data on nutrient concentrations is available either.

Another factor that has not been named yet but will have an influence on biological production is the amount of PAR. The influence this factor had on NCP could not be regarded independently though, as it is part of the calculations (see Eq.4). This is very likely the reason of a statistically significant positive correlation (R^2: 0.56, p value: <<0.01,) of surface PAR and residual NCP (Fig. 13). Generally speaking, the amount of PAR will influence production in a way that higher light availability will result in higher PP rates until the threshold of photoinhibition (see background information part 2.1). The heterotrophic respiration should not be influences by light, at least not directly. Indirectly, higher light levels will result in higher biomass which gives more organic matter to respire.

The effect PAR has on assimilation rates of the phytoplankton should also be reflected in the amount of chlorophyll, if higher amounts of light will result in higher biomass production, which could be used to build up chlorophyll. Chlorophyll concentrations were observed to rapidly respond at time scales shorter than a day to changed light conditions (Swart et al., 2014). Correlations of PAR and the amount of chlorophyll (measured by the glider, not calculated) were partly discussed in part 4.4. Comparing the surface PAR with either the surface Chl *a* or top 10 m average Chl *a* as two timeseries, there was a weak positive correlation (R^2: 0.28, p value: <<0.01, (surface Chl)/(R^2: 0.24 (average Chl top 10m)) (data not shown). Although sometimes, they seem to be anti-correlated. A reason for this could be that the amount of chlorophyll per cell can vary with the light conditions, as discussed earlier. If light conditions are already "good enough" to obtain maximum amounts of energy, an increase in light intensity might not result in an increase in chlorophyll and the cells might even reduce the amount of chlorophyll to avoid over-heating (Geider, 1987). In fact, the periods of anti-correlating PAR and Chl trends are also the phases where MLDs are shallow (24th-27th of October; 15th – 18th of November; 21st -25th of January), already trapping the plankton cells in the sunlit water anyway, which could result in too high light levels and a reduction of chlorophyll concentration. On the other hand, at some occasions, high surface PAR values appear to support high chlorophyll concentrations even to the MLD is getting deeper (3rd – 7th of November; 26th – 29th of November), limiting

sunlight exposure and diluting the amount of cells into deeper water masses. The finding by Swart et al. (2014) of Chl biomass rapidly reacting to sunlight exposure was based on mixing depth trapping plankton in the sunlit layers, the interaction of sunlight exposure by water depth and by the total amount of incoming radiation appears to be more complex.

It has to be noted though, that the just described time periods show simply a time lag of chlorophyll concentrations responding to changing MLDs, and have not much to do with PAR altogether. The used values are midday values showing the conditions at exactly the same time, which means that even if chlorophyll concentrations are able to respond quickly to altered light exposures, there would still be a time lag of at least 1-2 days for the effect to become visible in Chl concentrations. To conclude, the relationship between PAR and Chl is influenced by many processes, which is probably why there is no clear statistically relevant relationship visible between the two.

Huang et al. (2012) observed a statistically significant relationship of NCP towards the logarithm of surface Chl concentration ((R^2: 0.72, $p << 0.01$). As, for this study, surface chlorophyll concentration was a major component in the calculations for NCP, a strong relationship between the two for this study is expectable and should not be used to explain the drivers of NCP.

5.4.2 Physical factors influencing DIC fluxes

It was hypothesized and reasoned in discussion section 5.2 that the daily changes in surface water DIC concentration as they were calculated with the method presented in 3.3.2 are to a large extent caused by biological production and consumption. Hence, net community production was considered the main cause of the daily developments and a residual DIC caused by physical factors was derived. As described in 5.3, NCP and DIC followed the same inverse trend the majority of the season when looking at the smoothed running mean time series, although the DIC fluxes were fluctuating with greater amplitude. Looking at the residual DIC, the proportion that cannot be explained by NCP, shows that the DIC flux was approximately half the time larger and half the time lower than NCP. It was lower than expected by biological production in the second half of October, the first week of December and the first week of January, and positive the rest of the time. There was no correlation between residual DIC and any of the physical factors.

The NCP was controlled by the MLD for the majority of the time, the DIC flux was not. Also the other factors that were proven to be correlated with NCP didn't seem to have a significant impact on the DIC flux. The time period when NCP could not be explained by the MLD from the end of October until the middle of November (NCP was low even though the MLD was shallow) was the same as the time when the DIC flux could not be explained by NCP (increase in DIC concentration over the day). This lead to the assumption that DIC concentrations were increasing over the course of a day because the NCP is close to zero or negative. At the same time, this was the time period where NCP and DIC flux were not anticorrelated. The reason for this could be that the NCP was very close to zero at this time, so that already a small change of 10-20 mg m^{-2} d^{-1} would change the value's sign. Between the 11th and 17th of November however, the magnitude of NCP was bigger, so that during this time NCP and DIC flux are positively correlated and the DIC flux must be influenced by another factor than the biology.

On the 11th of November the wind was strong and the air-sea CO_2 flux was almost zero, which means the CO_2 uptake was not as strong as before and after this day and outgassing might have been more prominent. The here presented air-sea flux is a net value. A value close to zero could mean that both the uptake and release of gasses is very strong, i.e. on a stormy day, or that both are very small, on a windless day. The strong winds in the SAZ have been found to be of great importance in driving the CO_2 flux in that area (McNeil et al., 2007). This would explain the negative DIC flux during this day that was not in agreement with the NCP. The temperature is 0.5-1°C lower on this windy day compared to the days before and after, which could be attributed to high mixing (Kahru et al., 2010). Low temperatures increase the gas solubility and have been shown to have an impact on pCO_2 (McNeil et al., 2007). Possibly, the temperature difference is not big enough to have a large impact on the CO_2 flux and the increased mixing by wind is of greater importance. Two days later the windstress and CO_2 flux have decreased again and DIC fluxes become positive even though the NCP simultaneously started to increase.

During the first two weeks of the time series, the DIC data was experiencing a strong decline while the NCP was staying at almost constant slightly positive values. Consequently, the residual DIC was at very high negative values. The surface windstress during these days was continuously decreasing while the SST was increasing and the MLD shoals to 20m, which was likely the reason why NCP could stay at positive values. The air-sea CO_2 flux was increasing to almost zero while daily DIC fluxes were decreasing. Possibly, increased SST and thus a decrease in the solubility pump are responsible for decreased CO_2 uptake and lowered daily DIC consumption rates. According to Volk and Hoffert (1985) the solubility pump is important for carbon uptake in the SO. Except for the second half of October this is not evident in the here presented dataset, as there is no correlation between DIC flux and temperature.

Alternatively, the low air-sea flux could mean that both uptake and release were low, induced by the very low windstress. All physical factors whose influence was tested for the impact on DIC fluxes appeared to be only relevant at short timescales and when looking into few selected days, which is likely the reason why no correlation could be seen when looking at the whole datasets. McNeil et al. (2007) attribute the carbon sink which the SAZ presents to cooling and strong winds and highlights furthermore the importance of the seasonal development of strong mixing in winter and high PP in summer for the CO_2 flux in the South Atlantic. The influence of temperature and wind was evident at few selected time periods when they were driving the air-sea CO_2 flux and, in turn, appear to be of greater importance in regulating the DIC rate over the day than the biological production. Tortell et al. (2011) found a stronger correlation between carbon fluxes (pCO_2 instead of DIC) and NCP in spring than in summer. For this study, this is not the case. The correlation is stronger in summer (R^2: 0.1, p value: 0.01) and there is no correlation when looking only at the spring (R^2: ¡0.01, p value: 0.57).

The term of MLD entrainment and lateral advection of DIC can be large (Munro et al., 2015). When calculating NCP with changes in DIC concentrations, excluding the factor of MLD entrainment and advection can lead to an underestimation of NCP by 35% (Munro et al., 2015). McNeil et al. (2007) highlights that lateral Ekman transport is especially important for the SAZ. The episodic entrainment term is especially large during spring (Munro et al., 2015). To reduce the influence of MLD entrainment to the surface water DIC pool, only the fluxes between sunrise and sunset were considered, assuming that mixing majorly takes place

in the night and the morning DIC concentration is representative of a homogenously mixed layer, and the data was salinity normalized. For this dataset, there was neither a statistically significant relationship between MLD deepening and residual DIC for spring nor summer. Part of the days of MLD deepening (in December and February) resulted in positive residual DIC values, whereas some resulted in negative DIC values. Especially during November days of negative and positive residual DIC were alternating on days when the MLD was deepening, which suggests that there is no clear trend and other factors must be responsible. For the days between the 24th until 29th of December and the 2nd to 3rd of February, the change in DIC concentrations over the day could not be well explained by the NCP (both terms positive). During the same time MLD entrainment took place, which was likely the cause of increasing DIC concentrations throughout the day that explains positive DIC fluxes over the days when NCP was also positive. For this time (the whole time after the bloom peak), MLD entrainment and NCP are negatively correlated, which suggests that MLD deepening dilutes phytoplankton into deeper waters and thus decreases production.

As there was generally no statistically significant correlation between MLD entrainment and DIC fluxes when looking at the whole time series, it can be concluded that the DIC flux calculations presented here are not biased by having made assumptions about the MLD entrainment term, and that only during two short periods, 24th until 29th of December and the 2nd to 3rd of February, MLD entrainment is responsible for elevated DIC concentrations in the surface waters. Nevertheless, the fact that the amount of DIC that is added/ removed by lateral advection and entrainment cannot clearly be separated from the biological production is a deficiency of this method and something that should be investigated in future studies. The here presented method doesn't completely remove the effect of entrainment and advection, it just reduces it. Likely, the term of advection and entrainment of matter have a bigger impact regarding the DIC concentrations than Chl concentrations and are thus more prominent in the DIC flux than the NCP. This could be an explanation for the greater daily variability in the DIC data as opposed to the NCP data. Additionally, the glider is moving in a small circle, so that some of the observed variability in-between measurements might be attributed to horizontal gradients.

The concentration of DIC in the surface waters can progress over the course of a day due to CO_2 exchange with the atmosphere. The air-sea CO_2 flux was thus subtracted from the DIC concentration in the water. The air-sea CO_2 flux in the SO was in some parts found to be controlled to the same extend by temperature and biology, which would cancel each other out when they are of the same magnitude, and in some parts to be dominated by the biology (Takahashi et al., 2002). In spring, the control of NCP on the air-sea CO_2 flux is more evident than in summer (Tortell et al., 2011). Contrary to this, Munro et al. (2015) reports that physical forcings appear to be more relevant in regulating the pCO_2 during spring and winter (in Drake Passage), whereas during summer the biological influence gains importance. The flux between sea and atmosphere is also largely governed by wind (Takahashi et al., 2002). In this study, on the days where the diurnal change in DIC concentrations appeared to be controlled by the air-sea flux (end of October and middle of November), the NCP was either low and positive or negative. It was reasoned that the flux on these days was driven by wind and temperature. Nightingale et al. (2000) suggest, that the relationship between wind speed and air-sea CO_2 flux is not linear but might have a positive curvature and that the remaining part of the flux that can not be explained by wind speed might be controlled by breaking waves and surface films. This might have small implications on the calculated air-sea

CO_2 flux in this study, which was calculated with the method by Nightingale et al. (2000). The occurrence of high productivity was observed to reduce the air-sea gas exchange through the development of surface films (Nightingale et al., 2000; Frew, 1997), and at very high wind speeds the air-sea flux might be enhanced due to breaking waves and bubbles (Nightingale et al., 2000; Bates et al., 1998).

Concluding the analysis on the importance of physical drivers on NCP and DIC fluxes it can be said that there is not much analogy between the influencing components on the two processes, especially since there is not much agreement or correlation of DIC with anything at all. This could be 1. due to the fact that the daily variability is in the DIC data is higher than the variability in the forcing physical parameters, 2. due to the fact that a combination of multiple factors is driving the flux, possibly in different directions (the effects could cancel each other out), so that looking at only one cause will not show a significant correlation with the effect, or 3. due to the fact that the driving mechanisms have different effects on the biology and the oceanic processes/chemistry, that could furthermore be different over the season. For example on days in the beginning of the season when nutrients are not limiting, MLD deepening would not favor biological production through nutrient replenishment, it would rather reduce productivity and thus diurnal carbon uptake when plankton cells get transported and diluted into deeper water masses. Later in the season however (as it was observed by Swart et al. (2014) but not in this study) entrainment could promote productivity and thus increase DIC reduction over the day. Whereas looking solely at the oceanic process of MLD deepening, it would increase DIC concentrations in the surface water. To reduce this uncertainty, the residucal DIC was calculated and used for correlation analysis, however the correlation between NCP and DIC was not very high in the first place.

To summarize, the DIC fluxes over a day can be controlled by a variety of thermodynamical or chemical mechanisms, and thus by more complex processes and their interactions, than the biology. This could have implications on the here developed method of using DIC data to obtain NCP during times when the variability and strength of the physical parameters is high, for example when winds are stronger and periodic storm events are more frequent. This could be the case during early spring and autumn. Furthermore, biological production during this time is generally lower than during the peak bloom period, so possibly the impact of physical forcings could overshadow the impact of the biology.

6 Future Perspectives

For future studies, it should be experimentally investigated whether the assumption that production and DIC concentration behave the same way, and exponentially decrease with depth, is valid. Incubation experiments could be used to investigate how well daily changes in DIC and NCP resolved over depth match and how well the here used method works. Other studies (for example Merlivat et al., 2014 and Munro et al., 2015) are assuming a constant DIC concentration over depth. The knowledge of how exactly the amount of DIC changes going from the water surface into deeper waters would be very helpful to find the actual magnitude of integrated DIC concentration, which would allow for a better comparison of depth-integrated DIC flux and NCP.

It should further be investigated how well salinity, as being independent from the biology, functions as a proxy for advection and entrainment. Those processes can make up a fair

amount of DIC fluxes (Munro et al., 2015), and for this study, no direct data on lateral and vertical gradients is available.

It should furthermore be kept in mind, that the daily variability, and the time period where DIC flux and NCP are in disagreement most often, is during the time where the glider is moving to its permanent sampling location. Potentially, this could have let to the passage of vertical gradients in DIC concentrations, but it could also be that during this time (in spring) physical and thermodynamically simply have a forcing impact on the DIC flux and thus cause the disagreement with the NCP data. Nevertheless, the fewer the gliders are moving would probably be the better, to reduce the influence of spatial variability in-between the samplings.

For future studies, it could be interesting to start the experimental period a little bit earlier in the year. As I discussed, a lot of studies point out that the spring bloom is actually starting earlier in the season than reasoned in the Sverdrup Hypothesis, and it would be valuable to have information about the net community production and efficiency of the biological pump for this time of the year. Furthermore, the spring appears to be the time when NCP and DIC flux data have the highest rate of being in disagreement, so this time needs the most investigation on what factors are actually controlling the diurnal DIC flux.

7 Summary and Conclusion

Bio-optical and physical data sampled by a pair of a surface wave glider and a buoyancy glider during a 4.5 month period in the austral spring and summer in the Subantarctic zone of the Southern Ocean was processed and analyzed. The two different datasets from the two gliders offered a unique opportunity at investigating the response of carbon dynamics to biological production and at developing a new method to use DIC data to calculate NCP. According to the aim and first hypothesis of this study, the seasonal development and magnitude of NCP and daily DIC fluxes, which were hypothesized to follow the same pattern, were compared for their analogy. It was furthermore examined to what extend the biology is driving the daily DIC fluxes and conditions and events when other factors became more important were identified. Lastly, following the second aim for this study, controlling physical factors on both NCP and DIC flux, which were hypothesized to be the same, were examined and compared.

The magnitude of the NCP modeled from bio-optical glider data is strongly dependent on the bloom initiation date chosen. It ranges from -90 to 242 mg m^{-2} d^{-1} as a seasonal average. The average NCP of all bloom initiation dates is 118 mg m^{-2} d^{-1} and was used for further investigations. Chl concentrations as well as NCP peak in the beginning of December but are mainly positive before and after this time as well. For the majority of the investigated time period, the biology appears to be the driving force in DIC seasonality. Daily fluctuations in the DIC data are large and the seasonal pattern can best be seen when looking at a running mean smoothed dataset. The DIC fluxes are fluctuating with a greater amplitude to both positive and negative values than NCP but show a similar seasonal average of -235 mg m^{-2} d^{-1} nevertheless. Looking at trends instead of single days the majority of the time the same inverse pattern can be seen. Nevertheless, the correlation between NCP and DIC flux is weak. As the NCP and the daily DIC fluxes are largely following a similar trend and are also of comparable magnitude, I would still conclude that the first hypothesis is met.

The NCP was largely controlled by the MLD and by PAR, the DIC flux did not show any correlation with any of the physical drivers. Looking into the time periods when NCP and DIC flux are not behaving inversely, during spring variations in temperature and windstress could be held responsible in controlling an outgassing CO_2 flux which reduces the daily DIC rate, during the latter half of the season the days where NCP and DIC had the same sign coincided with periods of MLD entrainment. This means that, during some short-lived events, the DIC flux was controlled by thermodynamically forcings that have no impact on the biology. Altogether, these time periods make up $\sim$1/5 of the whole sampling time and could be found to greater extend during spring. Nevertheless, the hypothesis that both fluxes are controlled by the same physical mechanisms was not met.

In conclusion, it can be said that the here presented method is suitable to derive NCP from DIC measurements and will lead to community production rates in similar pattern and magnitude as Chl-based NCP calculation methods, even though none of the driving forces on NCP development were evident to be driving DIC fluxes. Thermodynamic processes, which are controlling the carbon uptake and release, and thus the diurnal DIC cycle but do not have an impact on the biology, are evident during few short-lived events. The approach is valuable for converting large scale DIC measurements into biological data, which can be used to estimate the effect the biological pump has for oceanic carbon uptake. The correct parameterization of factors like biological uptake and release, chemical solubility and physical upwelling and mixing, which are all controlling CO_2 uptake, release and burial, is necessary for making reliable model estimates of CO_2 dynamics (Resplandy et al., 2014).

8 References

André, J.M. (1992). Ocean colour remote-sensing and the subsurface vertical structure of phytoplankton pigments. *Deep Sea Reseach*, Part A, 39, 763-779

Babin, M., A. Morel, V. Fournier-Sicre, F. Fell, and D. Stramski (2003). Light scattering properties of marine particles in coastal and open ocean waters as related to the particle mass concentration. *Limnology Oceanography* 48, 843-859

Baker, A. R., and P. Croot (2010). Atmospheric and marine controls on aerosol iron solubility in seawater. *Marine Chemistry*, 120(1), 4–13

Banse K. (1991). Rates of Phytoplankton Cell Division in the Field and in Iron Enrichment Experiments. *Limnology Oceanography* 36, 1886–1898

Banse, K. (1992). Grazing, temporal changes of phytoplankton concentrations, and the microbial loop in the open sea, in Primary Productivity and Biogeochemical Cycles in the Sea. Environmental Science Research, Vol. 43, eds P. G. Falkowski and A. D. Woodhead (New York, NY: Plenum Press), 409–440

Bates, N.R., A.H. Knapp, A.F. Michaels (1998). Contribution of hurricanes to local and global estimates of air-sea exchange of CO_2. *Nature* 395, 58-61

Batten, S. D., and Mackas, D. L. (2009). Shortened duration of the annual *Neocalanus plumchrus* biomass peak in the Northeast Pacific. *Marine Ecology Progress Series*, 393, 189–198

Beaupre, Steven R. and Aluwihare, Lihini (2010). Constraining the 2-component model of marine dissolved organic radiocarbon. *Deep Sea Research Part II: Topical Studies in Oceanography* 57, 16, 1494–1503. Doi: http://dx.doi.org/10.1016/j.dsr2.2010.02.017

Behrenfeld, M.J. and Boss, E. (2003). The beam attenuation to chlorophyll ratio: an optical index of phytoplankton photoacclimation in the surface ocean? *Deep Sea Research* 50,

1537–1549. Doi:10.1016/j.dsr.2003.09.002

Behrenfeld, M.J. and Boss, E. (2006). Beam attenuation and chlorophyll concentration as alternative optical indices of phytoplankton biomass. *Journal of Marine Research* 64(3), 431–451. doi:10.1357/002224006778189563

Behrenfeld, M. J., and Boss, E. S. (2014). Resurrecting the ecological underpinnings of ocean plankton blooms. *Annual Review of Marine Science* 6, 167–194

Behrenfeld, M., Waine E. Esaias, Kevin R. Turpie (2002). Assessment of primary production at the global scale. In *Phytoplankton Productivity: Carbon Assimilation in Marine and Freshwater Ecosystems*, Chapter 7, 156–186. Edited by Peter J. le B. Williams, David N. Thomas, Colin S. Reynolds. Copyright by Blackwell Publishing Ltd

Behrenfeld, M. (2010). Abandoning Sverdrup's Critical Depth Hypothesis on phytoplankton blooms. *Ecology* 91, 977–989

Blain, S., et al. (2007). Effect of natural iron fertilization on carbon sequestration in the Southern Ocean. Nature, 446, 1070–1074 Boyd, Philip W. (2002). Environmental factors controlling phytoplankton processes in the Southern Ocean. *Journal of phycology* 38, 844-861

Boyd, P. W., and M. J. Ellwood (2010). The biogeochemical cycle of iron in the ocean. *Nature*, 3, 675–682. Doi:10.1038/ngeo964

Boyd, P. W., E. Ibisanmi, S. G. Sander, K. A. Hunter, and G. A. Jackson (2010). Remineralization of upper ocean particles: Implications for iron biogeochemistry. *Limnology and Oceanography Methods*, 55(3), 1271–1288

Brody, S. R., Lozier, M. S., and Dunne, J. P. (2013). A comparison of methods to determine phytoplankton bloom initiation. *Journal of Geophysical Research: Oceans*, 118, 2345–2357

Brown, Evelyn, AngelaColling, Dave Park, John Phillips, Dave Rothery, John Wright (2001). Ocean Circulation (2nd Edition). Oxford, UK: Butterworth-Heinemann. ISBN 0750652780

Cadule, P., P. Friedlingstein, L. Bopp, S. Sitch, C. D. Jones, P. Ciais, S. L. Piao, and P. Peylin (2010). Benchmarking coupled climate carbon models against long-term atmospheric CO2 measurements. *Global Biogeochemical Cycles* 24, GB2016. Doi:10.1029/2009GB003556

Carr, M.-E., et al. (2006). A comparison of global estimates of marine primary production from ocean color. *Deep Sea Research, Part II*, 53, 741–770. Doi:10.1016/j.dsr2.2006.01.028

Carranza, M. M., and Gille, S. T. (2015). Southern Ocean wind-driven entrainment enhances satellite chlorophyll-a through the summer. *Journal of Geophysical Research* 120, doi:10.1002/2014JC010203

Cassar, N., P. J. DiFiore, B. A. Barnett, M. L. Bender, A. R. Bowie, B. Tilbrook, K. Petrou, K. J. Westwood, S. W. Wright, D. Lefevre (2011). The influence of iron and light on net community production in the Subantarctic and Polar Frontal Zones. *Biogeosciences* 8, 227–237. Doi:10.5194/bg-8-227-2011

Cetinic, I., Perry,M.J., Briggs, N.T., Kallin, E., D'Asaro,E.A., Lee, C.M. (2012). Particlulate organic carbon and inherent optical properties during 2008 North Atlantic Bloom Experiment. *Journal of Geophysical Research, Ocean.* doi:10.1029/2011JC007771

Chapman, William L., Walsh, John E. (1993). Recent variations of sea ice and air temperature in high latitudes. *Bulletin American meteorological society* Vol. 74, 33-47

Chester, Roy (2000). Marine Geochemistry. Second edition, Blackwell Science Ltd, Oxford UK, ISBN 0-632-05432-8 Chiswell, S. (2011). Annual cycles and spring blooms in phytoplankton: don't abandon Sverdrup completely. *Marine Ecology-Progress Series* 443, 39–50

Constable, Andrew J. et al. (2014). Climate change and Southern Ocean ecosystems I: How changes in physical habitats directly affect marine biota. *Global Change Biology* 20(10), 1-22. Doi: 10.1111/gcb.12623

Cosgrove, Jeff, Borowitzka, Michael A. (2010). Chlorophyll Fluorescence Terminology, an Introduction. Chlorophyll *a* fluorescence in aquatic sciences: Methods and Applications, Developments in applied Phycology 4. Doi: $10.1007/978 - 90 - 481 - 9268 - 7_1$ Springer Science Business Media B.V. 2011

Cullen, J.J. (1982). The deep chlorophyll maximum: comparing vertical profiles of chlorophyll *a*. *Canadian Journal of Fisheries and Aquatic Sciences* 39(5), 791–803. Doi: 10.1139/f82-108

Dau, H. (1994). Short-term adaptation of plants to changing light intensities and its relation to photosystem II photochemistry and fluorescence emission. *Journal of Photochemistry and Photobiology* B 26, 3-27

de Baar, H. J. W., et al. (2005). Synthesis of iron fertilization experiments: From the iron age in the age of enlightenment. *Journal of Geophysical Research* 110, C09S16, doi:10.1029/2004JC002601

De Boyer Montegut, C. (2004). Mixed layer depth over the global ocean: an examination of profile data and a profile-based climatology. *Journal of Geophysical Research*, 109: C12003

De La Fuente, Patricia, Celia Marrase, Antonio Canepa, X. Anton Alvarez-Salgado, Marc Gasser, Noelia M. Fajar, Cristina Romera-Castillo, Josep L. Pelegria (2014). Does a general relationship exist between fluorescent dissolved organic matter and microbial respiration? - The case of the dark equatorial Atlantic Ocean. *Deep Sea Research Part I: Oceanographic Research Papers* 89, 44-55. Doi: http://dx.doi.org/10.1016/j.dsr.2014.03.007

Del Giorgio, P. A., Cole, J. J., and Cimbleris A. (1997). Respiration rates in bacteria exceed plankton production in unproductive aquatic systems. *Nature* 385, 148–151

Demers, S., S. Roy, R. Gagnon and C. Vignault (1991). Rapid light-induced changes in cell fluorescence and in xanthophyll-cycle pigments in *Alexandrium escavatum* (Dinophyceae) and *Thalussiosiru pseudonana* (Bacillariophyceae): a photoprotection mechanism. *Marine Ecology Progress Series* 76, 185-193

Dore, John E. (2009). Physical and biogeochemical modulation of ocean acidification in the central North Pacific. *PNAS* 106, 30, 12235-12240. Doi: 10.1073/pnas.0906044106

Dower, K. M., and Lucas, M. I. (1993). Photosynthesis-irradiance relationships and production associated with a warn-core ring shep from the Agulhas Retroflection south of Africa. *Marine Ecology*, 95, 141–154

Eppley, R.W. (1972). Temperature and phytoplankton growth in the sea. *Fisheries Bulletin* 70, 1063-1085

Eppley, R.W. (1989). New production: history, methods, problems. In: Berger, W.H., Smetacek, V.S., Wefer, G. (Eds), Productivity of the Ocean: Present and Past. Wiley, Chichester, pp. 85-97

Eppley, R.W., Chavez, F.P., Barber, R.T. (1992). Standing stocks of particulate carbon and nitrogen in the equatorial Pacific at 150∘W. *Journal of Geophysical Research* 97(C1), 655-661. doi:10.1029/91JC01386

Evans, G. T., and J. S. Parslow (1985). A model of annual plankton cycles. *Biological Oceanography* 3, 327-347

Falkowski, P., K. Wyman, A. Ley, D. Mauzerall (1986). Relationship of steady state photosynthesis to fluorescence in eucaryotic algae. *Biochemical Biophysical Acta* 849, 183-192

Ferrari, R., Merrifield, S., and Taylor, J. (2014). Shutdown of convection triggers increase of surface chlorophyll. *Journal of Marine Systems*, S0924-7963(14)00038-4. Doi:

10.1016/j.jmarsys.2014.02.009

Frew, N.M. (1997). The role of organic films in air-sea gas exchange. In: The Sea Surface and Global Change, edited by P.S. Liss and R.A. Duce, pp. 121 - 172, Cambridge Univ. Press, New York

Friedrichs, M. A. M., et al. (2009). Assessing the uncertainties of model estimates of primary productivity in the tropical Pacific Ocean. *Journal of Marine Systems*, 76(1–2), 113–133. Doi:10.1016/j.jmarsys.2008.05.010

Geerts, B. (1998). Antarctic sea ice: seasonal and long-term changes. Department of Atmospheric science, University of Wyoming. Retrieved May 2015.)

Geider, R. J. (1987). Light and temperature dependence of the carbon to chlorophyll ratio in microalgae and cyanobacteria: Implications for physiology and growth of phytoplankton. *New Phytology* 106, 1 –34

Goericke, R. and Montoya, J.P. (1998). Estimating the contribution of microalgal taxa to chlorophyll a in the field – variation of pigment ratios under nutrient- and light-limited growth. *Marine Ecology Progress Series* 169, 97-112. Doi:10.3354/meps169097

Granfors, Anna, Anders Karlsson, Erik Mattsson, W.O. Smith, Katarina Abrahamsson (2013). Contribution of sea ice in the Southern Ocean to the cycling of volatile halogenated organic compounds. *Geophysical Research Letters* 40(15):3950-3955. Doi:10.1002/grl.50777

Greve W, Lange U, Reiners F, Nast J (2001). Predicting the seasonality of North Sea zooplankton. In: Kroncke I, Turkay M, Sundermann J (eds) Burning issues of North Sea ecology. Proc 14th Int Senckenberg Conf 31:263–268

Greve,W., Prinage, S., Zidowitz, H., Nast, J., andReiners, F. (2005).On the phenology of North Sea ichthyoplankton. *ICES Journal of Marine Science*, 62, 1216–1223

Griffith, D. R., McNichol, A. P., Xu, L., McLaughlin, F. A., Macdonald, R. W., Brown, K. A., and Eglinton, T. I. (2012). Carbon dynamics in the western Arctic Ocean: insights from full-depth carbon isotope profiles of DIC, DOC, and POC. *Biogeosciences*, 9, 1217-1224, doi:10.5194/bg-9-1217-2012, 2012.

Gruber, N., Gloor, M., Fletcher, S. E. M., Doney, S. C., Dutkiewicz, S., Follows, M. J., Gerber, M., Jacobson, A. R., Joos, F., Lindsay, K., Menemenlis, D., Mouchet, A., Müller, S. A., Sarmiento, J. L., Takahashi, T. (2009) Oceanic sources, sinks, and transport of atmospheric CO_2. *Global Biogeochemical Cycles* 23, GB1005. Doi:10.1029/2008GB003349

Hill, R., C. Frankart, P.J. Ralph (2005). Impact of bleaching conditions on the components of non-photochemical quenching in the zooxanthellae of coral. *Journal of experimental marine biology and ecology* 322, 83-92

Hiscock, M. R. (2004). The regulation of primary productivity in the Southern Ocean. PhD thesis, Nicholas school of environmental and earth sciences, Duke University

Huang, K., Ducklow, H.,Vernet, M., Cassar, N., and Bender, M. L. (2012). Export production and its regulating factors in the West Antarctica Peninsula region of the Southern Ocean. *Global Biogeochemical Cycles* 26. Doi:10.1029/2010GB004028

Huisman, J., van Oostveen, P., and Weissing, F. J. (1999). Critical depth and critical turbulence: two different mechanisms for the development of phytoplankton blooms. *Limnology and Oceanography* 44, 1781–1787

Ishii, Masao, Hisayuki Y. Inoue, Hidekazu Matsueda, Eiichiro Tanoue (1997). Close coupling between seasonal biological production and dynamics of dissolved inorganic carbon in the Indian Ocean sector and the western Pacific Ocean sector of the Antarctic Ocean. *Deep Sea Research I* 45, 1187-1209

Johnson, G.C. and Lyman, J.M. (2015). Sea surfac salinity (SSS). *Bulletin of the American Meteorological Society.* Aug2016Supplement State of the Climate in 2015, pS71-S72.

2p. Ji, Rubao, Martin Edwards, David L. Mackas, Jeffrey A. Runge, Andrew C. Thomas (2010). Marine plankton phenology and life history in a changing climate: current research and future directions. *Journal of Plankton Research*, Volume 32, Issue 10, 1355-1368

Jiang, C., S.T. Gille, J. Sprintall, C. Sweeney (2014). Drake Passage oceanic pCO_2: Evaluating CMIP5 coupled carbon/ climate models using in-situ observations. *Journal of Climate* 27(1), 76–100. Doi: http://dx.doi.org/10.1175/JCLI-D-12-00571.1

Kahru, M., S. T. Gille, R. Murtugudde, P. G. Strutton, M. Manzano-Sarabia, H. Wang, and B. G. Mitchell (2010). Global correlations between winds and ocean chlorophyll. *Journal of Geophysical Research*, 115, C12040. doi:10.1029/2010JC006500

Kaiser, Michel J., Martin J. Attrill, Simon Jennings, David N. Thomas, David K. A. Barnes, Andrew S. Brierley, Nicholas V. C. Polunin, David G. Raffaeli, Peter J. B. Williams (2005). Marine Ecology – Processes, Systems and Impacts. New York, USA: Oxford University Press Inc. ISBN 019924975-X

Karl, D.M., Tilbrook, B.D., Tien, G. (1991). Seasonal coupling of organic matter production and particle flux in the western Bransfeld Strait, Antarctica. *Deep Sea Research* 38, 1097-1126

Knox, G. A. (2007). Biology of the Southern Ocean. *CRC Marine Biology Series*. CRC Press. ISBN 9780849333941

Kolber, Z., Falkowski, P. (1993). Use of active fluorescence to estimate phytoplankton photosynthesis in situ. *Limnology and Oceanography* 38, 1646-1665

Krause, G., Weis, E. (1991). Chlorophyll fluorescence and photosynthesis: the basics. *Annual Review of Plant Physiology and Plant Molecular Biology* 42, 313-349

Landschützer, P., N. Gruber, D. C. E. Bakker, U. Schuster (2014). Recent variability of the global ocean carbon sink. *Global Biogeochemical Cycles* 28, 927–949. Doi:10.1002/2014GB004853

Large, W., and Pond, S. (1981). Open ocean momentum flux measurements in moderate to strong winds. *Journal of Physical Oceanography* 11, 324–336

Lavigne, H., D'Ortenzio, F., Migon, C., Claustre, H., Testor, P., D'Alcala, M. R., Lavezza, R., et al. (2013). Enhancing the comprehension of mixed layer depth control on the Mediterranean phytoplankton phenology. *Journal of Geophysical Research: Oceans* 118, 3416–3430

Ledford, H.K., Niyogi, K.K. (2005). Singlet oxygen and photo-oxidative stress management in plants and algae. *Plant, Cell and Environment* 28, 1037-1045

Lee, Kitack, Lan T. Tong, Frank J. Millero, Christopher L. Sabine, Andrew G. Dickson, Catherine Goyet, Geun-Ha Park, Rik Wanninkhof, Richard A. Feely, Robert M. Key (2006). Global relationships of total alkalinity with salinity and temperature in surface waters of the world's oceans. *Geophysical research letters* 33, L19605. Doi:10.1029/2006GL027207

Lenton, A., Tilbrook, B., Law, R. M., Bakker, D., Doney, S. C., Gruber, N., Ishii, M., Hoppema, M., Lovenduski, N. S., Matear, R. J., McNeil, B. I.,Metzl, N., Mikaloff Fletcher, S. E., Monteiro, P. M. S., Rödenbeck, C., Sweeney, C., and Takahashi, T. (2013). Sea-air CO_2 fluxes in the Southern Ocean for the period 1990–2009. *Biogeosciences* 10, 4037–4054. Doi:10.5194/bg-10-4037-2013

Lindemann, C., and St John, M. A. (2014). A seasonal diary of phytoplankton in the North Atlantic. *Frontiers in Marine Science* 1, 1 – 6

Lovenduski, N. S., Ito, T. (2009). The future evolution of the Southern Ocean CO2 sink. *Journal of Marine Research* 67(5), 597–617. Doi: http://dx.doi.org/10.1357/002224009791218832

Lozowski, E.P., R.B. Charlton, C.D. Nguyen, J.D. Wilson (1989). The

Use of Cumulative Monthly Mean Temperature Anomalies in the Analysis of Local Interannual Climate Variability. *Journal of Climate* 2(9), 1059-1068. Doi: $10.1175/1520-0442(1989)002<1059:TUOCMM>2.0.CO;2$

Luo, C., N. Mahowald, and N. Meskhidze (2005). Estimation of iron solubility from observations and a global aerosol model. *Journal of Geophysical Research*, 110, D23307, doi:10.1029/2005JD006059

MacIntyre, Hugh L., Todd M. Kana, Tracy Anning, Richard J. Geider (2002). Photoacclimation of Photosynthesis Irradiance Response Curves and Photosynthetic Pigments in Microalgae and Cyanobacteria. *Journal of Phycology* 38, 17-38. Doi: 10.1046/j.1529-8817.2002.00094.x

Mahadevan, A., D'Asaro, E., Lee, C., and Perry, M. J. (2012). Eddy-driven stratification initiates North Atlantic spring phytoplankton blooms. *Science* 337, 54–58

Marinov, I., J. L. Sarmiento, J. R. Toggweiler, M. Follows, B. K. Mignone (2008). Impact of oceanic circulation on the biological carbon storage in the ocean and atmospheric pCO2. *Global Biogeochemical Cycles* 22, GB3007. Doi:10.1029/2007GB002958

Marra, John (1997). Analysis of diel variability in chlorophyll fluorescence. *Journal of Marine Research*, Volume 55, Number 4, pp. 767-784(18). Doi: http://dx.doi.org/10.1357/0022240973224274

Martin, J., R. Gordon, and S. Fitzwater (1990b). Iron in Antarctic waters. *Nature*, 345, 156–158

Martin, A. P. (2003). Phytoplankton patchiness: the role of lateral stirring and mixing. *Progress in Oceanography* 57, 125–174. Doi:10.1016/S0079-6611(03)00085-5

Masojidek, J., G. Torzillo, M. Koblizek, J. Kopecky, P. Bernardini, A. Sacchi, J. Kmenda (1999). Photoadaptation of two members of the Chlorophyta (Scenedesmus and Chlorella) in laboratory and outdoor cultures: changes in chlorophyll flurescence quenching and the xanthophyll cycle. *Planta* 209, 126-135

McNeil, Ben I., Nicolas Metzl, Robert M. Key, Richard J. Matear, Antoine Corbiere (2007). An empirical estimate of the Southern Ocean air-sea CO2 flux. *Global Biogeochemical Cycles* 21, GB3011. Doi:10.1029/2007GB002991

Merlivat, L., G. Caniaux, J. Boutin, M. Gonzalez-Davila, M. Levy, A. S. Kremeur, and L. Resplandy (2005). Space and time variability of total inorganic carbon and air-sea flux of CO2 in the north-east Atlantic ocean during the POMME experiment (2001): A study from the diurnal to the monthly time scale along langrangian buoys trajectory. Conference paper. Doi:10.13140/2.1.1907.5528

Merlivat, L., J. Boutin, D. Antoine (2014). Roles of biological and physical processes in driving seasonal air–sea CO2 flux in the Southern Ocean: New insights from CARIOCA pCO_2. *Journal of marine systems* 147, 9-20. Doi: http://dx.doi.org/10.1016/j.jmarsys.2014.04.015

Meskhidze, N., A. Nenes, W. Chameides, C. Luo, and N. Mahowald (2007). Atlantic Southern Ocean productivity: Fertilization from above or below? *Global Biogeochemical Cycles*, 21, GB2006, doi:10.1029/2006GB002711

Miller, Charles B. (2004). Biological Oceanography. *Blackwell Science Ltd.* pp. 56–58

Monteiro, P. M. S., L. Gregor, M. Lévy, S. Maenner, C. L. Sabine, S. Swart (2015). Intraseasonal variability linked to sampling alias in air-sea CO2 fluxes in the Southern Ocean. *Geophysical Research Letters* 42. Doi:10.1002/2015GL066009

Moore, J.K., Lindsay, K., Doney, S.C., Long, M.C., Misumi, K. (2013). Marine Ecosystem Dynamics and Biogeochemical Cycling in the Community Earth System Model [CESM1(BGC)]: comparison of the 1990s with the 2090s under the RCP4.5 and RCP 8.5 Scenarios. *Journal of climate* 26 (23), 9291–9312. Doi: http://dx.doi.org/10.1175/JCLI-D-12-

00566.1.

Mulholland, M., Rocha, A., Boneillo, G. (2011). Incorporation of Leucine and Thymidine by Estuarine Phytoplankton: Implications for Bacterial Productivity Estimates. *Estuaries and Coasts*, 34(2), 310. Doi:10.1007/s12237-010-9366-2

Munro, David R., Nicole S. Lovenduski, Britton B. Stephens, Timothy Newberger, Kevin R. Arrigo, Taro Takahashi, Paul D. Quay, Janet Sprintall, Natalie M. Freeman, Colm Sweeney (2015). Estimates of net community production in the Southern Ocean determined from time series observations (2002–2011) of nutrients, dissolved inorganic carbon, and surface ocean pCO_2 in Drake Passage. *Deep Sea Research* II 114, 49–63. Doi: http://dx.doi.org/10.1016/j.dsr2.2014.12.014

NASA Goddard Space Flight Center, Ocean Ecology Laboratory, Ocean Biology Processing Group; (2014): MODIS-Aqua Ocean Color Data; NASA Goddard Space Flight Center, Ocean Ecology Laboratory, Ocean Biology Processing Group. $http://dx.doi.org/10.5067/AQUA/MODIS_OC.2014.0Accessedon07/28/2015$

Nevison, C. D., R. F. Keeling, M. Kahru, M. Manizza, B. G. Mitchell, and N. Cassar (2012). Estimating net community production in the Southern Ocean based on atmospheric potential oxygen and satellite ocean color data. *Global Biogeochemical Cycles* 26, GB1020. Doi:10.1029/2011GB004040

Nicklisch, A., Koehler, J. (2001). Estimation of primary production with Phyto-PAM-Fluorometry. Annual Report, Institute of Freshwater Ecology, Inland Fish, Berlin, 13: 47-60

Nightingale, P. D., G. Malin, C. S. Law, A. J. Watson, P. S. Liss, M. I. Liddicoat, J. Boutin, R. C. Upstill-Goddard (2000). In situ evaluation of air-sea gas exchange parameterizations using novel conservative and volatile tracers. *Global Biogeochemical Cycles*, 14(1), 373–387. Doi:10.1029/1999GB900091

Olaizola, Miguel, Julie La Roche, Zbigniew Kolber, Paul G. Falkowski (1994). Non-photochemical fluorescence quenching and the diadinoxanthin cycle in a marine diatom. *Photosynthesis Research* 41, 357-370

Oubelkheir, K., Claustre, H., Sciandra, A., Babin, M. (2005). Bio-optical and biogeochemical properties of different trophic regimes in oceanic waters. *Limnology Oceanography* 50(6), 1795-1809. doi:10.4319/lo.2005.50.6.1795.

Papageorgiou, G., M. Tsimilli-Michael, K. Stamatakis (2007). The fast and slow kinetics of chlorophyll a fluorescence induction in plants, algae and cyanobacteria: a viewpoint. *Photosynthesis Research* 94, 275-290

Parslow, John S., Philip W. Boyd, Stephen R. Rintoul, F. Brian Griffiths, (2001). A persistent subsurface chlorophyll maximum in the Interpolar Frontal Zone south of Australia: seasonal progression and implications for phytoplankton–light–nutrient interactions. *Journal of Geophysical Research* 106, 31543–31557

Peloquin, J. A., Smith, W. O., Jr. (2007). Phytoplankton blooms in the Ross Sea, Antarctica: Interannual variability in magnitude, temporal patterns, and composition. *Journal of Geophysical Research: Oceans* 112 (C08013). Doi:10.1029/2006JC003816

Perkins, R., J.-L. Mouget, S. Levebvre, J. Lavaut (2006). Light response curve methodology and possible implications in the application of chlorophyll fluorescence to benthic diatoms. *Marine Biology* 149, 703-712

Piketh, S.J., Tyson, P.D., Steffen,W., (2000). Aeolian transport from southern Africa and iron fertilization of marine biota in the South Indian Ocean. *South African Journal of Science* 96 (5)

Pinet, Paul R. (2006). Invitation to Oceanography (4th Edition). Sudbury, MA: Jones and Bartlett Publishers. ISBN-10: 0763740799

Platt, T., Gallegos, C. L., and Harrison, W. G. (1980). Photoinibition of photosynthesis in natural assemblages of marine phytoplankton. *Journal of Marine Research*, 38, 687–701

Platt, T. (1986). Primary production of the ocean water column as a function of surface light intensity: Algorithms for remote sensing. *Deep Sea Research* 33, 149-163

Platt, T., Bird, D. F., and Sathyendranath, S. (1991). Critical depth and marine primary production. *Proceedings of the Royal Society B: Biological Sciences* 246, 205–217

Platt, T., and Sathyendranath, S. (1993). Estimators of primary production for interpretation of remotely-sensed data on ocean color. *Journal of Geophysical Research: Oceans*, 98, 14561–14576

Pollard, R., M. Lucas, and J. Read (2002). Physical controls on biogeochemical zonation in the Southern Ocean. *Deep Sea Research*, Part II, 49, 3289–3305

Pollard, R. T., et al. (2009). Southern Ocean deep-water carbon export enhanced by natural iron fertilization. *Nature* 457, 577–580

Racault, M-F., Raitsos, D. E., Berumen, M. L., Brewin, R. J.W., Platt, T., Sathyendranath, S., Hoteit, I. (2015). Phytoplankton phenology indices in coral reef ecosystems: application to ocean-colour observations in the Red Sea. *Remote Sensing of Environment* 160, 222–234

Ralph, Peter J., Christian Wilhelm, Johann Lavaud, Torsten Jakob, Katherina Petrou, Sven A. Kranz (2010). Fluorescence as a tool to understand changes in photosynthetic electron flow regulation. *Chlorophyll a fluorescence in aquatic sciences: Methods and Applications, Developments in applied Phycology* 4. Doi: $10.1007/978-90-481-9268-7_1$ Springer Science Business Media B.V. 2011

Raven J.A., Geider R.J. (1988). Temperature and algal growth. *New Phytology* 110, 441–461. doi:10.1111/j.1469-8137.1988.tb00282.x

Raven, J. A. and Falkowski, P. G. (1999). Oceanic sinks for atmospheric CO_2. *Plant, Cell and Environment* 22, 741–755

Raven, John A. and Geider, Richard J. (2003). Adaptation, Acclimation and Regulation in Algal Photosynthesis. *Photosynthesis in Algae*, 385-412. Doi: $10.1007/978-94-007-1038-2_17$

Reay, D., J. Priddle, D. Nedwell, M. Whitehouse, J. Ellis-Evans, C. Deubert, and D. Connelly (2001). Regulation by low temperature of phytoplankton growth and nutrient uptake in the Southern Ocean. *Marine Ecology Progress Series*, 219, 51–64

Resplandy, L., Boutin, J., Merlivat, L., (2014). Observed small spatial scale and seasonal variability of the CO_2-system in the Southern Ocean. *Biogeosciences* 11, 75–90. Doi: http://dx.doi.org/10.5194/bg-11-75-2014.

Richardson, K., A.W. Visser, F. Bo Pedersen (2000). Subsurface phytoplankton blooms fuel pelagic production in the North Sea. *Journal of Plankton Research* 22, 1663–1671. Doi: 10.1093/plankt/22.9.1663

Robinson, Carol and Williams, Peter J. le B. (2005). Respiration and its measurements in surface marine waters. In: Respiration in aquatic ecosystems, Chapter 9. Oxford University Press, USA. ISBN 0191523615, 9780191523618

Rolinski S, Horn H, Petzoldt T, Paul L (2007) Identifying cardinal dates in phytoplankton time series to enable the analysis of longterm trends. *Oceologia* 153, 997–1008

Rubin, S.I. (2003). Carbon and nutrient cycling in the upper watercolumn across the Polar Frontal Zone and the Antarctic Circumpolar Current along 170∘W. *Global Biogeochemical Cycles* 17 (3), 1087. Doi: http://dx.doi.org/10.1029/2002GB001900

Sackmann , B. S., M. J. Perry, and C. C. Eriksen (2008). Seaglider observations of variability in daytime fluorescence quenching of chlorophyll a in Northeastern Pacific coastal

waters. *Biogeosciences discussions* 5, 2839–2865

Sathyendranath, Shuba, Luigi Lazzara, Louis Prieur (1987). Variations in the spectral values of specific absorption of phytoplankton. *Limnology Oceanography*, 32(2), 403-415

Schimel, D., I. Enting, M.Heimann, T. Wigley, D. Raynaud, D. Alves, U. Siegenthaler (1994). Chapter CO_2 and the Carbon Cycle, in Climate Change 94, Radiative Forcing Of Climate Change, pp. 38-71, Intergovernmental Panel on Climate Change. Cambridge University Press, New York

Schlitzer, R. (2002). Carbon export fluxes in the Southern Ocean: Results from inverse modeling and comparison with satellite-based estimates. *Deep Sea Research, Part II*, 49, 1623–1644. Doi:10.1016/S0967-0645(02)00004-8

Schreiber, U., W. Bilger, H. Hormann, C. Neubauer (1998). Chlorophyll fluorescence as a diagnostic tool: basics and some aspects of practical relevance. In: Raghavendra, A. (ed). Photosynthesis: a comprehensive treatise. Cambridge University Press, Cambridge, pp 320-335

Schreiber, U. (2004). Pulse Amplitude Modulation (PAM) fluormetry and saturation pulse method: an overview. In: Papageorgiou, G. Govindjee (eds). Chlorophyll *a* fluorescence: a signature of photosynthesis. Springer, Dordrecht, pp 279-319

Seaton, G.G.R., Walker, D.A. (1990). Chlorophyll fluorescence as a measure of photosynthetic carbon assimilation. *Proceedings of the Royal Society of London, B* 242, 29-35

Siegel, D.A., S.C. Doney, J.A. Yoder (2002). The North Atlantic Spring Phytoplankton Bloom and Sverdrup's Critical Depth Hypothesis. *Science* Vol. 296, 730-733

Smayda, T. J. (1997b). What is a bloom? A commentary. *Limnology and Oceanography* 42, 1132–1136. doi: $10.4319/lo.1997.42.5_part_2.1132$

Smetacek, Victor and Passow, Uta (1990). Spring bloom initiation and Sverdrup's critical depth model. *Limnology and Oceanography* 35, 228–234

Sommer, Ulrich, Herwig Stibor, Alexis Katechakis, Frank Sommer, Thomas Hansen (2002). Pelagic food web configurations at different levels of nutrient richness and their implications for the ratio fish production:primary production. *Sustainable Increase of Marine Harvesting: Fundamental Mechanisms and New Concepts*, Volume 167 of the series Developments in Hydrobiology, 11-20. Doi: $10.1007/978-94-017-3190-4_2$

Stanley, R. H. R., Kirkpatrick, J. B., Cassar, N., Barnett, B. A., and Bender, M. L. (2010). Net community production and gross primary production rates in the western equatorial Pacific. *Global Biogeochemical Cycles*, 24. Doi:10.1029/2009GB003651

Steemann Nielsen, E. (1952). The use of radio-active carbon (^{14}C) for measureing organic production in the sea. *Journal du Conseil pour la Conservation Internationale pout l'Exploration de la Mer* 18, 117-140

Stramski, D., R., Reynolds, A., Kahru, M., Mitchell, B.G. (1999). Estimation of Particulate Organic Carbon in the Ocean from Satellite Remote Sensing. *Science*, 285(5425), 239–242. doi:10.1126/science.285.5425.239

Stuart, Venetia, Shubha Sathyendranath, Trevor Platt, Heidi Maass, Brian D. Irwin (1998). Pigments and species composition of natural phytoplankton populations: Effect on the absorption spectra. *Journal of Plankton Research* Vol. 20 no. 2, 187-217

Sunda, W., and S. Huntsman (1995). Iron uptake and growth limitation in oceanic and coastal phytoplankton. *Marine Chemistry*, 50, 189–206

Sutton, A. J., Sabine, C. L., Maenner-Jones, S., Lawrence-Slavas, N., Meinig, C., Feely, R. A., Mathis, J. T., Musielewicz, S., Bott, R., McLain, P. D., Fought, H. J., and Kozyr, A. (2014). A high-frequency atmospheric and seawater pCO_2 data set from 14 open-ocean sites using a moored autonomous system. *Earth System Science Data*, 6, 353-366,

doi:10.5194/essd-6-353-2014

Sverdrup, H. 1953. On conditions for the vernal blooming of phytoplankton. *Journal du Conseil* 18, 287–295

Swart, S., Thomalla, S. J., and Monteiro, P.M.S. (2014). The seasonal cycle of mixed layer dynamics and phytoplankton biomass in the Sub-Antarctic Zone: a high-resolution glider experiment. *Journal of Marine Systems*. Doi:10.1016/j.jmarsys.2014.06.002.

Takahashia, Taro, Stewart C. Sutherland, Colm Sweeney, Alain Poisson, Nicolas Metzl, Bronte Tilbrook, Nicolas Bates, Rik Wanninkhof, Richard A. Feely, Christopher Sabine, Jon Olafsson, Yukihiro Nojiri (2002). Global sea–air CO_2 flux based on climatological surface ocean pCO_2, and seasonal biological and temperature effects. *Deep-Sea Research II* 49, 1601–1622

Takahashi, T., Sutherland, S. C., Wanninkhof, R., Sweeney, C., Feely, R. A., Chipman, D.W., Hales, B., et al. (2009). Climatological mean and decadal change in surface ocean pCO_2, and net sea-air CO_2 flux over the global oceans. *Deep Sea Research, Part II: Topical studies in oceanography* 56, 554–577

Takahashi, T., C. Sweeney, B. Hales, D. Chipman, T. Newberger, J. Goddard, R. Iannuzzi, S. Sutherland (2012). The changing carbon cycle in the Southern Ocean. *Oceanography* 25(3), 26–37

Taylor, J. R., and Ferrari, R. (2011). Shutdown of turbulent convection as a new criterion for the onset of spring phytoplankton blooms. *Limnology and Oceanography* 56, 2293–2307

Thomalla, S. J., Fauchereau, N., Swart, S., Monteiro, P. M. S. (2011). Regional scale characteristics of the seasonal cycle of chlorophyll in the Southern Ocean. *Biogeosciences* 8, 2849–2866

Thomalla Sandy J., Marie-Fanny Racault, Sebastiaan Swart, Pedro M. S. Monteiro (2015). High-resolution view of the spring bloom initiation and net community production in the Subantarctic Southern Ocean using glider data. *ICES Journal of Marine Science*. Doi:10.1093/icesjms/fsv105

Thomalla S., Ogunkoya AG., Vichi M., Swart S. (2016a). Using optical sensors in gliders to estimate phytoplankton carbon concentrations and chlorophyll-to-carbon ratios in the Southern Ocean. Manuscript submitted for publication.

Thomalla, S., Erica Kean, Mike Lucas, Michael-John Gibbert, Ray Barlow (2016b). Photosynthesis versus irradiance relationsships in the Atlantik sector of the Southern Ocean. Manuscript submitted for publication

Thomas, Helmuth (2002). Remineralization ratios of carbon, nutrients, and oxygen in the North Atlantic Ocean: A field databased assessment. *Global Biogeochemical Cycles* 16(3), 1051. Doi:10.1029/2001GB001452

Tortell, P. D., Guéguen, C., Long, M. C., Payne, C. D., Lee, P., DiTullio, G. R. (2011). Spatial variability and temporal dynamics of surface water pCO_2, O_2/Ar and dimethylsulfide in the Ross Sea, Antarctica. *Deep-Sea Research Pt. I*, 58, 241–259. Doi:10.1016/j.dsr.2010.12.006, 2011

Townsend DW, Cammen LM, Holligan PM, Campbell DE, Pettigrew NR (1994). Causes and consequences of variability in the timing of spring phytoplankton blooms. *Deep Sea Research I* 41, 747-765

Tripathy, S.C., S. Pavithran, P. Sabu, H.U.K. Pillai, D.R.G. Dessai, N. Anilkumar (2015). Deep chlorophyll maximum and primary productivity in Indian Ocean sector of the Southern Ocean: Case study in the Subtropical and Polar Front during austral summer 2011. *Deep Sea Research II* 118, 240-149. http://dx.doi.org/10.1016/j.dsr2.2015.01.004

Valdés L, O'Brien T, López-Urrutia A (eds) (2006) Zooplankton monitoring results in the ICES area. *Summary status report 2004/2005*. ICES Coop Res Rep 281

Vernet, M., D. G.Martinson, R. A. Iannuzzi, S. Stammerjohn, W. Kozlowski, K. Sines, R. Smith, and I. Garibotti (2008). Primary production within the sea-ice zone west of the Antarctic Peninsula: I—Sea ice, summer mixed layer, and irradiance. *Deep Sea Research, Part II*, 55, 2068–2085

Volk, T. and Hoffert, M. I. (1985). Ocean Carbon Pumps: Analysis of Relative Strengths and Efficiencies in Ocean-Driven Atmospheric CO2 Changes, in The Carbon Cycle and Atmospheric CO_2: Natural Variations Archean to Present (eds E.T. Sundquist and W.S. Broecker), American Geophysical Union, Washington, D. C.. doi: 10.1029/GM032p0099

Wagener, T., C. Guieu, R. Losno, S. Bonnet, and N. Mahowald (2008). Revisiting atmospheric dust export to the Southern Hemisphere ocean: Biogeochemical implications. *Global Biogeochemical Cycles*, 22, GB2006, doi:10.1029/2007GB002984

Wallace, J. M., T. P. Mitchell, and C. Deser (1989). The influence of sea surface temperature variability on surface wind in the eastern equatorial Pacific: Seasonal and interannual variability *Journal of Climate* 2, 1492–1499

Wang, Xiujun and Matear, Richard J. (2001). Modeling the upper ocean dynamics in the Subantarctic and Polar Frontal Zones in the Australian sector of the Southern Ocean. *Journal of geophysical research* 106, NO. C12, 31,511-31,524

Weeding, B., Trull, T.W. (2014). Hourly oxygen and total gas tension measurements at the Southern Ocean Time Series site reveal winter ventilation and spring net community production. *Journal of Geophysical Research* 119, 348–358. http://dx.doi.org/10.1002/2013JC009302.

Weiss, R.F., Östlund, H.G., Craig, H. (1979). Geochemical studies of the Weddell Sea. *Deep Sea Research* 26, 1093-1120

White, M., et al. (2009). Intercomparison, interpretation, and assessment of spring phenology in North America estimated from remote sensing for 1982–2006. *Global Change Biology*, 15, 2335–2359, doi:10.1111/j.1365-2486.2009.01910.X.

Wilson, C., and V. J. Coles (2005). Global climatological relationships between satellite biological and physical observations and upper ocean properties. *Journal of Geophysical Research* 110, C10001. Doi:10.1029/2004JC002724

Woods, J.D. (1980). Diurnal and seasonal variation of convection in the wind-mixed layer of the ocean. *Quarterly Journal of the Royal Meteorological Society* 106, 379-394. Doi: 551.465.4551.465.7

Yacobi, Y.Z. and Zohary, T. (2010). Carbon:chlorophyll a ratio, assimilation numbers and turnover times of Lake Kinneret phytoplankton. *Hydrobiologia* 639, 185-196. doi:10.1007/s10750-009-0023-3

Zhang, H. M., Bates, J. J., and Reynolds, R.W. (2006). Assessment of composite global sampling: sea surfacewind speed. *Geophysical Research Letters* 33, L17714

Supporting background information

Deep Chlorophyll Maximum (DCM) The occurrence of deep chlorophyll maximum has previously been reported from the polar oceans, in particular the Southern Ocean (Tripathy et al., 2015; Parslow et al, 2001), although they are more common in the subtropic gyres and temperate oceans (Parslow et al., 2001). It can contribute significantly to the PP during the summer/ late summer (Richardson et al., 2000), a time when nutrient concentrations

are usually depleted within the MLD (Tripathy et al., 2015). At this time, a maximum of chlorophyll concentration can occur below the MLD at the depth of the nutricline (Cullen, 1982). A deep chlorophyll maximum can develop for two reasons. Firstly, in a layer of shade adapted phytoplankton cells that package their cells with a lot of chlorophyll and have thus a high chlorophyll to carbon ratio, and secondly, it can coincide with a high phytoplankton biomass (Miller, 2004). At depth where the light intensity is low but nutrient concentrations might be higher due to elevated mixing, phytoplankton can increase their intracellular chlorophyll content up to tenfold (Cullen, 1982). The DCM might also be a transient process of phytoplankton sinking out of the surface waters (Parslow et al., 2001).
No data on taxonomic species composition, zooplankton grazer abundance or nutrient concentration in the water column is present in this study. However, as it can be seen that the MLD had been rising to almost the surface 1 month before the deep chlorophyll maximum was present and there was a tail of Chl and C_{phyto} that seemed to be moving from the surface downwards as time passed on, it could be assumed that the DCM consisted of phytoplankton that had fallen out of the mixed layer and sunk to a depth where they were still actively living and photosynthesizing.

Supporting methods

Non-photochemical quenching The Phenomenon where a photon is emitted by an electron, element or molecule during its return from an excited state to the ground state and re-emitted at a longer wavelength is called fluorescence. It can be observed in various processes in nature, one of them being light absorbed by chlorophyll a in photoautotrophic cells. The fate of the absorbed light in chlorophyll cells is to either be used to conduct photosynthesis, to be lost as heat in non-photochemical quenching, or to be emitted via fluorescence (Falkowski et al., 1986; Seaton and Walker 1990; Kolber and Falkowski 1993; Nicklisch and Koehler 2001). The sum of the ratio of these processes is assumed to be constant (Cosgrove and Borowitzka, 2010). As chlorophyll fluorescence is at ambient temperatures arising to 90-95% in the photosystem II where oxygen evolution takes place (Krause and Weis, 1991; Papageorgiou et al., 2007), the fluorescence yield can be used to derive information about photosynthesis (Dau, 1994; Schreiber, 2004). When chlorophyll cells are situated in a dark environment (dark adapted) and all reaction centres are open, a sudden short flash of high intensity light will increase the proportion of closed PSII reaction centres as the QA get reduced. With closed reaction centres, photochemistry is zero and fluorescence maximum. Responsible for the closure of reaction centres, and thus the fluorescence yield, is the oxidation state of the ubiquinone (QA). The reduced state means the reaction centres are closed and unable to accept an electron (Schreiber et al., 1998). Reaction centres are closed when the level of irradiance is above the saturation irradiance, or when the cell's light environment suddenly changes from dark/low light to high light (Ralph et al., 2010), which helps the cells prevent oxidative stress (Ledford and Nyjogi 2005). If the cells are dark-adapted, the redundant energy in the cells is emitted as radiation. This process is used in marine sciences to quantify chlorophyll a concentrations in the water. A flash of light is emitted and fluorescence detected. As described above, this method will only work if the cells are dark-adapted. If the cells were not dark-adapted, fluorescence yield will not reach a maximum due to the induction of non-photochemical quenching. Non photochemical quenching (NPQ) is used to prevent the cells from getting damaged by excess energy and prevent photoinhibition (Krause and Weis, 1991), in cases where the amount of energy from light absorption is exceeding the amount that can be used in photosynthesis. The excess energy is released as heat before it reaches the PSII reaction centre. NPQ can directly reduce the emission fluorescence under high light conditions (Perkins et al., 2006) as it reduces the lifetime of excited chlorophyll. Since there is one component of NPQ that does to a small fraction cause photoinhibition by damaging the core protein D1 in PSII (Hill et al., 2005), it might take up to hours until the proteins in the PSII get repaired and photoinhibitory quenching stops (Masojidek et al., 1999). Quenching was observed to occur in depths of up to 50m and the magnitude of quenching is positively correlated with incoming solar radiation (Sackmann et al., 2008). This is the reason why daytime profiles of fluorescence need to be quenching corrected.

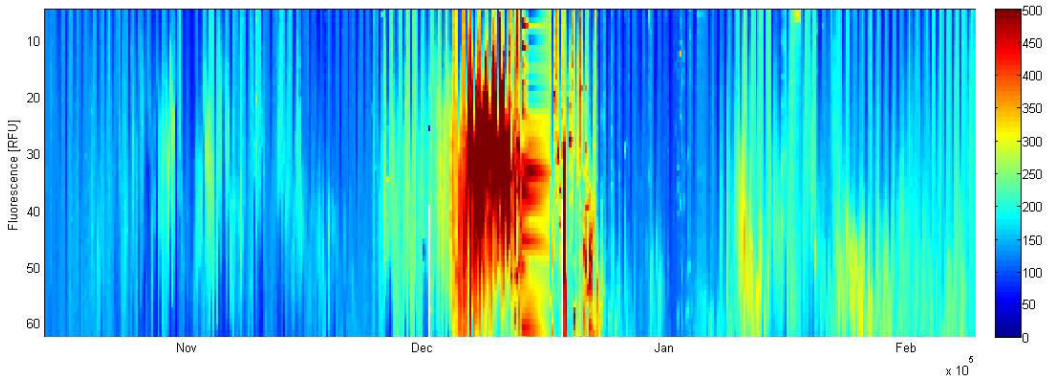

Figure 19: Fluorescence measured by the glider before applying the quenching correction method

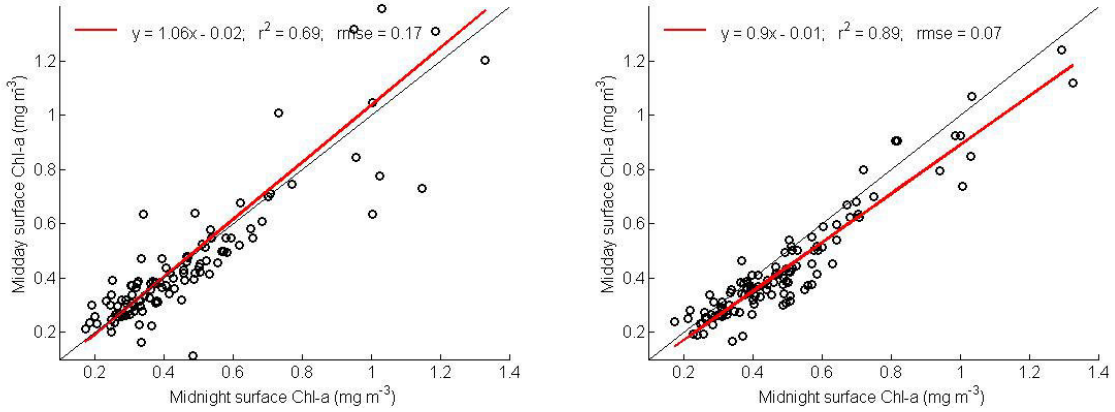

(a) (b)

Figure 20: Correlation analysis of daytime chlorophyll and nighttime chlorophyll values after the here developed quenching correction method was applied. The correlation was performed for the average Chl concentration for the 5 m below the depth of quenching correction (y=1.06x-0.02, R^2: 0.69, RMSE: 0.17) (a) and the average of the 5 m above the correction starting depth (y=0.9x-0.01, R^2: 0.89, RMSE: 0.07) (b)

Bloom initiation dates A bloom is defined as a condition with elevated phytoplankton concentrations (Behrenfeld and Boss, 2014). For being able to identify the day of spring bloom initiation, which is necessary when using the Sverdrup hypothesis, surface chlorophyll as well as MLD integrated chlorophyll values of the glider time series were compared to annual median surface chlorophyll values. This way, the time of unproportionally high increase in phytoplankton concentration relative to the rest of the annual phytoplankton cycle, and thus the beginning of a bloom, can be determined. Since glider data was not available for a whole year but for the spring and summer month from the middle October to the middle of February, averaging the chlorophyll concentration in these month would overestimate the annual value. Hence, satellite surface chlorophyll data extracted for the comprising area and year of the glider sampling period was used to mediate.
Annual surface Chlorophyll *a* data was derived via MODIS aqua satellite observations (NASA, 2014). For the time between April 2013 to March 2014, embedding the deployment period of the gliders, surface chlorophyll data was extracted with an 8 day average of 9 km resolution over

a square between 41,5° S – 44,5° S, 9° W– 7,6° W, centered at the sampling area of SOSCExII. The satellite derived Chlorophyll *a* concentration in the surface water can be used as a proxy for phytoplankton biomass (André, 1992). Satellite values of Chlorophyll *a* were ∼3 times lower than the glider data, which is in agreement with the findings of Thomalla et al. (2015) and Merlivat et al. (2014) who furthermore discuss various other studies who found the Southern Ocean satellite values to be systematically 2-5 times lower than modelling estimates. Thus, the annual satellite Chl data was multiplied by three to match the glider data.
The median annual satellite chlorophyll (april 2013 to march 2014) was then set in relation to the median satellite chlorophyll of the time of the experiment (October 2013 to February 2014). The comparison revealed the median of the data from the glider time series to be 16% higher than the annual median. Thus, the annual median value of chlorophyll (Chl_{annual}) was calculated as

$$Chl_{annual} = Chl_{glider} * 0.84 \tag{27}$$

Where Chl_{glider} is the median of the glider chlorophyll data.
Several different methods exist on the determination of spring bloom initiation dates (Brody et al., 2013; Ji et al., 2010). In this study, I compare the results of four different approaches using both, surface chlorophyll data and MLD integrated chlorophyll data.

Cumulative Sum Method The cumulative sum method builds a cumulative sum of the annual chlorophyll data and identifies the first day where the cumulative integration of the chlorophyll data of the glider time series reaches more than 15% of the maximum annual cumulative sum. This method has been used in various different zooplankton studies (Greve et al., 2001; Greve et al., 2005; Valdes et al., 2006; Batten and Mackas, 2009) as identification of the "start-of-season".

Cumulative Sum of Anomalies Method This method finds the period within the year where chlorophyll biomass increases most rapidly (Brody et al., 2013). It uses a time series of anomalies (chlorophyll biomass of each day minus the annual median chlorophyll biomass) to create a cumulative summation and find the day where it changes direction from a decreasing to an increasing trend (local minimum). This day will be identified as the date of bloom initiation and is simultaneously the day at which chlorophyll biomass rises above the threshold of annual median biomass. Lozowski, Charlton, Nguyen and Wilson (1989) applied this method to investigate temperature anomalies, and Racault et al. (2015) used this method to characterize phytoplankton seasonality in the Red Sea.

Rate of Change Method The rate of change method compares the rate of change in chlorophyll biomass (difference between two days) of the glider time series with the median rate of change of the annual time series. The day at which the daily rate of change has exceeded 15% of the annual median for 8 days or more will be identified as the start of the phytoplankton bloom. This method has previously been investigated and approved by Rolinski et al. (2007) in an aquatic ecosystem and by White et al. (2009) in terrestrial ecosystems.

Cumulative Sum of Anomalies of Positive Growth Rate Method Here, the bloom initiation is defined as the day with the largest anomaly in positive growth rate. Growth rates are calculated as the difference between the consecutive days and positive and negative slopes are separated. Multiple succeeding rates of the same sign are averaged. The growth rates of each time step are being subtracted by an annual median cumulative sum to find the anomaly of

each time step. The minimum of the cumulative sum of this difference is the day (or the period of days) where the community undergoes the biggest change in growth rate, which indicates it is shifting from a net biomass loss to a net biomass gain. This method was developed by Thomalla et al. (2015) and applied for finding the spring bloom initiation date in the Southern Ocean in 2012.

Method	Chl data	Bloom Initiation Date
Cumulative Sum	surface	8 Nov
Cumulative Sum	MLD integr.	25 Oct
Cumulative Sum of Anomalies	surface	25 Nov
Cumulative Sum of Anomalies	MLD integr.	13 Oct
Cum. Sum of Anom. Pos. Growth Rate	surface	15-16 Oct
Cum. Sum of Anom. Pos. Growth Rate	MLD integr.	15-16 Oct
Rate of Change	surface	3 Nov
Rate of Change	MLD integr.	26 Nov

Table 2: Bloom initiation dates were calculated with four different methods for both surface and MLD integrated chlorophyll values and resulted in seven different bloom initiation dates

The bloom initiation dates have been calculated using 4 different methods with surface chlorophyll as well as mixed layer integrated chlorophyll. The eight different approaches resulted in 7 different dates. The derived dates were all used individually and not grouped together as one date when a couple of days were close together, as it became clear that calculated NCP with the different bloom initiation dates can vary a lot between adjacent days. This is mainly due to fluctuations in mixed layer depth, which is used to integrate respiration and is thus directly related to NCP. If one date was to be preferred over the other when rounding up, it might calculate a very low NCP, whereas calculating NCP with a bloom initiation date only a day later might result in a high NCP (comparing the 25th and the 26th of November). For the cumulative sum of anomalies of positive growth rate method, which gave a range of 2 and 3 dates as output, only one date was chosen as representative for this method. This way all methods are represented by two dates and thus equally weighed when calculating the mean NCP. As shown in Fig. bla, the mean of all NCPs is identical to the NCP calculated with the bloom initiation date of the 8th of November (cumulative sum method), which is why from now onwards the NCP calculated with this date is used for further investigations.

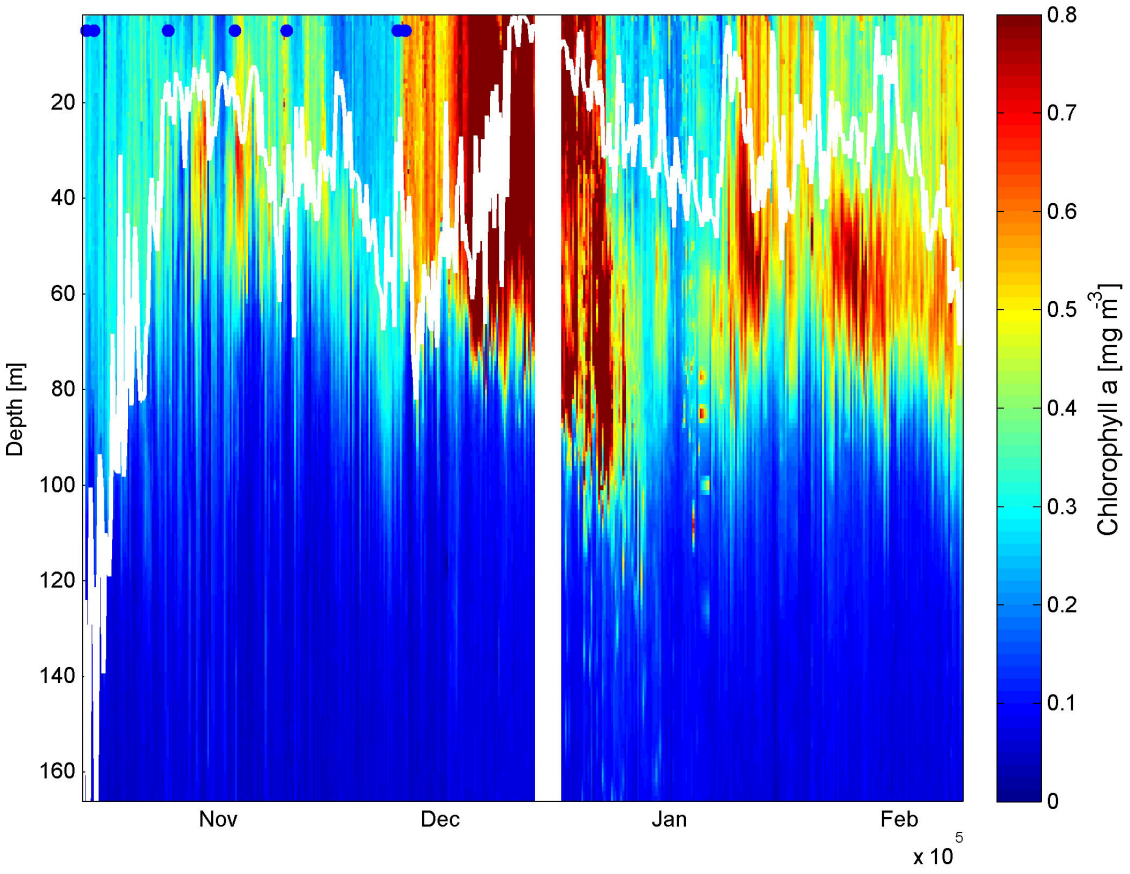

Figure 21: Concentrations of Chl *a* in the upper ocean over the samling period. The 7 different bloom initiation dates found by the 8 different calculation approaches (13th,15th and 25th of October, 3rd, 8th, 25th and 26th of November) are plotted as blue circles

Supporting figures .

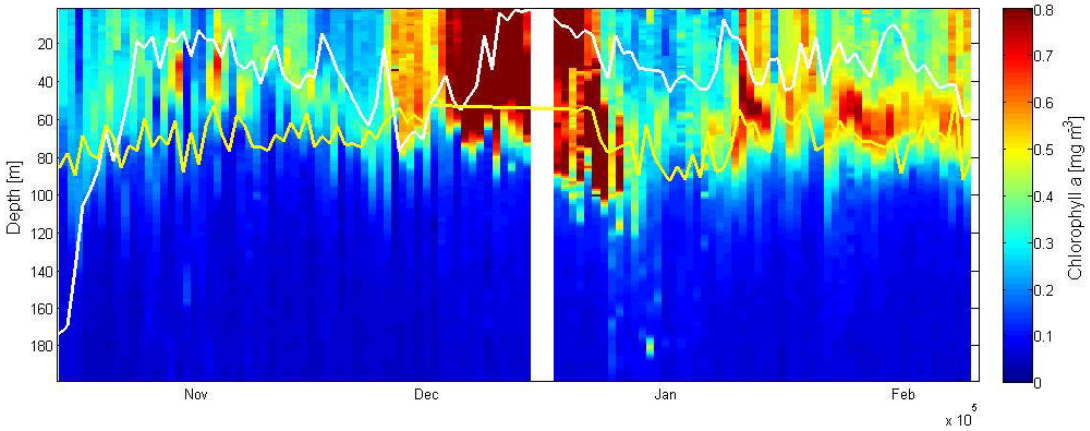

Figure 22: Concentrations of Chl *a* in the upper ocean over the samling period. The MLD is plotted in white, the ED, which was chosen as integration depth in the NCP calculations, is plotted in yellow

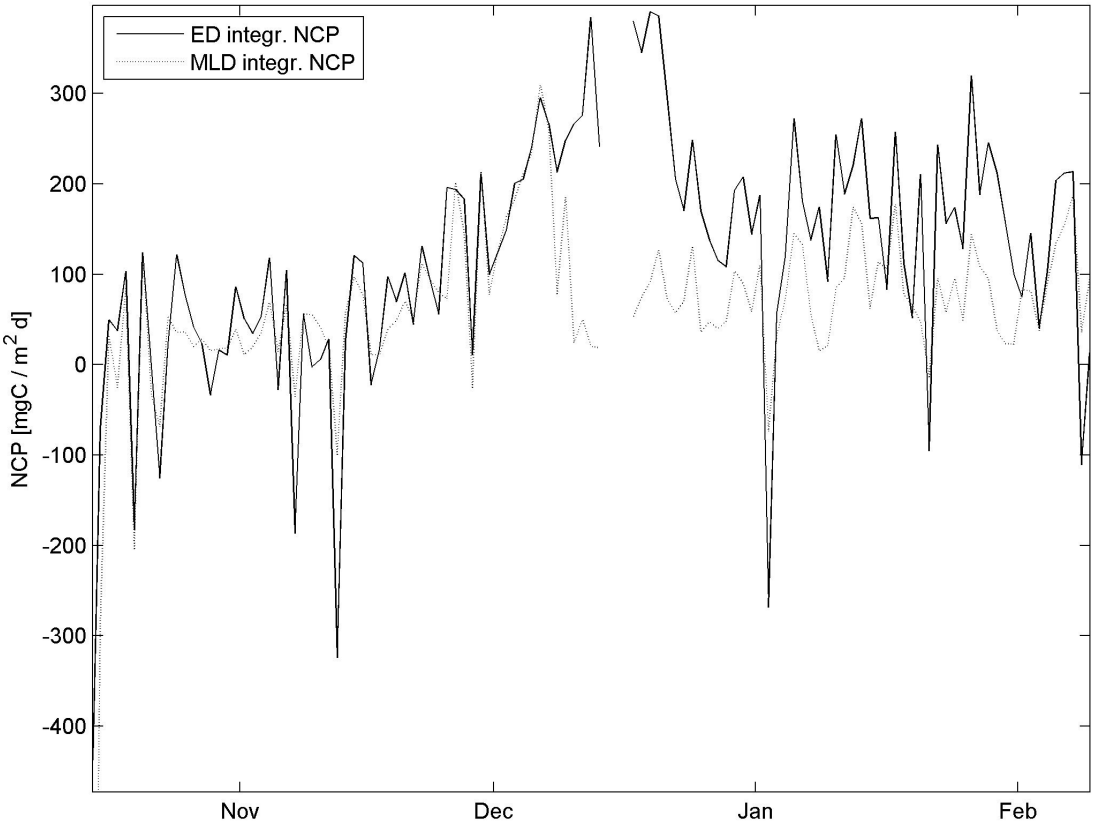

Figure 23: Time series of net community production (NCP) integrated over the mixed layer depth (MLD) (dotted line) and the euphotic depth (ED) (solid line)

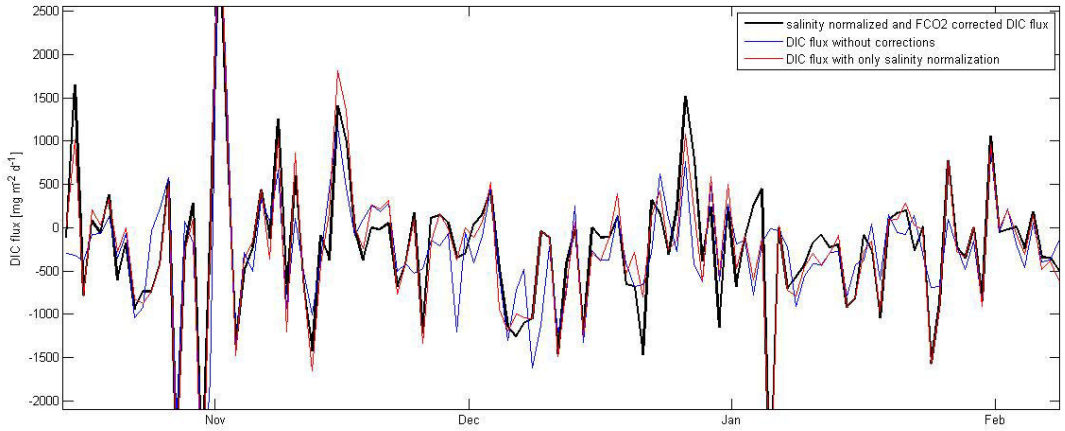

Figure 24: DIC flux time series with normalizing to salinity and subtracting the air-sea CO_2 flux (thick black line), without any of those corrections (blue line) and with only salinity normalization without subtracting FCO_2 (red line)

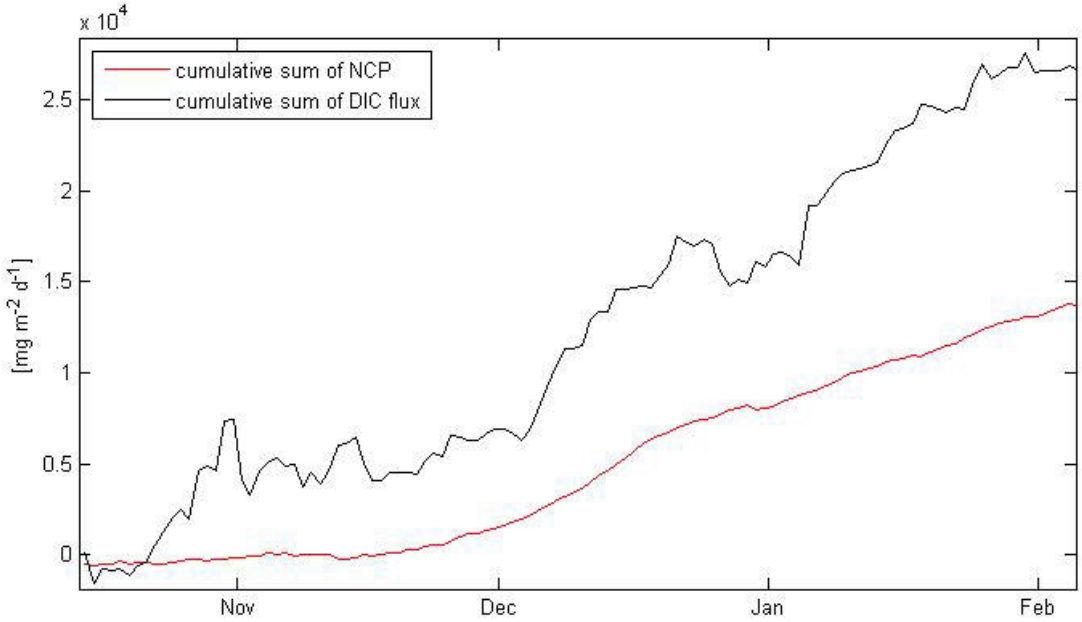

Figure 25: The cumulative sum of DIC flux (black line) peaks 1.5 weeks before the end of the sampling period, the cumulative sum of NCP rate does not peak until the end of the measurements (red line). The slope of the DIC cum.sum. is slightly steeper and the total DIC flux cum.sum. is higher than the NCP, but otherwise both rates show a similar slope

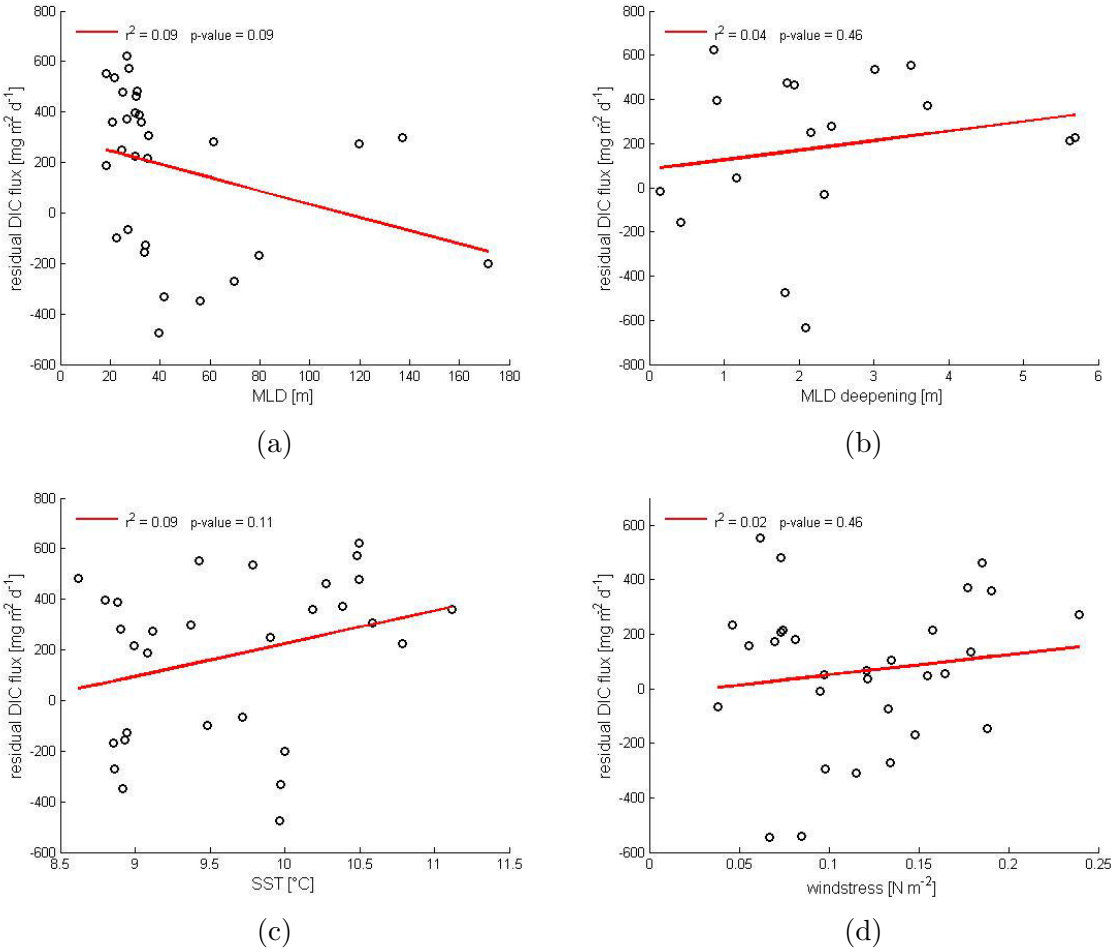

Figure 26: Correlation analysis of dayily DIC fluxes and the MLD (R^2: 0.09, p value: 0.09) (a), MLD deepening (R^2: 0.04, p value: 0.46) (b), surface temperature (R^2: 0.09, p value: 0.11) (c) and surface windstress (R^2: 0.02, p value: 0.46) (d)

http://iis4.nateko.lu.se/files/doc/Gulaserien.doc

Institutionen för naturgeografi och ekosystemvetenskap, Lunds Universitet.

Student examensarbete (Seminarieuppsatser). Uppsatserna finns tillgängliga på institutionens geobibliotek, Sölvegatan 12, 223 62 LUND. Serien startade 1985. Hela listan och själva uppsatserna är även tillgängliga på LUP student papers (https://lup.lub.lu.se/student-papers/search/) och via Geobiblioteket (www.geobib.lu.se)

The student thesis reports are available at the Geo-Library, Department of Physical Geography and Ecosystem Science, University of Lund, Sölvegatan 12, S-223 62 Lund, Sweden. Report series started 1985. The complete list and electronic versions are also electronic available at the LUP student papers (https://lup.lub.lu.se/student-papers/search/) and through the Geo-library (www.geobib.lu.se)

372 Andreas Dahlbom (2016) The impact of permafrost degradation on methane fluxes - a field study in Abisko

373 Hanna Modin (2016) Higher temperatures increase nutrient availability in the High Arctic, causing elevated competitive pressure and a decline in *Papaver radicatum*

374 Elsa Lindevall (2016) Assessment of the relationship between the Photochemical Reflectance Index and Light Use Efficiency: A study of its seasonal and diurnal variation in a sub-arctic birch forest, Abisko, Sweden

375 Henrik Hagelin and Matthieu Cluzel (2016) Applying FARSITE and Prometheus on the Västmanland Fire, Sweden (2014): Fire Growth Simulation as a Measure Against Forest Fire Spread – A Model Suitability Study –

376 Pontus Cederholm (2016) Californian Drought: The Processes and Factors Controlling the 2011-2016 Drought and Winter Precipitation in California

377 Johannes Loer (2016) Modelling nitrogen balance in two Southern Swedish spruce plantations

378 Hanna Angel (2016) Water and carbon footprints of mining and producing Cu, Mg and Zn: A comparative study of primary and secondary sources

379 Gusten Brodin (2016) Organic farming's role in adaptation to and mitigation of climate change - an overview of ecological resilience and a model case study

380 Veränika Trollblad (2016) Odling av *Cucumis Sativus* L. med aska från träd som näringstillägg i ett urinbaserat hydroponiskt system

381 Susanne De Bourg (2016) Tillväxteffekter för andra generationens granskog efter tidigare genomförd kalkning

382 Katarina Crafoord (2016) Placering av energiskog i Sverige - en GIS analys

383 Simon Nåfält (2016) Assessing avalanche risk by terrain analysis An experimental GIS-approach to The Avalanche Terrain Exposure Scale (ATES)

384 Vide Hellgren (2016) Asteroid Mining - A Review of Methods and Aspects

385 Tina Truedsson (2016) Hur påverkar snömängd och vindförhållande vattentrycksmätningar vintertid i en sjö på västra Grönland?

386 Chloe Näslund (2016) Prompt Pediatric Care Pediatric patients' estimated travel times to surgically-equipped hospitals in Sweden's Scania County

387 Yufei Wei (2016) Developing a web-based system to visualize vegetation trends by a nonlinear regression algorithm

388 Greta Wistrand (2016) Investigating the potential of object-based image analysis to identify tree avenues in high resolution aerial imagery and lidar data

389 Jessica Ahlgren (2016) Development of a Web Mapping Application for grazing resource information in Kordofan, Sudan, by downloading MODIS data automatically via Python

390 Hanna Axén (2016) Methane flux measurements with low-cost solid state sensors in Kobbefjord, West Greenland

391 Ludvig Forslund (2016) Development of methods for flood analysis and response in a Web-GIS for disaster management

392 Shuzhi Dong (2016) Comparisons between different multi-criteria decision analysis techniques for disease susceptibility mapping

393 Thirze Hermans (2016) Modelling grain surplus/deficit in Cameroon for 2030

394 Stefanos Georganos (2016) Exploring the spatial relationship between NDVI and rainfall in the semi-arid Sahel using geographically weighted regression

395 Julia Kelly (2016) Physiological responses to drought in healthy and stressed trees: a comparison of four species in Oregon, USA

396 Antonín Kusbach (2016) Analysis of Arctic peak-season carbon flux estimations based on four MODIS vegetation products

397 Luana Andreea Simion (2016) Conservation assessments of Văcărești urban wetland in Bucharest (Romania): Land cover and climate changes from 2000 to 2015

398 Elsa Nordén (2016) Comparison between three landscape analysis tools to aid conservation efforts

399 Tudor Buhalău (2016) Detecting clear-cut deforestation using Landsat data: A time series analysis of remote sensing data in Covasna County, Romania between 2005 and 2015

400 Sofia Sjögren (2016) Effective methods for prediction and visualization of contaminated soil volumes in 3D with GIS

401 Jayan Wijesingha (2016) Geometric quality assessment of multi-rotor unmanned aerial vehicle-borne remote sensing products for precision agriculture

402 Jenny Ahlstrand (2016) Effects of altered precipitation regimes on bryophyte carbon dynamics in a Peruvian tropical montane cloud forest

403 Peter Markus (2016) Design and development of a prototype mobile geographical information system for real-time collection and storage of traffic accident data

404 Christos Bountzouklis (2016) Monitoring of Santorini (Greece) volcano during post-unrest period (2014-2016) with interferometric time series of Sentinel-1A

405 Gea Hallen (2016) Porous asphalt as a method for reducing urban storm water runoff in Lund, Sweden

406 Marcus Rudolf (2016) Spatiotemporal reconstructions of black carbon, organic matter and heavy metals in coastal records of south-west Sweden

407 Sophie Rudbäck (2016) The spatial growth pattern and directional properties of *Dryas octopetala* on Spitsbergen, Svalbard

408 Julia Schütt (2017) Assessment of forcing mechanisms on net community production and dissolved inorganic carbon dynamics in the Southern Ocean using glider data

409 Abdalla Eltayeb A. Mohamed (2016) Mapping tree canopy cover in the semi-arid Sahel using satellite remote sensing and Google Earth imagery

410 Ying Zhou (2016) The link between secondary organic aerosol and monoterpenes at a boreal forest site

411 Matthew Corney (2016) Preparation and analysis of crowdsourced GPS bicycling data: a study of Skåne, Sweden